Thomas Alexandre Rodrigues

Licenciatura em Bioquímica

Preparation and characterization of hydrogels based on biopolymers: FucoPol and Chitin-glucan complex (CGC)

Dissertação para obtenção do Grau de Mestre em Biotecnologia

Orientador: Doutora Maria Filomena Andrade de Freitas, Professora Auxiliar, FCT-NOVA

Júri:

Presidente: Professora Isabel Sá Nogueira

Arguente: Professor Vítor Alves

Vogal: Professora Filomena Freitas

FACULDADE DE CIÊNCIAS E TECNOLOGIA
UNIVERSIDADE NOVA DE LISBOA

Dezembro, 2020

Thomas Alexandre Rodrigues

Licenciatura em Bioquímica

Preparation and characterization of hydrogels based on biopolymers: FucoPol and Chitin-glucan complex (CGC)

Dissertação para obtenção do Grau de Mestre em Biotecnologia

Orientador: Doutora Maria Filomena Andrade de Freitas, Professora Auxiliar, FCT-NOVA

Júri:

Presidente: Professora Isabel Sá Nogueira

Arguente: Professor Vítor Alves

Vogal: Professora Filomena Freitas

Dezembro, 2020

Preparation and characterization of hydrogels based on biopolymers: FucoPol and Chitin-glucan complex (CGC)

Agradecimentos

Em primeiro lugar gostaria de agradecer à Professora Filomena Freitas pela oportunidade de me receber no seu laboratório, por toda a disponibilidade, pela preocupação, pela orientação e por todo o conhecimento transmitido ao longo deste ano bastante atípico.

Um muitíssimo obrigado à Diana por tudo, desde toda a paciência para as minhas dúvidas, pela resolução de todos os problemas que surgiam com os géis, que nunca nos facilitaram a vida, até à mini formação sobre todo o processo de gravidez.

Aos membros do 407, nomeadamente à Asiyah, Patrícia Reis, Ana Teresa, João, Rita, Inês, Patrícia Freitas e Sílvia pelo ambiente incrível, amizade, e pelo esclarecimento de todas as minhas dúvidas laboratoriais. Às minhas colegas de mestrado Marta, Cristiana e Kleyde por me acompanharem nesta jornada e por todas as conversas fora de horas.

Aos meus amigos e vizinhos do serrado que sempre me apoiaram e integraram desde que entrei na faculdade, nada teria sido igual sem vocês.

Aos rapazes do Rodízio por toda a amizade, jantares, e companheirismo de sempre, e pelas nossas fantásticas apresentações noite fora pelo zoom, durante a quarentena.

Aos rapazes de Fátima e à Bajouco por estarem sempre ao meu lado, desde sempre.

Aos meus incansáveis companheiros de casa Carlos e Bruno pela fabulosa vivência e por esperarem até às 23h para jantar por causa do meu futebol.

À minha família sem que nada disto teria sido possível, pelo incondicional apoio e por estarem sempre lá.

A todos, um profundo obrigado!

Abstract

In this thesis, two polysaccharides were produced, FucoPol and chitin-glucan complex (CGC). FucoPol is an exopolysaccharide synthesised by the bacterium *Enterobacter* A47, composed of fucose, glucose, galactose and glucuronic acid, and also with acyl groups. CGC is a copolymer of chitin and glucan, extracted from the cell wall of the yeast *Komagataella pastoris*. Both biopolymers were produced using glycerol as the source of carbon, through fed-batch cultivation processes. The gel-forming capacity of these two biopolymers was recently demonstrated, and thus, the aim of this thesis was the production and characterization of FucoPol and CGC based hydrogels in terms of texture, mechanical, viscoelastic, and drug loading and release properties.

As FucoPol has the ability to form hydrogels in the presence of some metal cations, different dialysis techniques against Fe^{3+} solutions were performed to obtain FucoPol hydrogels, as well as different concentrations of iron solutions. On the other hand, CGC solutions obtained by freezing-thawing cycles were subjected to dialysis to induce the polymer's spontaneous gelation. Different freeze-thaw cycles, freezing time, dialysis temperature, polymer concentration and centrifugation conditions were tested in order to optimize the final properties of CGC hydrogels. All the resulting polymeric structures exhibited high water content (above 95%). The optimized FucoPol hydrogels were more brittle and presented a reduced iron content (below 0.15%), whereas the prevalent ductileness of CGC hydrogels in all the conditions tested provided an easier characterization of texture properties, in which the hydrogel with better hardness (16547 Pa) was obtained with the higher CGC concentration. The ability of CGC hydrogels to load and release model compounds (blue food dye E133/E122, and theophylline 99%) was demonstrated for different gels. However, the drug-release capacity was lower with the increase of CGC concentration. The fact that the resulting hydrogels display different textures, rheological and drug loading and release properties support their use as promising biomaterials in distinct areas including biomedicine, bioremediation, and agriculture.

Keywords: FucoPol, Chitin-glucan Complex (CGC), hydrogels, drug delivery system, skin.

Resumo

Dois polissacáridos foram produzidos nesta tese, o FucoPol e o complexo quitina-glucanos (CQG). O FucoPol é um exopolissacárido sintetizado pela bactéria *Enterobacter* A47, composto por fucose, glucose, galactose, e ácido glucurónico, e também por grupos acilo. O CQG é um co-polímero de quitina e glucanos, extraído da parede celular da levedura *Komagataella pastoris*. Ambos os polímeros foram produzidos utilizando glicerol como fonte de carbono, através de crescimentos em modo de operação fed-batch. A capacidade de gelificação destes dois polímeros foi recentemente demonstrada e, portanto, o propósito desta tese foi a produção e caracterização de hidrogéis baseados em FucoPol e CGC, nomeadamente, das propriedades texturais, mecânicas, viscoelásticas e libertação controlada de substâncias.

Como o FucoPol possui a capacidade de gelificação na presença de catiões metálicos, foram realizadas diferentes técnicas de diálise em Fe^{3+} para a obtenção de hidrogéis de FucoPol, assim como soluções com diferentes concentrações de ferro. Por outro lado, as soluções de CGC obtidas por ciclos de congelamento/descongelamento foram submetidas a diálise de modo a induzir a gelificação espontânea. Diferentes condições de ciclos de congelamento/descongelamento, tempo de congelação, temperatura de diálise, concentração de polímero e centrifugação foram testadas com o intuito de otimizar as propriedades finais dos hidrogéis de CGC. Todas as estruturas poliméricas obtidas apresentaram elevados conteúdos em água (acima de 95%). Os hidrogéis de FucoPol otimizados mostraram-se mais frágeis, enquanto que a predominante ductilidade dos hidrogéis de CGC testados em todas as condições providenciaram uma caracterização mais acessível das suas propriedades texturais, em que o hidrogel com a maior dureza (16547 Pa) foi obtido com a maior concentração de CGC. A capacidade dos hidrogéis de CGC em adsorver e libertar compostos modelo (corante alimentar azul E133/E122, e teofilina 99%) foi demonstrada para diferentes géis. Contudo, a capacidade de libertação foi menor com o aumento da concentração de CGC. O facto de os hidrogéis desenvolvidos revelarem diferentes propriedades texturais, reológicas e de adsorção e libertação de fármaco reforça o seu uso como promissores biomateriais em áreas distintas incluindo biomedicina, biorremediação e agricultura.

Palavras-chave: FucoPol, complexo quitina-glucano (CQG), hidrogéis, sistema de libertação controlada de fármaco, pele.

List of Contents

List of Figures

List of Tables

Abbreviations

CDW	Cell dry weight
CGC	Chitin-glucan complex
DNA	Deoxyribonucleic acid
DTDT	Diffusion through dialysis tubing
EFSA	European Food Safety Authority
EPS	Exopolysaccharide
FT-IR	Fourier-transform infrared spectroscopy
HA	Hyaluronic acid
HPLC	High-performance liquid chromatography
ICP-AES	Inductively Coupled Plasma-Atomic Emission Spectrometry
IPN	Interpenetrating polymer network
LB	Luria Bertani
$\overline{M}_c$	Molecular weight of the polymer chain between cross-links
MWCO	Molecular weight cut-off
OD	Optical density
PBS	Phosphate buffered saline
PHA	Polyhydroxyalkanoate
ppm	Parts per million
RNA	Ribonucleic acid
rpm	Rotations per minute
SEM	Scanning electron microscopy
SLPM	Standard litres per minute
TFA	Trifluoroacetic acid
UV	Ultraviolet
Vis	Visible

Variables

μ_{max}	Specific cell growth rate (h^{-1})
ΔX	Active biomass ($g_{Biomass}$/L)
ΔS	Substrate consumed ($g_{Glycerol}$/L)
ΔP	EPS produced (g_{EPS}/L)
Δt	Variation of time (days)
$Y_{X/S}$	Biomass yield on substrate ($g_{Biomass}$ /$g_{Glycerol}$)
$Y_{P/S}$	Product yield on substrate (g_{EPS} /$g_{Glycerol}$)
r_p	Volumetric productivity (g_{EPS}/(L*d))

Chapter 1- Introduction and Motivation

1.1. Introduction

1.1.1. Biopolymers

Biopolymers are high molecular weight molecules which may be produced by animals, plants, microorganisms, and algae. They are broadly divided, depending on their monomeric units, as polysaccharides (polymerized sugars), polypeptides (proteins), polyesters and polynucleotides (DNA and RNA)[1,2]. Since a few decades, the interest in biopolymers has grown as a result of industrialization rising and with the increase of research, development and optimization of a wide variety procedures to obtain polymers, some has reached commercial scale (e.g. PHA) or even industrial scale (e.g. cellulose acetate), serving diverse fields such as agriculture and medical applications[3]. Currently, the expansion of biomaterials based on biopolymers with their biocompatibility, biodegradability and low toxicity has been rising an ideal competition against fossil fuel-based materials, particularly in functional properties[2,4]. However, concerning numbers, the use of non-degradable biopolymer in several functional areas is rather higher than of the biodegradable ones[4].

In fact, synthetic polymers own great mechanical and thermal properties, as well as they are good barriers against microorganisms. Even though synthetic polymers are being produced at low-cost, they are non-renewable and non-biodegradable materials[5]. In this view, taking into consideration environmental issues, it is increasingly important to fabricate new products and materials based on green chemistry and eco-friendly engineering[4,5].

1.1.2. Polysaccharides

Polysaccharides (or glycans) are polymers composed of sugar monomers, monosaccharides. Approximately 90 % of the carbohydrate mass is present in the form of polysaccharides, making them the largest component of biomass in nature[6]. They can be produced and obtained through algae, crustacean, plants as well as a broad range of microorganisms. Actually, the emerging interest in microorganisms' polysaccharides is attributed to the advantages of production process over the other sources (e.g. algae or plants cell wall), which allow the efficiency to obtain specific polysaccharides with low properties variability at a constant production rate, by the control of microbial cultivation conditions[7,8]. Also, the time production (hours or days) is way lower comparing with plants (3-6 months), despite required infrastructures associated with the cost of production[9].

Regarding these biopolymers that are produced with a vast range of molecular weights and branching degrees, they can be classified as homopolysaccharides, in which the polymer is only made up of one type of monomer unit, such as cellulose that is assembled by β-D-glucose sugars. On the other hand, those that are made up of two or more monomer units are classified as heteropolysaccharides, such as alginates that are assembled by β-D-manuronyl linked with α-L-guluronyl residues[6,9,10].

In terms of microbial polysaccharides, they carry out different biological functions according to their location in the cell. Therefore, polysaccharides can be intracellular, related

with the storage and energy source (e.g. glycogen)[9,10], extracellular (e.g. alginate, xanthan), or with structural properties which are closely associated with the cell surface (e.g. peptidoglycans)[8,9,11].

Extracellular polysaccharides (EPS) are secreted by microorganisms in two possible ways, where either the polymer stays attached to the cell envelope as a capsule or forms a slime which is loosely bound to the cell surface, as a biofilm[9,12]. Depending on their composition, which varies according to the type of sugar monomer (most common are glucose and galactose), EPS may also have non-sugar components such as organic groups (e.g. acetyl)[8]. Essentially, EPS main biological function is to protect the cell against the environment, by surrounding the cell with EPS layers, which assures resistance to desiccation and predation from other microorganisms, for example. Likewise, they support the cell against abiotic stresses (e.g. pH, temperature), make cell-cell recognition and help to sorption essential nutrients and ions, due to their anionic nature[9,13].

Regarding the cell wall polysaccharides that provide rigidity, shape and protection to the cell, there exists a diversity in their composition among microorganisms. For instance, cell walls from gram-positive bacteria, mostly composed by peptidoglycan, differ from gram-negative bacteria[14]. Yeast and fungi present similar cell wall structure, which has an outer layer constituted of mannoproteins responsible for the porosity of the cell wall, and a microfibrillar layer mainly formed by glucan and chitin (50–60% of cell wall's dry weight) which confers mechanical strength to the cell wall[14,15].

As so, the concern about finding biomaterials has increased over the last years since polysaccharides possess several interesting commercial properties, such as film-forming capacity, water retention capacity and rheology (e.g. gelling agents)[8]. Additionally, they are environmentally friendly, being biodegradable and biocompatible. Thus, polysaccharides can have a wide range of applications, like cosmetics, pharmaceuticals, industrials, and biomedical uses[10,12].

1.1.3. Hydrogels

Hydrogels are three-dimensional network structures composed of hydrophilic polymers, which are capable of absorbing a large amount of water through the presence of hydrophilic moieties[16–18]. The network structure (mesh), that leads to the solid form, is created as a result of cross-links among the polymer chains and their resistance to dissolution is a consequence of network chains[16,18]. Usually, hydrogels water content exceeds 90% of their composition[17]. The most relevant properties which delineate the hydrogel structure, at the molecular level, are the mesh size, and the molecular weight of the polymer chain between cross-links ($\overline{M}_c$). Regarding the cross-linking type, they can be physical, such as hydrogen bonding and entanglement, and chemical, like covalent bonding[16] (Figure 1). Macroscopically, they express forms as beads, films, microspheres, papers, and even aerogels[19].

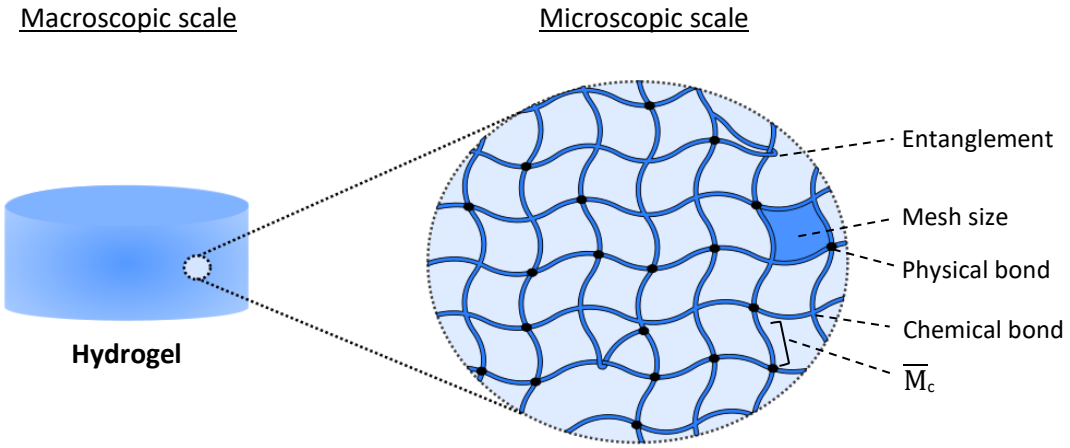

Figure 1: Design of hydrogels structure at macroscopic and microscopic level.

The process in which water diffuses into the hydrogel is named swelling and consists of three stages. Firstly, water molecules adhere to hydrophilic groups (primary bound water). Secondly, water molecules interact with the existing hydrophobic groups (secondary bound water). Thirdly, at the equilibrium swelling, water fills the empty spaces (free water), like pores. The percentage of swelling depends on the polymer concentration and cross-linking degree. Therefore, a higher cross-linking density will lead to less swelling ratio and hydrogel brittleness[16,17,20].

Hydrogels present a porous network structure and possess solid and liquid properties. This "solid-like fluid" can be synthesized by chemical or physical methods[19,21,22]. Chemical hydrogels are mostly connected through a covalently cross-linked network, in which the addition of cross-linking agents makes capable the reaction with existing functional groups present on polymer chains[17,22]. Nevertheless, chemical hydrogels will always contain physical interactions caused by the aggregation of polymer hydrophobic parts and cross-linking agents[22]. On the other hand, the cross-linking network of physical hydrogels is held by non-covalent interactions, such as ionic bonds, hydrogen bonds, entanglement, and Van der Waals interactions[17,22]. An example that has been extensively utilized to produce hydrogels over ionic interactions is alginate, in which gelling occurs by Ca^{2+} ions[23]. Commonly, chemical hydrogels are easier to reproduce and more stable, while physical ones have higher hardness, in spite of their reversible bonds and shape instability. In both physical and chemical hydrogels, it is essential to understand and to adapt hydrogels properties to targeted applications[22].

Concerning the composition of the polymer network, hydrogels can be separated into homopolymer (only one type of monomer unit), copolymers (two or more types of monomer unit, at least one hydrophilic), interpenetrating polymer network (IPN), in which two independent cross-linked networks are partially interlaced at a molecular level (not covalently bonded to each other), and semi-interpenetrating polymer network (semi-IPN). IPN differs from semi-IPN in the way that IPN requires breaking of covalent bonds to separate polymers chain from the original polymer network[16,18,20].

In terms of their physical properties, hydrogels may be sensitive to stimulus from environmental conditions such as pH, temperature, light, pressure, sound, ionic strength, mechanical stress, magnetic and electric fields. Responding to the external condition these stimuli-responsive hydrogels can experience unexpected modifications on their growth actions, network structure, permeability, and mechanical strength[16,17,20,24]. Chitosan is an example of a pH-sensitive hydrogel, wherein an acid solution solubilizes the polymer and the neutralization of solution (above pH 6.2) induces gelation[25]. These "smart" hydrogels, thanks to all their features, are quite appropriate for biomedical applications (e.g. drug delivery systems)[16,17,20,24].

Hydrogels can also be classified depending on their source, configuration, ionic charge, response and degradability. Figure 2 sums up the different characteristics of each hydrogel classifications[16,17,20].

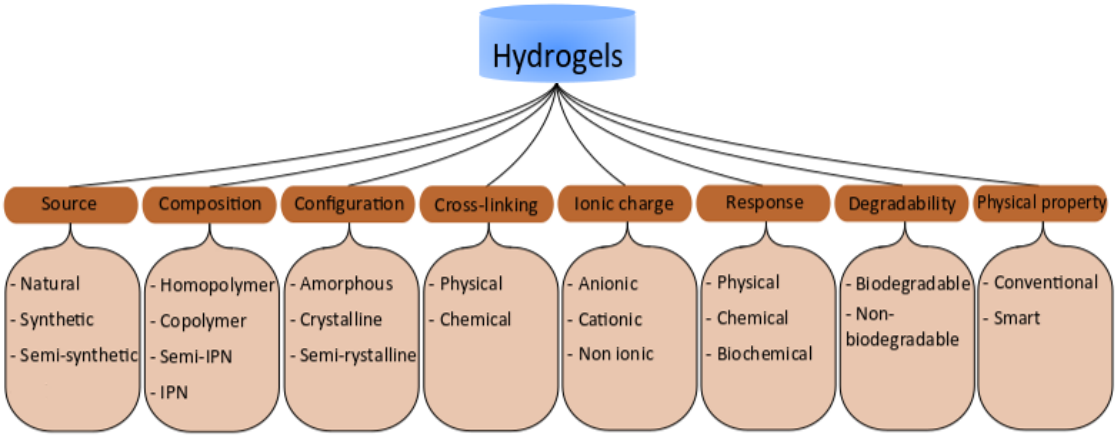

Figure 2: Schematic illustration of hydrogels classifications.

The interest in polymeric hydrogels has increased, due to plenty of desirable features, namely their biodegradability, biocompatibility, and low immunogenicity. Besides, hydrogels own high holding water capacity, soft structure and stimuli-responsive. All these properties make hydrogels versatile, flexible and quite resembling with biological tissues, in which arises various applications, such as agriculture, food industry and biomedicine[16–18].

Recently, a lot of research has been focused on polysaccharides thanks to their biodegradability, biocompatibility and hydrophilic properties, that are suitable to the elaboration of hydrogels for targeted applications, especially biomedicine (e.g. drug delivery, wound dressing, contact lenses and tissue engineering)[19,21,26]. In fact, a major part of the biomaterials obtained from nature exists in the form of polysaccharides because of their sugar constituents (e.g. nature, properties), amount of chain branching and the molecular length chains. Hydrogels based on polysaccharides can be simply obtained through hydrogen bonding and linked networks from hydroxyl groups. Also, different solvents have been investigated in order to dissolve native polysaccharides, such as ionic liquids, polar solvents and urea/alkaline solvents[19]. Besides, they can be prepared as a solid moulded form, microparticles, coating, films (or membranes) and encapsulated solids[21].

Many common polysaccharides have been used as structuring agents to produce hydrogels such as alginate, cellulose, xanthan, chitosan and starch[19,21] but others have been

arising with particular and interesting properties, like FucoPol, a fucose rich polysaccharide, and chitin-glucan complex (CGC), a copolymer formed by chitin and glucan polysaccharides[5,27].

1.1.4. Human skin

1.1.4.1. Structure

As the biggest organ of the human body, which covers 16% of total body weight[28–30], the human skin plays a part in the homeostasis of the body as a barrier, control of temperature, and repair function, by avoiding losses of body fluids and passing of harmful compounds or microorganisms from the environment[28,30]. Also, the skin functions as a protective barrier against the stress of mechanical forces, thanks to its great elasticity, and regulates the body temperature through sweating and blood flow rate[30]. The human skin structure is assembled in three types of tissues with different structure, composition and embryological origin: hypodermis, dermis and epidermis[30–33] (Figure 3).

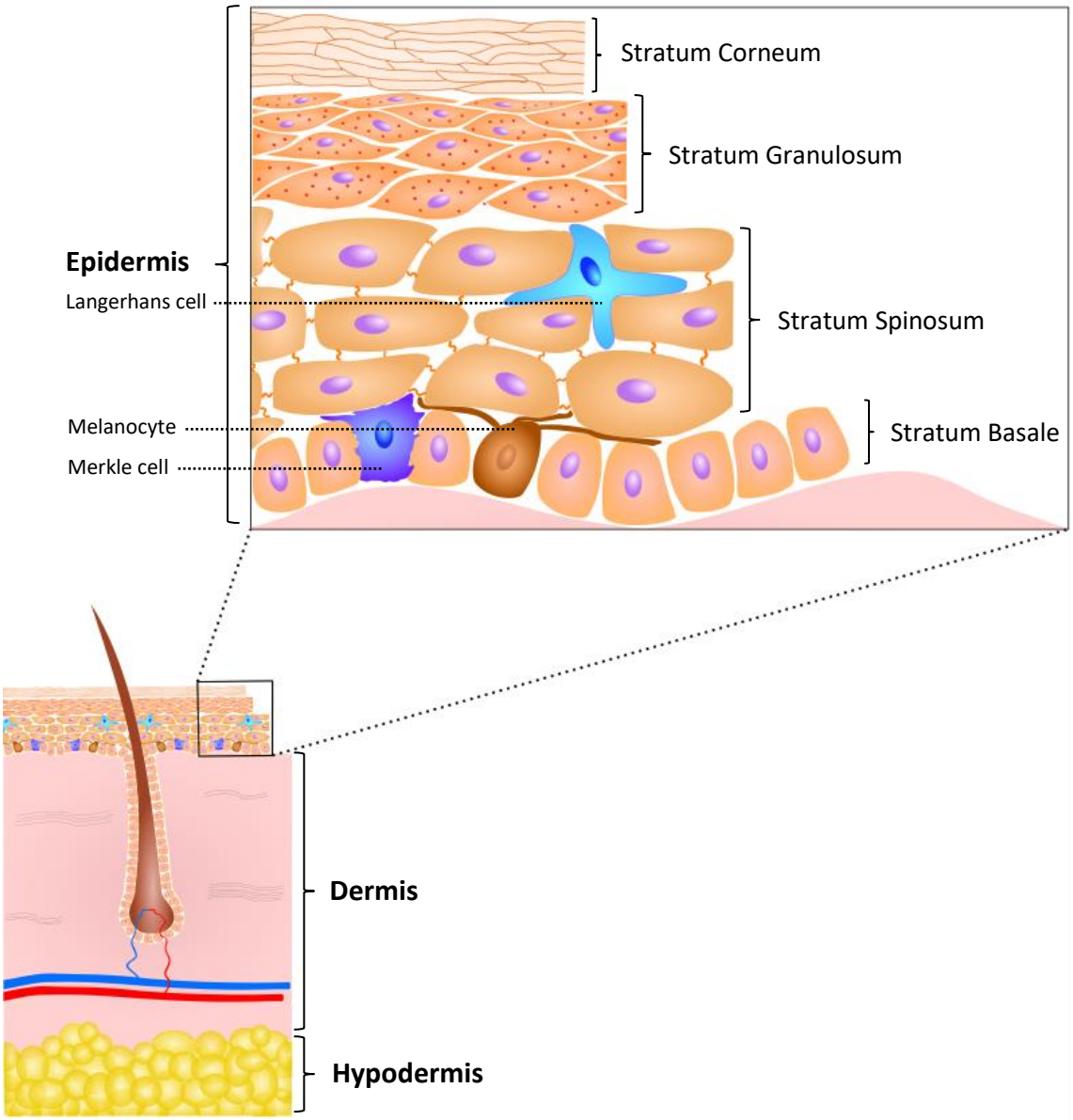

Figure 3: Schematic representation of the human skin structure.

The hypodermis, also called subcutaneous tissue, is the innermost layer of the skin formed by aggregates of fat lobules (lipocytes) and acts as a reservoir of energy for the body and has endocrine function, controlling the production of hormones which contribute to the regulation of appetite and metabolic energy[31–33]. Additionally, lipocytes also assist to insulate the body against cold and cushions deeper tissues from mechanical stresses[33].

Above the hypodermis, there is the dermis which is mostly composed of fibrous proteins such as collagen fibres (70% of the dry weight of the skin), elastic fibres and extrafibrillar matrix, which gives mechanical strength and elastic properties to the dermis. This skin structure which also includes nerves, blood vessels and cutaneous appendages, interacts and controls cells' functions that supply structural integrity and biological activity[32,33].

The outermost layer of skin is the epidermis, and it is mainly composed by keratin producing cells, keratinocytes, that undergo to division and differentiation from the *stratum basale* to the *stratum corneum*[30,32,33]. The epidermis also contains melanocytes that protect the skin from ultraviolet radiation, Langerhans cells which act as the first immunologic barrier, and Merkle cells which function as mechanoreceptors.

The *stratum basale* contains undifferentiated and proliferating cells that give rise to keratinocytes which migrate upward, making up the *stratum spinosum*. The continuous differentiation process proceeds to the *stratum granulosum*, where cells become more flattened and granules are composed of fibrous proteins that are responsible for the aggregation of keratin filaments in the *stratum corneum*[33]. The most external layer of the epidermis, the *stratum corneum*, is made up of denucleated, flattened, non-living cells filled with keratin, named corneocytes, making a semi-impenetrable barrier that acts as the larger physical barrier, protecting the body from the environment[30,31,33].

1.1.4.2. Drug delivery

Drug delivery is known as the safe administration of a drug to an animal or human, employing a group of technologies, in order to achieve a specific and desirable therapeutic effect. The drug delivery system is based on the incorporation of the drug, the controlled delivery of its active substances, and the release of these substances to the targeted site at an effective rate[16,29,34]. Some factors determine the choice of a drug delivery method like the desired effect, disease or even the patient's preferences[34].

Transdermal drug delivery systems are applied to insert medications through the skin into the systemic circulation at a predetermined rate and own several advantages[34,35] when compared to other delivery systems such as oral, intramuscular, and intravenous administration. This method is painless, non-invasive, cheap, can be self-administered, the drug release can be for extensive periods (up to a week), and it is avoided the gastrointestinal degradation and the first-pass effect of the liver which may prematurely metabolize medications[34,36,37]. Typically, they arise as creams, gels, drug carriers and patches. A well-known example of the transdermal drug delivery system is the nicotine patch, which releases controlled doses of nicotine to help with cessation of tobacco[34,35].

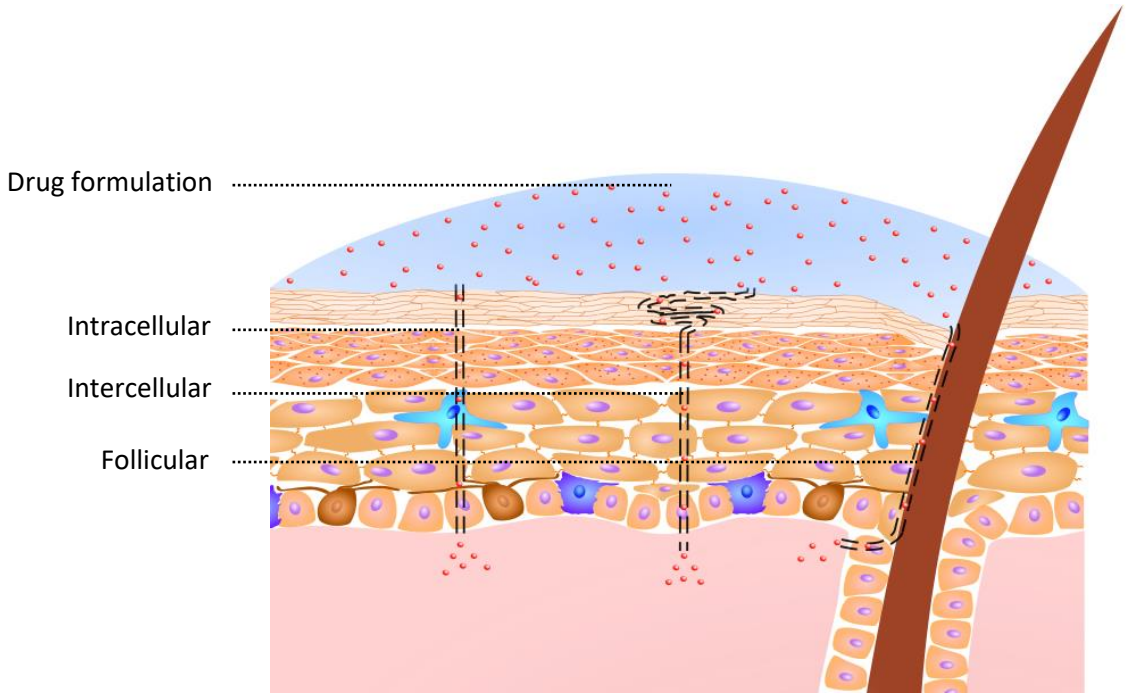

Figure 4: Schematic representation of the three possible drug permeation pathways through the skin: intracellular, intercellular, and follicular routes.

Drugs can cross the skin through three possible pathways (Figure 4): intracellular (transcellular), intercellular (paracellular), and follicular routes. In the intracellular pathway the substances cross all the epidermis layers of cells and extracellular matrix. However, since the hydrophilicity quite varies in the epidermis, this route involves sequences of diffusion and partitioning by the drug between the different layers. In the intercellular route, the substances travel the *stratum corneum* through the extracellular matrix, without traversing the cells. Small hydrophilic molecules usually prefer the intracellular route rather the intercellular route. In contrast, small lipophilic molecules favour intercellular route. The follicular route implies the drug permeation through hair follicles or sweat ducts. In fact, hair follicles compose about 0.1% of the skin surface, where the *stratum corneum* is thinner compared to other skin areas[30,38]. Nevertheless, the main challenge is to overcome the low diffusion across the impermeability of the *stratum corneum*, which constitutes the rate-limiting step of transdermal drug delivery systems[16,29,30,34,36,38].

1.1.4.3. Wound dressings

Usually, when the body undergoes an injury, it can restore the healed skin with the coordination between cells, proteins, proteases, growth factors, blood cells and extracellular matrix components, with minimal scars through a succession of four time-dependent physiological events[19,39–42]. It starts at the site of the injury with the *hemostasis* where platelets and inflammatory cells produce a clot through the release of fibrin proteins and clotting factors, in order to stop bleeding (lasts for 1 hour). Simultaneously, and up to 3 days, occurs the inflammatory phase in which involves cellular and vascular responses via releasing of vasoactive

mediators and chemotactic factors that causes the increase of phagocytes at the injury site. Afterwards and for 2-3 days, with the reduction of mediators and inflammatory cells, the proliferation phase comes until the wound is closed. Epithelial and fibroblast movement towards injury area repair damaged tissues and replace lost tissue. Then, fibroblast proliferation and collagen synthesis replace the provisional fibrin matrix. Lastly and for a year, maturation and remodelling phase increases the tensile strength up to 70% of new epithelium compared to normal skin, and forms cellular connective tissue, whereas all the processes involved in the inflammation and proliferation phases end[41–44].

The human body can readily provide all the needs for the wound healing process, except for severe skin functional anomalies or massive fluid losses. The wound healing is conditioned by diverse factors like depth of the wound, gender, medications, pressure, age, diseases, among others[16,39]. Regardless, providing suitable conditions to the wound such as pH, oxygen pressure, moisture, and protection against microorganisms, can help and accelerate the wound healing process[19].

Wound dressings should protect the wound from external pathogens agents or mechanical stress, be permeable to gas diffusion, generate and hold a moist environment to accelerate wound healing and minimize scarring[39–41]. Mostly made of polymers, drug delivery dressings used to provide therapeutic agents to the wound comprise hydrogels, hydrocolloids, silicone gels and alginates, which commonly appears in the form of foam sheets, thin films, or gels. These dressings should be capable of releasing the drug at a prefixed rate and have to maintain its therapeutic activity[16,41,43].

A lot of research has been done concerning hydrogels-based wound dressings, due to their great potential. The production of hydrogels with stretchability, shape-memory and self-healing capacity for purposes such as wound healing, drug delivery and tissue engineering has increased, especially due to possibility of the deliverance of dosages at desired rates in predetermined time intervals[19,39,45]. Hydrogel-based wound dressings appear in amorphous or sheet forms, or even as impregnated gauze. They are the most promising approach in wound treatment since they fill many requirements of an ideal wound dressing like keep a moist environment, allow gas exchange, pain reduction, and isolate from external bacteria[16,19,45]. Further, as hydrogels are mainly composed of water, they can easily carry on different types of hydrophilic drugs and the release are achieved thanks to the physical properties of hydrogels, like porosity. The drug incorporation into the hydrogel can be achieved by two possible methods, either the drug is mixed with the polymer followed by polymerization with crosslinker agent, or the formed hydrogel is immersed in a drug solution[16,29,40,41]. Hydrogels are desirable in all four stages of wound healing, except for infected or severely exuding wounds[43], have fewer side effects, great drug utilization efficiency and low cost in drug delivery systems[19]. However, hydrogels wound dressings need to be changed frequently, possess low tensile strength, and have issues with the incorporation of hydrophobic drugs[16,43].

1.2. Motivation

In recent years, the use of polysaccharides to develop novel biomaterials has increased, not only because of their interesting commercial properties but also due to their environmental-friendly features, being biodegradable and biocompatible[8,10]. Polysaccharide-based hydrogels are emerging as promising biomaterials thanks to their resemblance to biological tissues, arising in areas such as the food industry and biomedicine[16].

The skin, as the largest organ of the human body, plays an important role in the homeostasis of the body as a barrier, control of temperature, and avoids the passing of harmful compounds and microorganisms from the environment[28,30]. Transdermal drug delivery systems have increased the interest of research because of the painless, cheap, and non-invasive characteristics of the method[34,35]. Additionally, the drug release can be administered for long periods at a predetermined rate[34].

Two natural polysaccharides with particular and interesting properties, FucoPol and chitin-glucan complex (CGC), have been recently demonstrated with gel-forming capacity[26,46]. As so, the present work aims the preparation and characterization of hydrogels-based on these two biopolymers. Afterwards, the objective is the incorporation of a drug in the hydrogels and study the release over time, aiming for their use in targeted applications, mainly as a transdermal drug delivery systems and wound dressings.

Chapter 2- Biopolymer production and extraction

2.1. Introduction

2.1.1. FucoPol

Polysaccharides enriched in rare sugars such as rhamnose, uronic acids, and fucose have been studied due to their antioxidant and anti-inflammatory characteristics. Such rare sugars possess valuable properties that confer polysaccharides biological activity. In fact, fucose is nowadays used as a component of anti-inflammatory and anticarcinogenic drugs in creams, which act as hydrating and anti-ageing additives, and in case of injury, increase wound healing[47]. Fucose-containing polysaccharides can be produced through a broad range of bacteria, fungi and microalgae[8,48]. Another attractive sugar is glucuronic acid, due to its detoxifying activity in the liver, act as an anti-thrombotic and anti-arthritic drug, making it a desirable target to applications like surgery, regenerative medicine, and tissue engineering[49,50].

A new fucose-rich exopolysaccharide has been extensively studied, named FucoPol, which is synthesized by the gram-negative bacterium *Enterobacter* A47[5,12,51]. This high molecular weight biopolymer is composed of fucose (32–36% mol), galactose (25–26% mol), glucose (28–34% mol), glucuronic acid (9–10% mol), but also contains acyl groups substituents, mainly acetyl, pyruvyl and succinyl[7,52,53], which gives to the polysaccharide an anionic character[5,26]. Regarding the biopolymer production, it can be quite versatile because of the possibility to vary physicochemical factors of the cultivation conditions, affording a final FucoPol with different composition of bioactive sugars (fucose and glucuronic acid), and thus be used in different applications as well[12,49,54]. Moreover, FucoPol possesses a high molecular weight, which is comprised between 1.7×10^6 and 5.8×10^6 Da[26,53].

FucoPol forms viscous solutions and has demonstrated several interesting properties, namely the capacity of film-forming, thickening, gel-forming, flocculating, stabilize emulsions of hydrophobic substances in water, and shear thinning behaviour[7,12,26,47]. All these properties added to the fucose biological activity, increase significantly the market value of FucoPol, making it an ideal target to areas such as emulsion-based cosmetics, food products, pharmaceutical applications, medical devices and drug delivery systems[47,49,52].

2.1.2. Chitin-glucan complex (CGC)

In 1823, chitin was first isolated from the mushrooms cell-wall. Today, it is known that chitin is the major component of crustacean's shells and exoskeleton of insects and molluscs, which represent the dominant commercial sources of chitin and chitosan[5,55]. Very similar to cellulose, chitin is a polysaccharide composed of N-acetyl-D-glucosamine units, which often forms complexes with β-glucans, originating chitin-glucan complexes (CGC) covalently linked through β-(1,3) and β-(1,6) glycosidic linkages[27,56] (Figure 5).

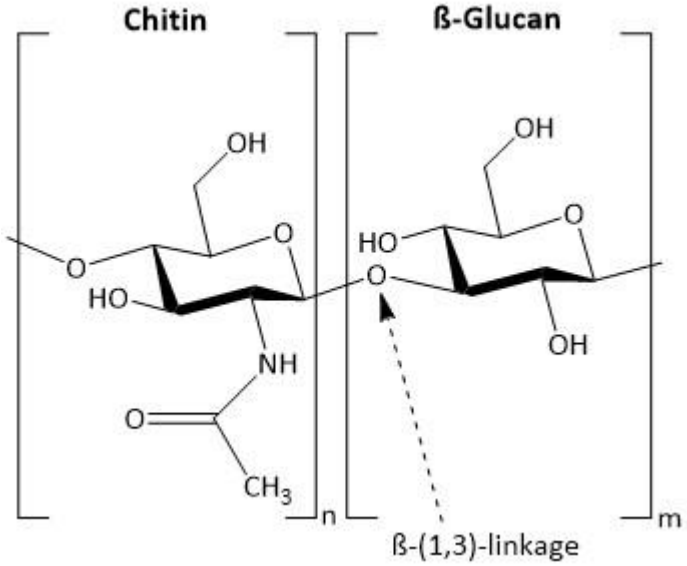

Figure 5: Structure of chitin-glucan complex (CGC).

In terms of chemical structure, chitin presents a degree of acetylation around 70%, whereas in chitosan, the deacetylated form of chitin, is lower than 30–40%. Such structural differences lead to variations in their material properties, particularly the solubility, where the presence of hydrophobic acetyl group makes chitin insoluble in water and most common organic solvents[57–59]. Typically, these two polysaccharides are extracted from shell wastes of crabs, shrimp, and lobster consumption through harsh chemical procedures. On the other hand, most fungal and yeast species also contain chitin and chitosan in their cell-walls, where the extraction methods are simpler, allowing the control of polymer composition and avoid the negative impact of the extraction conditions in the environment. Additionally, it is a non-animal alternative source, which prevents any allergenic risks of crustacean sources[57,60,61].

CGC is produced by most fungi and yeasts, and as the main component of cell-walls, it provides stiffness and rigidity to the cell[46,56]. This copolymer can be extracted from the cell wall of the yeast *Komagataella pastoris* wherein the production process reaches high cellular densities combined with a relatively high amount of CGC in the biomass. Besides, cheap operating costs and the capacity of *K. pastoris* to use a broad range of substrates with fast cell growth rates make the production process economically viable and sustainable[56,62].

Despite its high hydrophilicity, CGC is only soluble in toxic and/or corrosive polar solvents, which cause the resulting solutions frequently unstable and turn the processing harder[46,59]. The insolubility of this copolymer is due not only because of inter- and intra-molecular hydrogen bonds among CGC chains but also to its strong covalent linkages between chitin and glucan polymers[27,59]. Strategies like chemical (e.g. carboxymethylation) and physical (e.g. sonication) procedures have been developed to enhance its solubility, even though these modifications may change physical-chemical properties of the biopolymer, namely its bioactivity and biodegradability[27]. Despite its intractability, some green alternatives strategies have been explored in order to dissolve this biopolymer, such as ionic liquids[59], deep eutectic solvents and alkali or alkali/urea aqueous solutions[27,57]. Furthermore, as it combines two bioactive polysaccharides chitin and β-glucan, CGC owns many desirable features like antioxidant, antibacterial, anti-inflammatory, anti-ageing and anti-cancer properties, as well as biodegradable and biocompatible[27,46,59]. All these properties render CGC a valuable biomaterial to a wide range of applications such as cosmetics, food complement (EFSA Panel on Dietetic Products Nutrition and Allergies, 2010), pharmaceuticals, tissue engineering, wound dressings, and drug delivery systems[27,57,61,62].

2.2. Materials and Methods

2.2.1. FucoPol

2.2.1.1. Microorganism and media

The biopolymer FucoPol was produced by the bacteria *Enterobacter* A47, that was cryopreserved in 20% (v/v) glycerol, at -80°C. The reactivation of the culture was done by plating a sample of the cryopreserved vials, in agar plates (CHROMagar™ Orientation) and incubation at 30°C, for 24 h. Subsequently, the obtained isolated cultures were plated again in agar and incubated for another 24 h, to obtain single colonies.

Hereafter, for the pre-inocula, a single colony was inoculated into 50 mL liquid Luria Bertani (LB) medium (10.0 g/L peptone; 5.0 g/L yeast extract; 10.0 g/L NaCl; pH 7.0), in 250 mL shake flasks, and incubated in an orbital shaker at 30°C, and 200 rpm for 24 h.

The inocula for the bioreactor experiments were prepared in 500 mL baffled shake flasks by transferring 20 mL of the pre-inocula into 200 mL of Medium E* (K_2HPO_4, 5.8 g/L; KH_2PO_4, 3.7 g/L; $(NH_4)_2HPO_4$, 3.3 g/L; pH 7.0), supplemented with 2 mL of 100 mM $MgSO_4$ solution, 2 mL of micronutrients solution (per litre of 1 N HCl: $FeSO_4 \bullet 7H_2O$, 2.78 g; $MnCl_2 \bullet 4H_2O$, 1.98 g; $CoSO_4 \bullet 7H_2O$, 2.81 g; $CaCl_2 \bullet 2H_2O$, 1.67 g; $CuCl_2 \bullet 2H_2O$, 0.17 g; $ZnSO_4 \bullet 7H_2O$, 0.29 g)[54] and 40 g/L of glycerol (ReagentPlus 99% w/w, Sigma-Aldrich), as carbon source. The inocula were incubated at 30°C and 200 rpm, for 72 h.

2.2.1.2. Bioreactor Assays

The bioreactor assays were performed in a 10 L bioreactor (BioStat B-Plus, Sartorius, Germany), in which 7.2 L (90% (v/v)) of Medium E*, supplemented with 40 g/L glycerol, was inoculated with 0,8 L (10% (v/v)) of the inocula, operating in batch mode for the first 8 h. Then, a feeding solution was supplied to the reactors starting a fed-batch mode for 88 h. This feeding solution was composed of Medium E* supplemented with 1000 g/L of glycerol at a constant rate of 5 mL/h.

Throughout all the process the pH was controlled, automatically, at 7.00±0.05 by the addition of HCl (2 M) or NaOH (5 M). Also, the temperature was maintained at 30.0±0.1°C and the aeration rate was kept constant (1.6 SLPM, standard litres per minute, of compressed air). The dissolved oxygen concentration (DO) was controlled at 10% of air saturation by the automatic adjustment of the stirring rate (300-800 rpm). Foam formation was automatically controlled by the addition of Antifoam A (Sigma-Aldrich).

Samples (24 mL) were periodically collected from the culture broth and centrifugated at 15777 x g, 4°C, for 15 min (Sigma 4-16 KS, Germany) to separate the cell-free supernatant from the biomass pellet. Viscous samples recovered from the bioreactor were diluted in deionized water, as the viscosity increased. The cell-free supernatant was conserved at -20°C for further

analysis of glycerol and ammonium concentration, as well as quantification of FucoPol production.

2.2.1.3. Analytical techniques

2.2.1.3.1. Cell growth

The culture broth samples withdrawn during the process had the purpose of monitoring the cellular growth by measuring the optical density at 450 nm (OD_{450nm}) in a UV-Vis spectrophotometer (VWR, V-1200 spectrophotometer, Portugal). As necessary, the samples were diluted in order to obtain an OD_{450nm} below 0.3, using deionized water as zero reference. The cell dry weight (CDW) was calculated considering that one unit of OD_{450nm} is equivalent to 0.26 g/L CDW[12]. All the measurements were performed in duplicate.

2.2.1.3.2. Glycerol quantification

The glycerol concentration in the cell-free supernatant samples was evaluated by high-performance liquid chromatography (HPLC), with a VARIAN Metacarb column (BioRad). The analysis was performed at 50°C, using H_2SO_4 0.01 N as eluent, at a flow rate of 0.6 mL/min. The samples were diluted (1:50 v/v) with the eluent solution and filtered with centrifuge filters (Vectra Spin Micro Polysulfone filters, Whatman, 0.2 μm), at 3000 rpm for 10 min. All the measurements were done in duplicate. Glycerol (99% w/w, Sigma-Aldrich) was used as a standard in a concentration range from 0.0625 g/L to 1 g/L, in order to obtain a standard calibration curve (Figure A1).

2.2.1.3.3. Ammonium quantification

The ammonium concentration in the cell-free supernatant samples was determined by colourimetry using a flow segmented analyser (Skalar 5100, Skalar Analytical, The Netherlands). The samples were diluted (1:200 v/v) in deionized water and analysed. Ammonium chloride (Panreac) was used as a standard solution in a concentration range from 4 ppm to 20 ppm. All the analysis was done in duplicate.

2.2.1.3.4. Exopolysaccharide quantification

For the quantification of exopolysaccharide, the cell-free supernatant samples were dialysed with 12-14 kDa MWCO (molecular weight cut-off) membrane (Nadir® dialysis tubing, Carl Roth, Karlsruhe, Germany) against deionized water, at a constant stirring (200 rpm). The water was often changed until a constant value of conductivity was reached (bellow 10 μS/cm). To avoid polymer degradation by microorganisms, sodium azide (10 mg/L) was added to the dialysis water. Then, the dialyzed samples were freeze-dried (CoolSafe 4-15L, LaboGene) at -110°C, for 48 h) and the EPS content, throughout the cultivation run, was quantified by weighing the freeze-dried samples. All the measurements were done in duplicate.

2.2.1.4. Kinetic parameters

2.2.1.4.1. Specific growth rate

The maximum specific cell growth rate (μ_{max}, h^{-1}) was calculated from the linear regression slope of the exponential phase Ln (CDW_t/CDW_0) versus time (h).

2.2.1.4.3. Product yield

The product yield ($Y_{P/S}$) on a substrate during the cultivation was determined by the following equation (2):

$$Y_{P/S} = \frac{\Delta P}{\Delta S} \ (g_{EPS}/g_{Glycerol}) \quad (2)$$

where ΔP is the EPS produced (g_{EPS}/L) and ΔS is the substrate consumed ($g_{Glycerol}$/L).

2.2.1.4.4. Volumetric productivity

The EPS volumetric productivity (r_p) was calculated using equation 3:

$$r_p = \frac{\Delta P}{\Delta t} \ (g_{EPS}/(L*d)) \quad (3)$$

where ΔP is the amount of EPS produced (g_{EPS}/L) in time interval Δt (days).

2.2.1.5. Extraction and purification

At the end of the cultivation assay, the culture broth obtained was diluted with deionized water (1:10 v/v) to reduce the viscosity, and the biomass was removed by centrifugation (Beckman Avanti J-26 XPI) at 11325 x g, 4°C for 45 min. Then, the cell-free supernatant was submitted to thermal treatment (70°C, for 1 h), in order to denature remaining proteins. The processed supernatant was centrifugated (11325 x g, 4°C for 45 min) to remove remaining cells debris and denatured proteins.

Subsequently, to purify the polymer solution by the elimination of undesirable components, such as salts, glycerol and low molecular weight compounds, the treated supernatant was dialyzed with a 100 kDa MWCO membrane (Hydrosart® Ultrafiltration Cassette, Sartorius) through a continuous diafiltration process, with a crossflow module (Sartocon Slide Holder, Sartorius), until the polymer solution's conductivity reached values bellow 150 µS/cm. Afterwards, the process was switched to an ultrafiltration mode, to concentrate the polymer solution. Finally, the dialyzed polymer solution was freeze-dried and stored at room temperature.

2.2.1.6. Polymer characterization

2.2.1.6.1. Sugar monomers

To determine FucoPol's composition in terms of sugar monomers and acyl groups, samples of dried FucoPol (~ 5 mg) dissolved in deionized water (5 mL) were hydrolyzed with

trifluoroacetic acid (TFA) (0.1 mL TFA 99%), at 120°C for 2 h. The hydrolysate was used for the identification and quantification of the constituent monosaccharides by HPLC, using a CarboPac PA10 column (Dionex), equipped with an amperometric detector. The analysis was done using 4 mM NaOH as eluent, at 30°C and a flow rate of 0.9 mL/min. Standard solution of sugar monomers composed of D-(+)-galactose 98% (Alfa Aesar), D-(+)-glucose anhydrous 99% (Fisher Chemical), D-(+)-fucose 99% (Sigma-Aldrich), D-glucuronic acid 98% (Alfa Aesar) and D-(+)-galacturonic acid monohydrate 97% (Fluka) was prepared in deionized water in a concentration range from 1 to 100 ppm (Figure A2). The measurements were performed in quadruplicate.

The acid hydrolysate was also used for the identification and quantification of acyl groups by HPLC, with an Aminex HPX-87H 300x7.8 mm (Biorad) column, coupled to a UV-detector. The analysis was performed using sulphuric acid (H_2SO_4 0.01 N) as eluent, at 30°C and a flow rate of 0.6 mL/min. Standard solution of acetate 99% (Fischer Chemicals), succinate 99% (Merck) and pyruvate 99% (Sigma-Aldrich) were prepared in deionized water in a concentration range from 10 to 1000 ppm (Figure A3).

2.2.2. Chitin-glucan complex (CGC)

2.2.2.1. Biopolymer production

2.2.2.1.1. Microorganism and media

The biopolymer CGC was produced by the yeast *Komagataella pastoris* DSM 70877, that was cryopreserved in 20% (v/v) glycerol, at -80°C. The culture was cultivated in medium K[63], which was composed of (per litre of deionized water): KH_2PO_4, 37.33 g; $CaSO_4.2H_2O$, 0.1667 g; $MgSO_4 \bullet 7H_2O$, 2.67 g; $(NH4)_2SO_4$, 18.07 g and 2 mL of a trace mineral solution comprising the following composition (per litre of deionized water): $CuSO_4 \bullet 5H_2O$, 0.20 g; $MnSO_4 \bullet H_2O$, 3.00 g; $ZnCl_2$, 7.00 g; $FeSO_4 \bullet 7H_2O$, 22.00 g; biotin, 0.20 g; H_2SO_4, 5 mL. The pH of the medium K was adjusted to 5.0 with NaOH 5 M and sterilized by autoclaving at 121°C and 1 bar, for 20 min. The trace mineral solution was filter-sterilized (0.2 µm, Whatman), and stored at 4°C.

The inocula for the bioreactor experiments were prepared in 500 mL baffled shake flasks by inoculating the cryopreserved culture (1 mL) into 200 mL Medium K, supplemented with 40 g/L of glycerol (ReagentPlus 86-88% w/w, Scharlau), as carbon source. The inocula were incubated at 30°C and 200 rpm, for 40 h.

2.2.2.1.2. Bioreactors Assays

The bioreactor assays were performed in a 10 L bioreactor (BioStat B-Plus, Sartorius, Germany), in which 7.2 L (90% (v/v)) of Medium K, supplemented with 40 g/L glycerol, was inoculated with 0.8 L (10% (v/v)) of the inocula, operating in batch mode for the first 24 h. Then, a feeding solution was supplied to the reactor, starting a fed-batch mode for 24 h. The feeding solution was composed of glycerol supplemented with trace mineral solution, at a proportion of 24 mL mineral solution per litter of glycerol.

During the experiments, the pH was controlled, automatically, at 5.00±0.02 by the addition of ammonium hydroxide 25% (v/v) or HCl (2 M). Also, the temperature was maintained

at 30.0±0.1°C and the aeration rate was kept constant (1.4 SLPM, standard litres per minute, of compressed air). The dissolved oxygen concentration (DO) was controlled at 15% of air saturation by the automatic adjustment of the stirring rate (300-1500 rpm), followed by supplementation of the air stream oxygen. Foam formation was automatically controlled by the addition of Antifoam A (Sigma-Aldrich).

Samples of 10 mL were periodically collected from the culture broth and centrifugated at 7012 x g, 4°C, for 15 min (Sigma 4-16 KS, Germany), to separate the cell-free supernatant from the biomass pellet. The biomass pellets were conserved at -20°C for further analysis of biomass and CGC quantification.

2.2.2.2. Extraction and purification

The broth samples were centrifugated at 17418 x g, for 15 min, for cell separation. The cell pellet was washed twice with deionised water (re-suspended in water, centrifugated at 17418 x g, for 15 min) and freeze-dried. For CGC extraction from the yeast biomass, the freeze-dried samples (100-300 mg) were subjected to a hot alkaline treatment with NaOH 5 M (30 mL), for 2 h, at 65°C, under constant stirring, for solubilisation of cell wall components. The mixture was centrifugated (17418 x g, 15 min) and the resulting alkali-insoluble material was re-suspended in deionised water (30 mL) and neutralised with HCl 6 M. Then, after centrifugation (17418 x g, 15 min) the polymer was washed twice with deionised water (30 mL) to remove the soluble alkali components, and freeze-dried.

2.2.2.3. Kinetic parameters

The specific growth rate (μ_{max}, h^{-1}), biomass yield ($Y_{X/S}$, g_X/g_S) and volumetric productivity (r_P, g/L.h)) were assessed as described in section **2.2.1.4**.

2.2.2.4. Polymer characterization

2.2.2.4.1. Elemental analysis and degree of acetylation

The elemental analysis of freeze-dried CGC was performed by a Flash EA 1112 Series CHNS analyzer (Thermo Scientific). Chitin content (Q, %) was calculated based on samples' nitrogen content, by equation (4) as follows[27]:

$$Q = 14.199\ N \quad (4)$$

where N is the nitrogen content (%) in the sample.

The degree of acetylation (DA, %) was calculated using the following equation (5)[27]:

$$DA = \frac{\frac{C}{N} - 5.14}{1.72} \text{ x } 100\ (\%) \quad (5)$$

where C/N is the ratio (%) of carbon to nitrogen contents, as determined by elemental analysis.

2.3. Results and discussion

2.3.1. FucoPol

2.3.1.1. FucoPol production

Figure 6 presents the fed-batch cultivation profile of *Enterobacter* A47 using glycerol as the sole carbon source.

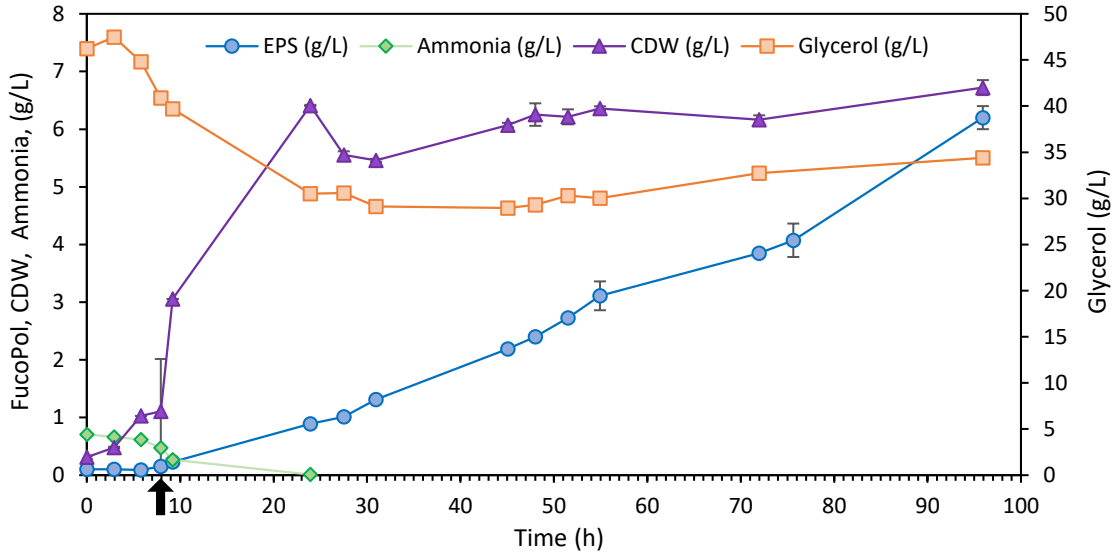

Figure 6: Cultivation profile of *Enterobacter* A47 using glycerol as the sole carbon source. The fed-batch phase was initiated after 8 hours of cultivation (⬆).

FucoPol production is partially growth associated[8] and it is enhanced in the stationary cell growth phase through low nitrogen and oxygen conditions associated with glycerol availability, as the source of carbon[54]. As so, during the fed-batch phase, the ammonia was present in the broth at limiting concentrations (<0.1 g/L) and the feeding solution was rich in glycerol (1000 g/L). Under such conditions, no growth was observed due to the limiting oxygen and nitrogen conditions imposed. As can be seen in Figure 6, after a few hours and up to the first 24 h, glycerol concentration decreased quickly (from 47.5 to 30.5 g/L) and the fed-batch phase was initiated at 8 h of cultivation and it was kept at a constant flow rate during the assay (5 ml/h). During the stationary phase, since the cells were not multiplying the substrate was being used mainly for EPS synthesis.

The synthesis of EPS slightly started in the batch phase with a 0.15 g/L value detected at 8 h (Figure 6), followed by a significant improvement in the stationary phase. Indeed, the EPS synthesis reached 6.20 g/L at the end of cultivation (Table 1).

Table 1: Kinetic parameters obtained by the bioreactor cultivation assay of *Enterobacter* A47 using glycerol as the sole carbon source, compared with previous studies.

	Cultivation assay	Literature[8,48,54,64]
EPS (g/L)	**6.20 (±0.013)**	7.23–7.97
CDW_{max} (g/L)	**6.72 (±0.20)**	5.80–7.68
μ_{max} (h^{-1})	**0.26**	0.27–0.36
$Y_{P/S}$ (g_P/g_S)	**0.52 (±0.36)**	0.28–0.47
r_P (g/(L.d))	**1.55 (±0.20)**	1.89–3.72

The EPS production (6.20±0.013 g/L) was slightly lower than the values reported in the literature (7.23–7.97 g/L) (Table 1). This might be due to the different quantification methods, in which a higher dilution (1:10 instead of 1:2) was used for EPS extraction from the broth, increasing the error.

As observed in Table 1, considering the overall cultivation time of 96 h, a 6.72±0.20 g/L of CDW was achieved, which is in the range of values reported in the literature (5.80–7.68 g/L). Associated with this, it was obtained a specific growth rate of 0.26 h^{-1} during the exponential cell growth phase, a value close to those of previous studies (0.27–0.36 h^{-1}). The net yield of EPS on glycerol was 0.52±0.36 $g_{EPS}/g_{Glycerol}$, which is slightly higher than the values reported in the literature, meaning that the substrate was effectively used for EPS synthesis. Additionally, a 1.55±0.20 g/(L.d) of productivity was achieved at the end of the cultivation assay, a close value comparing with previous studies (1.89–3.72 g/(L.d)).

2.3.1.2. EPS composition

The EPS composition can change depending on the cultivation conditions. As so, the EPS were characterized in terms of sugar composition and acyl groups (Table 2).

Table 2: Chemical composition of FucoPol produced by *Enterobacter* A47, using glycerol as sole carbon source (Fuc: fucose; Gal: galactose; Glu: glucose; GlucA: glucuronic acid; Acet: acetate; Succ: succinate; Pyr: pyruvate).

	Sugar composition (mol.%)				Acyl groups (wt.%)		
	Fuc	Gal	Glu	GlucA	Acet	Succ	Pyr
Cultivation assay	**35.7**	**26.0**	**33.1**	**5.2**	**3.5**	**0.55**	**3.7**
Literature[8,48,54,64]	30–36	22–29	25–34	9–10	3–5	3	13–14

As observed in Table 2, the EPS exhibited typical FucoPol composition: 35.7 mol.% of fucose, 26.0 mol.% of galactose, 33.1 mol.% of glucose, and 5.2 mol.% of glucuronic acid. Although the glucuronic acid value was slightly lower comparing with literature (9–10 mol.%), all the other sugars presented consistent values with those reported in previous studies. In terms of acyl groups, acetate values are in the range of those reported (3–5 wt.%), in spite of the values obtained for succinate (0.55 wt.%) and pyruvate (3.7 wt.%) were lower compared with the literature (3 2 wt.% and 13–14 wt.%, respectively).

2.3.2. CGC

2.3.2.1. CGC production

Figure 7 presents the fed-batch cultivation profile of Komagataella pastoris DSM 70877 using glycerol as the sole carbon source.

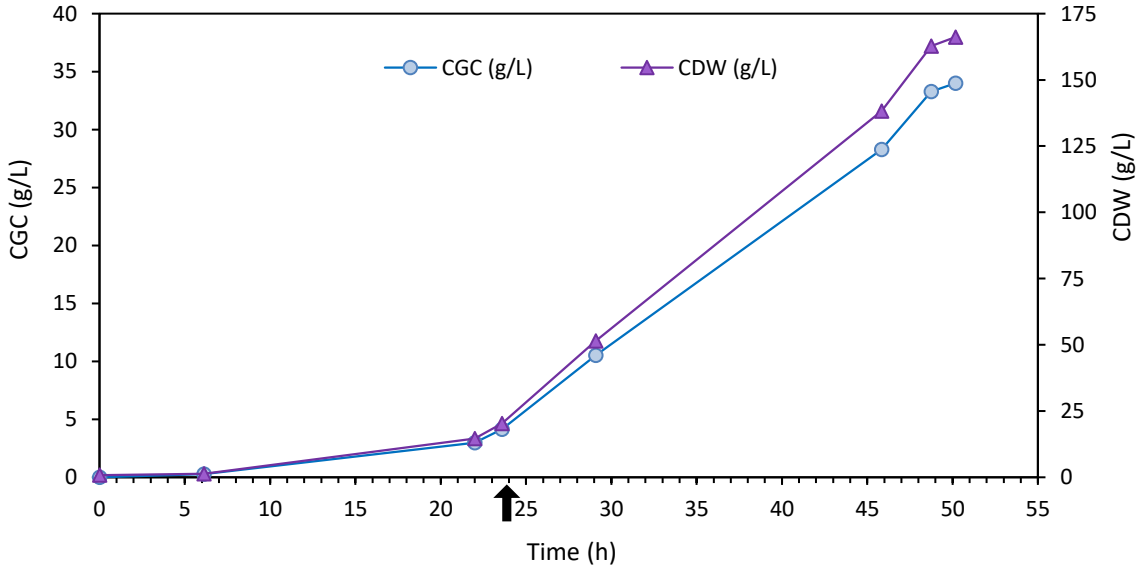

Figure 7: Cultivation profile of *Komagataella pastoris* DSM 70877 using glycerol as the sole carbon source. The fed-batch phase was initiated after 24 h of cultivation (⬆).

The CGC synthesis is growth associated[62] and as can be observed by Figure 7, during the initial batch phase, *Komagataella pastoris* cells reached a biomass concentration of 14.62 g/L at a maximum specific growth rate of 0.15 h^{-1}. At 24 h of cultivation run, the feeding solution of glycerol was added to the bioreactor, operating in batch mode overall the assay, reaching high biomass concentration (166.2 g/L) during fermentation.

Table 3: Kinetic parameters obtained by the bioreactor cultivation assay of *Komagataella pastoris* using glycerol as the sole carbon source, compared with previous studies.

	Cultivation assay	Literature[51,56,61–63]
CDW_{max} (g/L)	**166.2**	38.9–179.4
CGC (%)	**20.5**	13.4–19
CGC (g/L)	**34.0**	5.6–34.6
μ_{max} (h^{-1})	**0.18**	0.16–0.18
r_P (g/(L.d))	**16.3**	7.7–17.5

As can be seen in Table 3, considering the overall cultivation time of 50 h, all the kinetic parameters are within the range of values reported in the literature. The obtained CDW (166.2 g/L) associated to a high CGC content (20.5%) allowed to reach significant CGC concentration (34.0 g/L), compared with previous studies (5.6–34.6 g/L). Besides, a specific growth rate of 0.18 g/L was achieved during the log phase, which is within the range of reported studies (0.16-0.18 g/L). The overall volumetric productivity reached high values (16.3 g/(L.d)) as well, which are consistent with those reported in the literature (7.7–17.5 g/(L.d)).

2.3.2.2. CGC composition

The chemical characterization of the final CGC was assessed in order to evaluate the chitin content and degree of acetylation (Table 4).

Table 4: Chemical characterization of CGC, compared with literature

	Sample	**Elemental analysis (%)**			**Chitin content (%)**	**DA (%)**
		C	**H**	**N**		
Literature[27,61]	CGC	43.6	7.2	1.7	23.8–25	61.3
This study	CGC	43.9	7.2	2.5	35.6	63.4

As observed in Table 4, as determined by elemental analysis, the chitin content (35.6%) was higher compared with the values reported in the literature (23.8–25%). This might be due to the lower chitin/glucan ratio presented in the sample of the literature, or the high content of proteins. On the other hand, the degree of acetylation of the obtained CGC was slightly higher (63.4%) compared with previous studies (61.3%).

2.4. Conclusion

The production and extraction of both biopolymers reached appreciable values, associated with a great chemical composition of the final polysaccharides. FucoPol bioreactor achieved 6.2 g/L of FucoPol, with a composition of 35.7 mol.% of fucose, 26.0 mol.% of galactose, 33.1 mol.% of glucose, and 5.2 mol.% of glucuronic acid. CGC bioreactor reached high biomass values, combined to a high polymer content, allowed a final CGC concentration of 34.0 g/L, with a chitin content of 35.6% and a degree of acetylation of 63.4%.

Chapter 3- FucoPol-based hydrogels

3.1. Introduction

3.1.1. Ionotropic gelation

Ionotropic gelation occurs when polyelectrolytes are mixed with a counter ion solution, forming a hydrogel. Typically, this mechanism involves the electrostatic interaction of polysaccharides negatively charged with cations, which induces ionic cross-links among different polymer chains[26,65,66]. These hydrogels are produced in the form beads, microparticles or nanoparticles[66].

Beads are usually obtained through syringe dropping method, where an aqueous solution of polysaccharide is added dropwise into a cation solution[26,65] (Figure 8). Several natural polysaccharides have been used to prepare hydrogels through ionotropic gelation, including gellan gum, alginate, and chitosan-complexes[26,66] because of mild conditions, relatively cheap, quickness, and simplicity of the process, avoiding the use of toxic organic solvents[65,66].

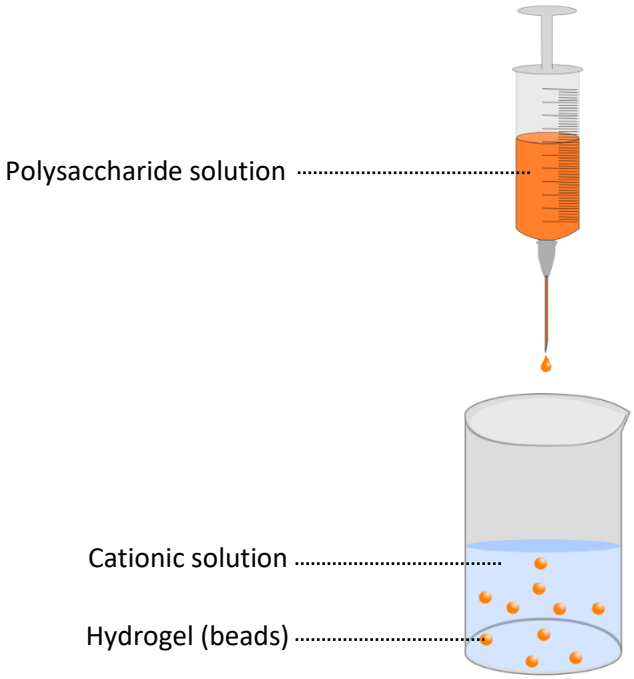

Figure 8: Schematic representation of ionotropic gelation method.

The ionotropic gelation is influenced by the concentration and chemical nature of cations in solutions[67,68]. For example, sodium alginate, gellan gum and pectin can easily form hydrogels when mixed with polyvalent ions (e.g. Ca^{2+})[67,69,70], resulting in strong and thermally stable gels[67,68,70], whereas monovalent cations may influence gelation by inducing aggregation, but cannot produce a hydrogel structure[71]. Alginate-based hydrogels are biocompatible, low cost, and obtained through a cross-linking method, commonly by the addition of divalent cations like Ca^{2+},[69,72] having suitable properties in biomedical applications, such as wound healing[72] and

tissue engineering[69,73]. However, the absence of enzymes that degrade alginate in mammals limits its full potential[73,74]. On the other hand, chitosan, due to amino groups, possesses a cationic nature and its hydrogels-based are obtained through cross-link with multivalent anions[23,75]. This feature enables the formation of chitosan complexes, namely chitosan-alginate complex, with the dropwise addition of alginate into a chitosan solution[23,65].

Therefore, the use of these natural polysaccharides by ionotropic gelation have shown great interest in biomedical's areas as a novel advanced drug delivery system[26,66,76]. In fact, this technique allows the efficient encapsulation of drugs (when the interactions between polymer and drug are great), along with the biocompatibility of polysaccharides provide formulations with relevant biological properties[65,76].

Recently, it was demonstrated for the first time that FucoPol, due to its anionic character, is able to develop polymeric structures through ionotropic gelation. Among mono -, di-, and trivalent ions tested, only iron (III) and copper (II) reveal the capacity to obtain hydrogels. Both the performed beads present stability in water, NaCl 0,9%, and PBS, but Copper–FucoPol beads are more fragile, which leads to its disintegration and release of copper to the medium, affecting cell differentiation and proliferation. However, this feature may find applicability in applications like chronic myeloid therapy, due to its antiproliferative action. In contrast, Fe–FucoPol beads are stabler and non-cytotoxic, which support their potential application as drug delivery carrier and wound dressings[26].

3.2. Materials and Methods

3.2.1. Preparation of FucoPol hydrogels

The ability of FucoPol to form hydrogels in the presence of trivalent cation, namely, Fe^{3+}, was demonstrated[26]. For that, freeze-dried FucoPol (25 mg) was dissolved in deionized water (5 mL) under constant and vigorous stirring (900 rpm) for 1.5 h, to obtain a homogenous solution. Afterwards, FucoPol hydrogels were prepared by dialysis of the FucoPol solutions with a 12-14 kDa MWCO membrane against different concentrations of iron ($FeCl_3 \cdot 6H_2O$, Sigma-Aldrich) solutions, for 24 h at 25°C. Then, to remove the excess of iron, the formed hydrogels within the membrane were dialyzed against deionized water, for 48 h, at 20 °C, until constant conductivity values were achieved (~10 µS/cm).

The effect of iron concentration was evaluated by testing different concentrations of iron solutions in a range of 0.01 g/L to 10 g/L of Fe^{3+}. To evaluate the ability of iron cation to cross the membrane, FucoPol hydrogels were prepared in a vertical position under constant stirring (Figure 9) or in a horizontal position without stirring (Figure 10). To prepare FucoPol hydrogels in a vertical position, 5 mL of FucoPol solution (5 g/L) were placed inside the dialysis membrane and dialyzed against iron solutions (250 mL). Several aqueous solutions containing different concentrations of Fe^{3+} (0.01–10 g/L of Fe^{3+}) were performed in 500 mL flasks. Then, the dialysis membranes containing the FucoPol solution were placed inside each iron solution and the flask was stirred (200 rpm) in an orbital shaker at room temperature, for 24 h. Afterwards, the iron solution was replaced by deionized water and the flask was stirred in the same conditions, for 48 h. Figure 9 shows a schematic representation of this type of FucoPol hydrogels preparation.

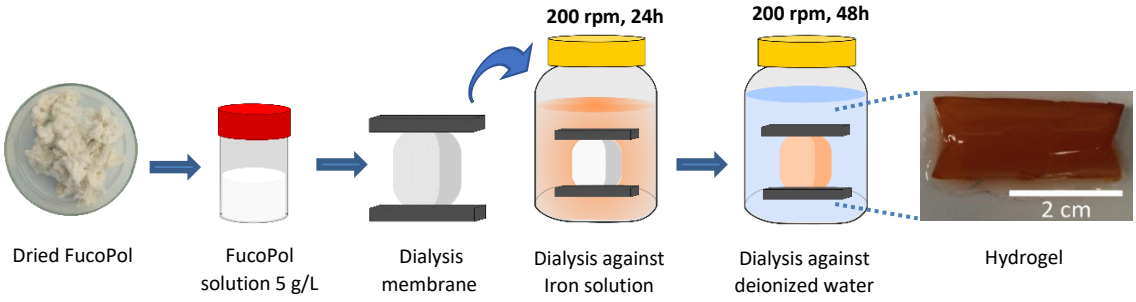

Figure 9: Schematic representation of FucoPol hydrogel (5 mL) in a vertical position preparation.

To prepare FucoPol hydrogels in a horizontal position, 10 mL of FucoPol solutions (5 g/L) were placed inside the dialysis membrane and dialyzed against iron solutions (300 mL) (Figure 10). Three different concentrations of iron were tested (0.05 g/L, 0.1 g/L and 0.5 g/L of Fe^{3+}) and prepared in a 1 L beaker. The dialysis membrane containing the FucoPol solution was carefully placed inside each iron solution and remained at the bottom of the beaker at room temperature, for 24 h. Then, the dialysis membrane was transferred to another beaker containing deionized water and the excess of iron was removed by dialysis at room temperature, for 48 h.

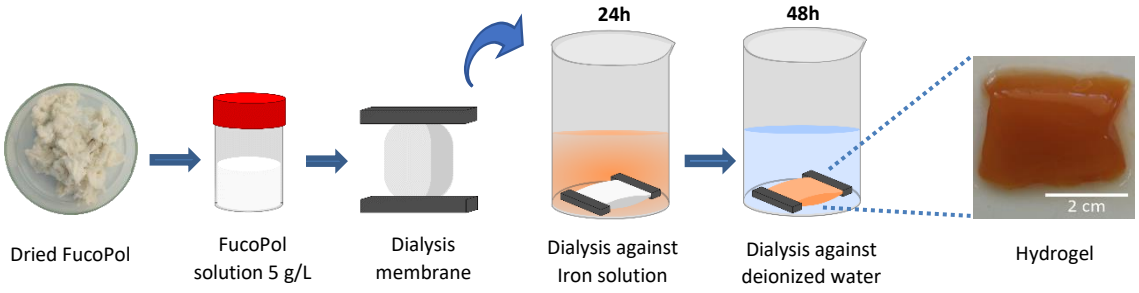

Figure 10: Schematic illustration of FucoPol hydrogels (10 mL) in a horizontal position preparation.

3.2.2. Characterization of FucoPol hydrogels

3.2.2.1. Water Content

The water content present in the hydrogels was determined by gravimetry. For that, the obtained hydrogels were weighed, freeze-dried at -110°C for 48 h and weighed again. The water content (%) was assessed with the following equation (6):

$$Water\ content = \frac{m_{wet} - m_{dry}}{m_{wet}} * 100\ (\%) \quad (6)$$

where m_{wet} is the initial wet hydrogel mass (g) and m_{dry} is the dried hydrogel mass (g). The measurements were done in triplicate for vertical (0.05–10 g/L of Fe^{3+}) and horizontal gels (0.05 g/L, 0.1 g/L and 0.5 g/L of Fe^{3+}).

3.2.2.2. Iron quantification

For the quantification of iron in the hydrogels, freeze-dried FucoPol hydrogel samples (~5 mg) were hydrolysed with nitric acid (5 mL of 5 % v/v HNO_3) (HNO_3 65%, Panreac). The hydrolysis was performed at 120°C for 2 h. The hydrolysed samples were filtered (0.2 µm, Whatman), and their content in iron was analysed by Inductively Coupled Plasma-Atomic Emission Spectrometry (ICP-AES) (Horiba Jobin-Yvon, France, Ultima), coupled with a 40.68 MHz RF generator, Czerny-Turner monochromator with 1.00 m (sequential), autosampler AS500 and

CMA (Concomitant Metals Analyzer). A solution of nitric acid (HNO_3 5 % v/v) was submitted to the same hydrolysis procedure and used as zero reference.

Standard solutions were prepared to obtain a calibration curve through the preparation of solutions with different iron concentrations (0.00–1.00 mg/L, Figure A4). The iron content (%) of a freeze-dried hydrogel (Iron $_{dry}$) was calculated as follows:

$$Iron_{\,dry} = \frac{m_{\,iron}}{m_{\,dry}} * 100\ (\%) \quad (6)$$

where m_{iron} is the iron mass (g) obtained by ICP-AES and m_{dry} is the dried hydrogel mass (g) weighed for the hydrolysis.

The iron content (%) of a wet hydrogel (Iron $_{wet}$) was determined by equation (7):

$$Iron_{\,wet} = Iron_{\,dry} * \frac{m_{\,dry}}{m_{\,wet}}\ (\%) \quad (7)$$

where m_{dry} is the dried mass (g) of the full hydrogel and m_{wet} is the wet hydrogel mass (g).

The measurements were done for vertical (0.05–10 g/L of Fe^{3+}) gels.

3.2.2.3. Rheology

The evaluation of rheological properties of the horizontal FucoPol hydrogels was analysed using a controlled stress rheometer (HAAKE MARS III, Waltham, MA, USA Thermo Scientific) equipped with a plate-plate serrated geometry (diameter 20 mm) with a 1.5 mm gap. The hydrogels samples with a similar thickness (~ 3 mm) were equilibrated at 25± 0.03°C, for 5 min. The stress sweep was applied under oscillatory shear of 1 Hz within a stress range between 0.01–1000 Pa (Figure A5). Then, viscoelastic properties were determined by applying frequency sweeps at a constant tension within the linear region, for a frequency range of 0.01 to 1 Hz. The analysis was performed in duplicate for horizontal gels (0.05 g/L, 0.1 g/L and 0.5 g/L of Fe^{3+}).

3.2.2.4. Fourier-transform infrared spectroscopy

FucoPol and freeze-dried horizontal hydrogels (0.05 g/L, 0.1 g/L and 0.5 g/L of Fe^{3+}) were analysed by Fourier-transform infrared spectroscopy (FT-IR). The analysis was conducted with Nicolet 6700 FT-IR (Thermo Electron Corporation, Walthman, USA) with a diamond crystal attenuated total reflectance (ATR) accessory. The spectra were recovered between 400 and 4000 cm^{-1} resolution with 10 scans, at room temperature.

3.3. Results and discussion

3.3.1. Hydrogels formation

The ability of FucoPol to gel in the presence of metal cation was recently demonstrated by Fialho *et al*.[26] and was used for the preparation of hydrogel beads. In this study, FucoPol hydrogels were obtained by a new technique recently used for alginate hydrogels called diffusion through dialysis tubing (DTDT)[77], which involves the diffusion of Fe^{3+} into FucoPol solution (Figure 9 and 10, section **3.2.1.**), allowing the crosslinking among iron and polymer within the dialysis tube and, subsequently, enables its spontaneous gelation. Polymer solutions (5 g/L) were dialysed against iron solutions in a range of 0.1 to 10 g/L of Fe^{3+}. Different dialysis procedures were assessed to evaluate the properties of final hydrogels.

Fe^{3+} solution (g/L)	0.05	0.1	0.5
Vertical technique	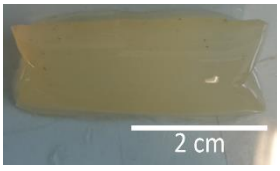	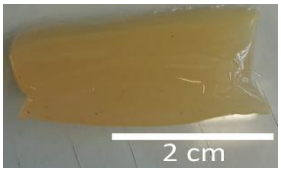	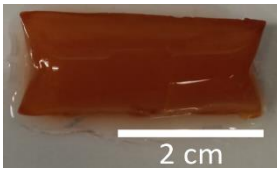
Water content (%)	99.52	99.14	98.73

Fe^{3+} solution (g/L)	1	5	10
Vertical technique	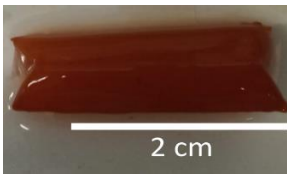	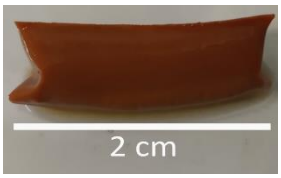	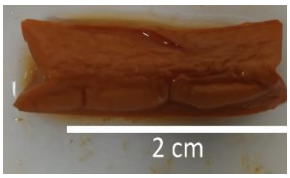
Water content (%)	98.32	95.57	96.63

Figure 11: Photographs of hydrogels and the respective water content (%) obtained by vertical dialysis technique against Fe^{3+} solutions (0.05, 0.1, 0.5, 1, 5, and 10 g/L).

The polymer solutions dialysed against solutions of 0.01 and 0.025 g/L of Fe^{3+} did not generate a hydrogel structure. This fact suggests that the concentration of iron was not enough to crosslink with FucoPol and perform a solid mesh, leading to brittle gelation (Figure 12).

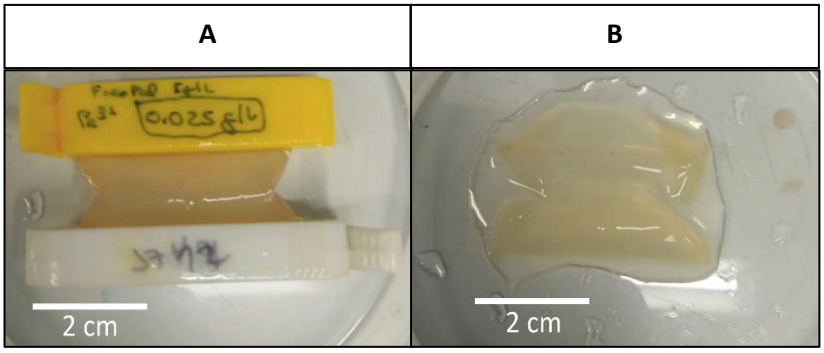

Figure 12: Photographs of FucoPol hydrogel obtained by dialysis of FucoPol (5 g/L) against 0.025 g/L of Fe^{3+} (**A**: hydrogel in the dialysis tube; **B**: hydrogel).

As can be seen in Figure 11, all the hydrogels presented a water content in the range of 95.57–99.52%, which is common for this type of structure. Indeed, the gellan gum- and xanthan gum-based hydrogels showed water content values of 95%[78] and 92.3%[79], respectively, as well as the hydrogel beads (98.60%) reported by Fialho *et al.*[26]. As the concentration of iron in the dialysis solution increased, the colour of the final hydrogels became more intense, from a translucid yellow to a dark brown. This fact should be caused by the higher diffusion of iron cations through the dialysis tube, as the salt ($FeCl_3 \cdot 6H_2O$) presents this typical brown colouration. Following the same line of thought, the water content decreased as the iron concentration in dialysis solution increased, except when used the 5 g/L of iron solution, which presented lower value than the 10 g/L, probably since these experiments were only performed once, without hydrogels replicas, increasing the error. Additionally, the size of the gels seemed to decrease as the iron concentration increase (Figure 11), probably due to the higher compacting of the polymer structure caused by the higher ionic strength.

Afterwards, FucoPol solutions with the same concentration (5 g/L) with higher volume (15 mL) were performed in order to study their physical properties. However, and as can be observed in Figure 13, the obtained hydrogels did not present a homogenous structure, being stiffer at the periphery and becoming softer as it crosses to the inner layers of the hydrogel.

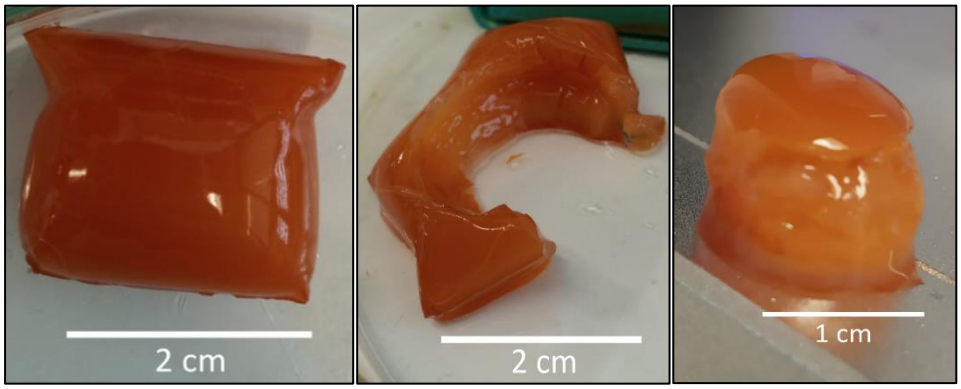

Figure 13: Photographs of FucoPol hydrogel (15 mL) dialysed with the horizontal technique against 0.5 g/L of Fe^{3+} solution.

Then, to obtain homogenous hydrogels, a horizontal dialysis technique was attempted in order to facilitate the iron diffusion uniformly, all over the hydrogel.

Fe^{3+} solution (g/L)	0.05	0.1	0.5
Horizontal technique	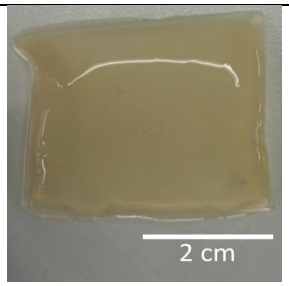	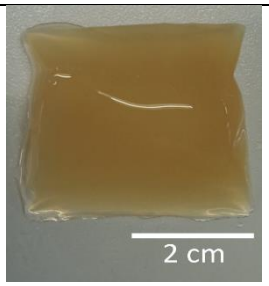	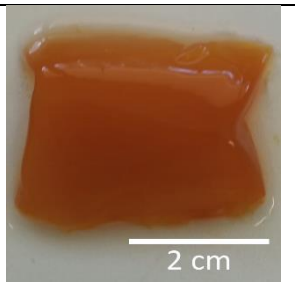
Water content (%)	99.79 (±0.03)	99.77 (±0.05)	99.34 (±0.05)

Figure 14: Photographs of hydrogels and the respective water content (%) obtained by horizontal dialysis technique against Fe3+ solutions (0.05, 0.1, and 0.5 g/L).

As observed in Figure 14 the colouration of the hydrogels was similar to those obtained with the vertical technique (Figure 11) and the water content exhibited values in the same range in both horizontal (99.34–99.79%) and vertical procedures (98.73–99.52%). The hydrogels obtained by the horizontal procedure presented significantly improved properties in terms of homogeneity, but they were still not uniform all over the structure, as can be observed in Figure 15.

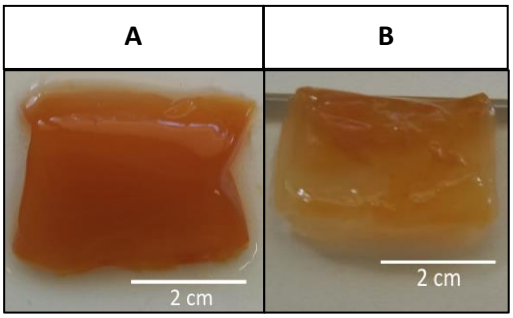

Figure 15: Photographs of FucoPol hydrogel dialysed with the vertical technique against 0.5 g/L of Fe^{3+} (**A**) and the cross-section of the same hydrogel (**B**).

As assumed by Dobashi *et al*.[80] during the dialysis, the inflow of cations through the inner layers is limited by a nonequilibrium thermodynamics, in which the iron atoms are not able to access the inner polymer layers, due to the already formed gel layers at the external sites of the structure.

3.3.2. Chemical composition

The FucoPol hydrogels obtained through vertical dialysis procedure were characterized in terms of their iron content (Table 5).

Table 5: Iron content (Iron wet, %) of FucoPol hydrogels obtained by vertical dialysis procedure against different iron concentrations.

Technique	Vertical					
Solution of Fe^{3+} concentration (g/L)	0.05	0.1	0.5	1	5	10
FucoPol Hydrogels						
$Iron_{wet}$ (%)	0.011	0.037	0.123	0.230	1.025	0.833

As observed in Table 5, the iron content in all hydrogels was relatively low (0.011–1.0230%) and, for the vertical technique, are approximately in the same order of magnitude of the iron solutions. For example, the iron content of the hydrogel dialysed against 0.05 g/L of Fe^{3+} (0.011%) was about one hundred times lower than that dialysed against 5 g/L of Fe^{3+} (1.025%). The control of iron content in hydrogels for controlled release dosages, associated to its non-toxicity[26] and bioactivity[7], enables the possibility of using FucoPol hydrogels in applications such as drug delivery systems in iron deficiency anaemia, being an attractive alternative of the oral therapy, which its bioavailability is low and severely dependent of gastric factors. However, the passage of hydrophilic drugs or molecules such as iron through the skin is quite complicated, and the release of iron in the systemic circulation is a major concern, due to the possibility of generation of reactive oxygen species[81].

The Fe^{3+} based FucoPol hydrogels beads performed by Fialho *et al*.[26] by ionotropic gelation, with dropwise addition of polymer solution through a syringe into the cation solution, exhibited values quite higher (0.15%, for 0.73 mg/L of Fe^{3+} solution) compared with those obtained with vertical dialysis procedure (Table 5), which may be related to the fact that the dialysis membrane functions as a permeable physical barrier. On the other hand, the hydrogels beads produced through ionotropic gelation crosslinks with a higher content of iron available in the solution. As the hydrogels obtained through the horizontal procedure presented higher homogeneity than those obtained with the vertical procedure, they were characterized in terms of their functional groups (FTIR) and viscoelastic properties (rheology).

3.3.3. Horizontal procedure

3.3.3.1. FT-IR

FTIR analysis was conducted to evaluate the interaction between FucoPol's functional groups and iron.

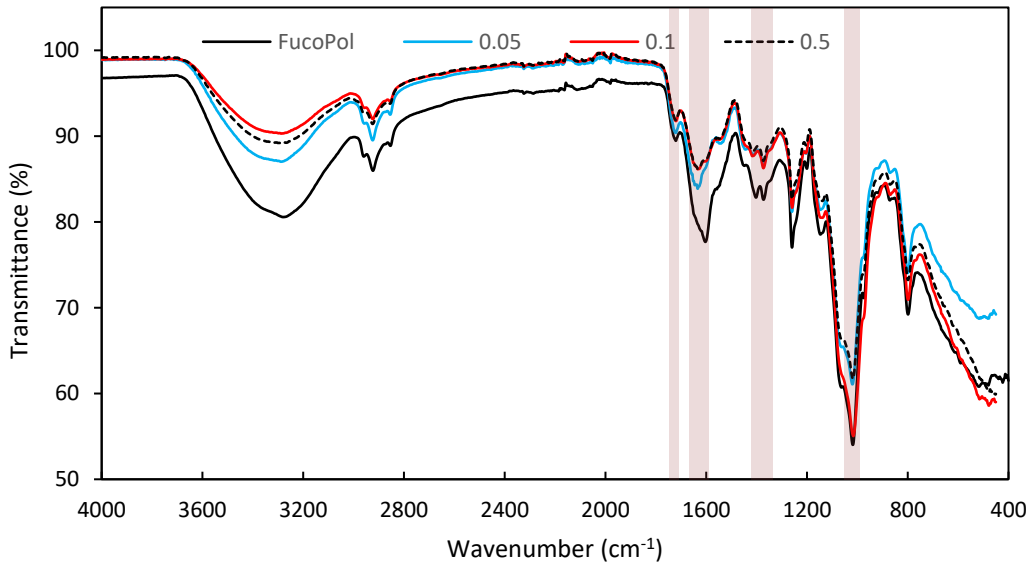

Figure 16: FTIR spectra of FucoPol and dried FucoPol hydrogels obtained with horizontal technique by dialysis against iron (0.05, 0.1, 0.5 g/L of Fe^{3+}).

As shown in Figure 16, all the FTIR spectra exhibited the bands characteristic of FucoPol. Even so, it can be observed that the interaction of FucoPol with iron led to shifts of some absorption peaks, namely those attributed to hydroxyl and carboxylate groups, as well as reported in previous studies[26]. The broad band corresponding to the stretching frequencies of FucoPol hydroxyl (O–H) groups observed at 3280 cm^{-1} was shifted to 3289 cm^{-1}, for all hydrogel's spectra. The absorption peak attributed to the carbonyl (C=O) stretching moieties found in acyl substituents and C–O corresponding to glycosidic bonds[26,48] appeared in the same region (1721 cm^{-1} (FucoPol)) for all the hydrogels spectra (1721 cm^{-1} (0.05), 1720 cm^{-1} (0.1 and 0.5)). Nonetheless, the C–C peaks attributed to pyranoid ring[26] (1018 cm^{-1} (FucoPol)) appeared slightly shifted (1020 cm^{-1} (0.05), 1016 cm^{-1} (0.1), 1017 cm^{-1} (0.5)). Also, C–H stretching peak corresponding to CH_2 groups of FucoPol[26,61] (2923 cm^{-1}) slightly shifted to 2924 cm^{-1} for all hydrogel's spectra. However, the peak at 1602 cm^{-1} and the absorption region at 1372–1402 cm^{-1} attributed to the asymmetric and symmetric stretching of carboxylates from glucuronic acid[26], shifted to 1634 cm^{-1} and 1373–1416 cm^{-1}, respectively, for all hydrogel's spectra.

3.3.3.2. Rheology

The rheology of FucoPol hydrogels was studied in order to envisage their potential purposes according to their viscoelastic properties.

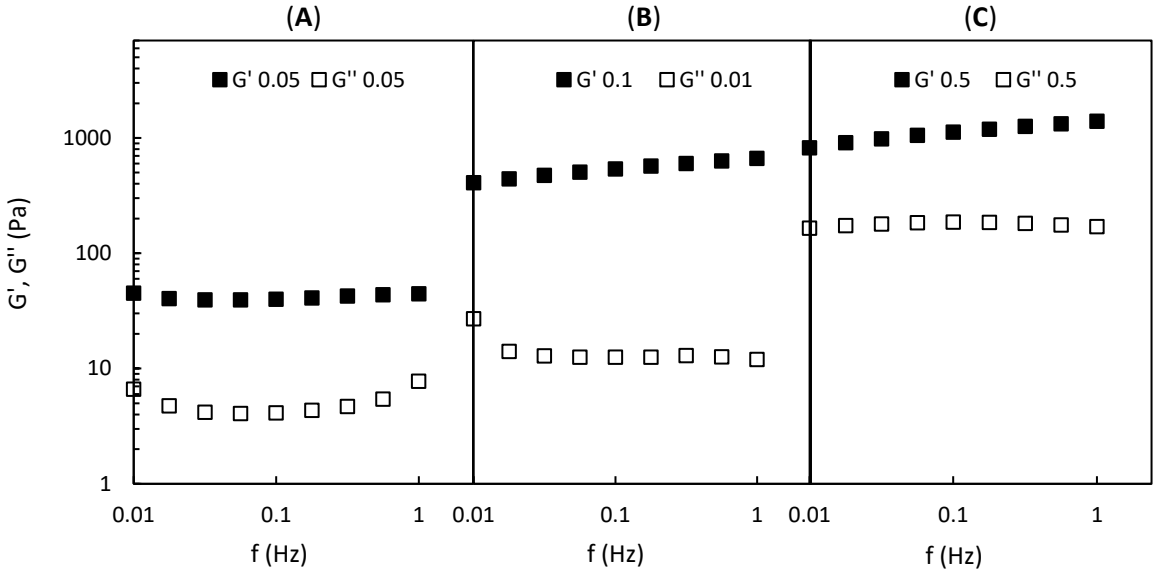

Figure 17: Rheological properties of horizontal FucoPol hydrogels prepared with dialysis against different iron concentrations (g/L) (**A**: 0.05; **B**: 0.1; **C**: 0.5). Mechanical spectrum storage (G', solid symbols) and loss moduli (G'', open symbols).

As it can be observed in Figure 17, for the three types of horizontal FucoPol hydrogels obtained with dialysis against different iron solutions, the storage moduli (G') values are higher in one order of magnitude when compared with loss moduli (G'') values, in the whole range of frequencies. This characteristic is in congruence with the gel-like nature of the samples. Comparing with literature, hydrogels based on xanthan showed a similar profile[82], as well as gellan gum-based hydrogels using calcium as a gelling agent[83]. Besides, FucoPol hydrogels dialysed against 0.5 g/L of Fe^{3+} revealed to have improved mechanical properties. In fact, for frequencies between 0.01–1 Hz, these FucoPol hydrogels (Figure 17**C**) presented a storage modulus of 820–1386 Pa, which is quite higher than the values reported by xanthan based (G'~400–600 Pa)[82] and gellan based (G'~200–300 Pa)[83] hydrogels. A high storage modulus (G') indicates that FucoPol hydrogels presented higher elastic properties when the stress is applied. Considering the same frequencies, the loss moduli of the FucoPol hydrogels (G''= 165–170 Pa, Figure 17**C**)) also exhibited higher values than xanthan-based (G''~40–90 Pa)[82] and gellan-based (G''~20 Pa)[83] hydrogels.

The effect of iron concentration can be observed in Figure 17, as the concentration of Fe^{3+} in the dialysis increased (**A**<**B**<**C**, Figure 17), the dynamic moduli of the resulted hydrogels also increased, which is related to stronger mechanical properties. Indeed, it was reported that the hydrogelation and modulation of hydrogels' properties can be largely influenced by the ionic strength present during the formation of hydrogels structures[84].

3.4. Conclusion

This study demonstrated for the first time the production of FucoPol-based hydrogels by diffusion through dialysis tubing. FucoPol hydrogels obtained by the vertical dialysis procedure were obtained with a relatively low content of iron (0.011–1.02%) in the hydrogel structure. However, their non-homogeneity led to the production of FucoPol hydrogels through a horizontal procedure, which allowed the characterization in terms of their viscoelastic properties. The FTIR analysis allowed to conclude that the crosslinked iron present in the hydrogels did not affect the characteristic bands of FucoPol, only leading to shifts of some absorption peaks. The rheology of hydrogels dialysed against 0.5 g/L of Fe^{3+} solution revealed improved mechanical properties compared with xanthan- or gellan- based hydrogels. Despite the final hydrogels were not totally homogeneous, the possibility of control the iron content combined with regulable viscoelastic properties of the final hydrogels are valuable characteristics for their use in the development of drug delivery carriers.

Chapter 4- Chitin-glucan complex-based hydrogels

4.1. Introduction

4.1.1. CGC-based hydrogels

Native cellulose and chitin hold numerous inter- and intra-molecular hydrogen bonds, which make these biopolymers insoluble in most solvents[59,85]. Therefore, the process to obtain hydrogels through chitin and cellulose require a specific solvent system, followed by gelation. Usually, it is necessary to add a second component to perform hydrogels with specific structure and morphology, and thus for specific applications (e.g. wound dressings and drug delivery). For example, the addition of lignin in cellulose-based hydrogel leads to a less dense and more homogenous structure. This is ideal in controlled release of drugs since as lignin increase the release rate increase too[85]. Nevertheless, the use of organic solvents with toxic and corrosive features unable batch production and restrain the potential applications of chitin[59,85,86] and cellulose hydrogels[85].

As hydrogels preparation normally require the polymer dissolution in a suitable solvent system followed by cross-linking, it is important to have a solvent able to overtake the insolubility of CGC[46]. In recent years, alkali solvents based on NaOH or KOH have appeared to be quite promising in the dissolution of chitin[87] and CGC[27]. In fact, it was demonstrated that NaOH solutions are capable of CGC solubilization, up to 68% through a freeze/thaw procedure (four cycles of freezing at -20°C and thawing at room temperature)[27]. Also, GCG has the ability to form hydrogels when dissolved in alkali solutions of NaOH or KOH, and the resulted solutions are submitted to dialysis, which induces the spontaneous gelation[46]. Although this process dissolves CGC and generates hydrogels, the degree of acetylation decreased from 61.3% to 33.9–50.6%, which indicates that chitin is converted to chitosan[27]. Furthermore, CGC hydrogels have been demonstrated as biocompatible[46,57,88], non-cytotoxic[46,89] and biodegradable[57,90]. Given those properties, CGC-based hydrogels reveal to have a large potential as novel biomaterials to biomedical applications, such as tissue engineering, wound healing, and drug delivery systems[46,88].

4.2. Materials and Methods

4.2.1. Production

To prepare CGC hydrogels, CGC powder (0.5 g) was dissolved in NaOH 5 M (25 g) and stirred at 500 rpm, for 1 h. The samples were frozen at -20°C for 48 h, and during this period, four freeze/thaw cycles were applied by stirring the thawed suspensions 500 rpm, for 1h, at room temperature. Afterwards, the insoluble polymer fraction was removed by centrifugation (20000 × g, 4°C, for 30 min) and the soluble fractions were dialyzed with a 12 kDa MWCO membrane (Nadir®, dialysis tubing, Carl Roth) against deionized water, under constant stirring (200 rpm), for 48 h, until the conductivity reached values bellow 20 µS/cm, as described by Araújo *et al.*[46]. Figure 18 shows a schematic representation of the general procedure of hydrogels preparation. All the CGC hydrogels were performed in triplicates.

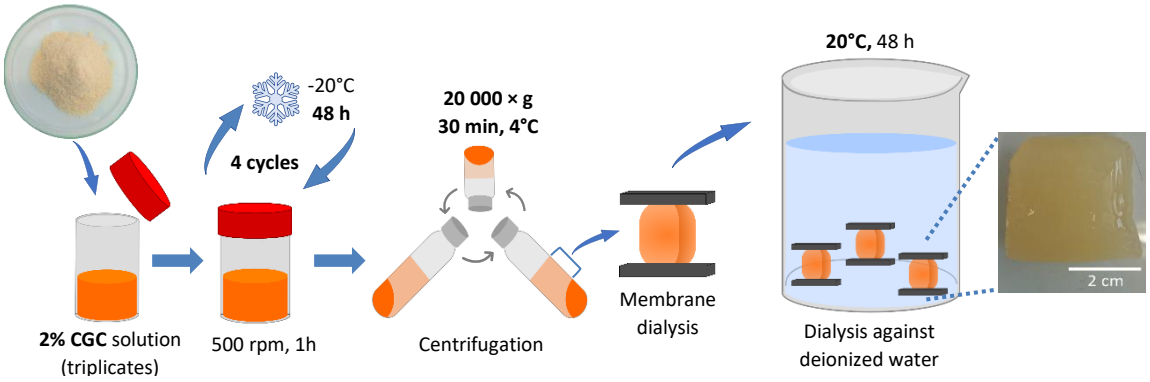

Figure 18: Schematic representation of CGC Hydrogels preparation.

To study and optimize the properties of the final CGC hydrogels, the effect of the number of freeze/thaw cycles, freezing time, dialysis temperature, polymer concentration and centrifugation conditions were assessed.

4.2.1.1. Effect of freeze/thaw cycles and freezing time

To investigate the effect of the number of freeze/thaw cycles, CGC suspensions (2% w/w) were submitted to 0, 1, 2, 3 or 4 freeze/thaw cycles while the other conditions were maintained, as illustrated in Figure 18. The freezing time effect was evaluated by changing the freezing time of CGC suspensions (2% wt.) to 18 h, instead of 48 h (Table 6). Based on the results, the later effects were tested using all the CGC solutions with 1 freeze/thaw cycle, for 18 h frozen.

Table 6: Performed CGC hydrogels changing the number of freeze/thaw cycles and freezing time.

CGC concentration (% wt)	Number of freeze/thaw cycles	Freezing time (h)	Centrifugation speed (g)	Dialysis temperature (°C)	Labelled
2%	0	48	20 000	20	0cycle
	1				1cycle
	2				2cycle
	3				3cycle
	4				4cycle
2%	1	18	20 000	20	1cy

4.2.1.2. Effect of dialysis temperature

The dialysis temperature of 2% CGC solutions was evaluated at 4, 10 and 30°C while the other conditions were kept constant (Table 7).

Table 7: Performed CGC hydrogels changing the dialysis temperature.

CGC concentration (% wt)	Number of freeze/thaw cycles	Freezing time (h)	Centrifugation speed (× g)	Dialysis temperature (°C)	Labelled
2%	1	18 h	20 000 × g	4°C	1cy4°C
				10°C	1cy10°C
				30°C	1cy30°C

4.2.1.3. Effect of polymer concentration and centrifugation conditions

The effect of CGC content was evaluated, changing to 4% and 6% while the other conditions were maintained constant. Finally, CGC solutions of 4% and 6% were centrifugated at 40 000 × g and 60 000 × g, respectively (Table 8).

Table 8- Performed CGC hydrogels changing the CGC content and centrifugation.

CGC concentration (% wt)	**Number of freeze/thaw cycles**	**Freezing time** (h)	**Centrifugation speed** (× g)	**Dialysis temperature** (°C)	**Labelled**
4%	1	18 h	20 000 × g	20°C	1cy4%
6%					1cy6%
4%	1	18 h	40 000 × g	20°C	1cy40
6%			60 000 × g		1cy60

4.2.2. Characterization of GCC hydrogels

4.2.2.1. Water content

The water content of CGC hydrogels was determined by gravimetry, as described in section **3.2.2.1**. The measurements were performed in triplicate for all hydrogels.

4.2.2.2. Elemental analysis and degree of acetylation

The elemental analysis was performed in original CGC powder and freeze-dried hydrogels (4cycle, 1cy and 1cy60) as described in section **2.2.4.1.**

4.2.2.3. FT-IR

CGC and the freeze-dried CGC hydrogels (4cycle, 1cy and 1cy60) were analysed by FT-IR as described in section **3.2.2.4**.

4.2.2.4. Texture analysis

The formed hydrogels were shaped through a 13.8 mm diameter mould (Figure 19) and cut with 7–11 mm height.

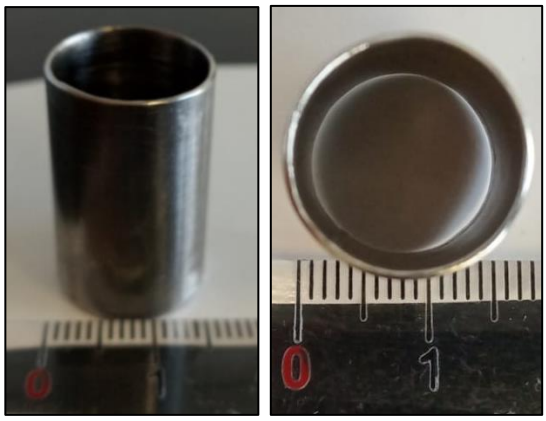

Figure 19: Mould used to shape the hydrogels with a constant diameter (13.8 mm).

The texture properties of hydrogels were assessed with a TMS-Pro texture analyzer (Food Technology Corporation, England) equipped with a 50 N load cell. The assays were performed applying a double compression cycle up to 50 % strain of the sample original height, at a speed rate of 60 mm/min, using a 60 mm aluminium plunger. The experiments were done in quintuplicate for all hydrogels.

The carried-out load (N) was converted to stress (Pa) according to equation (8):

$$Stress = \frac{Load}{\pi * 0.0069^2} \quad (Pa \; or \; N/m^2) \quad (8)$$

where the $Load$ is the load applied (N), 0.0069 is the constant radius (m) and $\pi * 0.0069^2$ is the cross-section area of hydrogels (m^2).

The maximum tension of the first compression corresponds to hardness as well as the springiness was defined by the ratio between the second and the first compression distances until maximum forces. Finally, the ratio between the positive force over the second cycle and the positive force over the first cycle was defined as cohesiveness[46].

4.2.2.5. Rheology

The evaluation of the rheological properties of CGC hydrogels was assessed by applying the same parameters of stress sweep (Figure A6 and A7) and frequency sweeps within the linear region, as described in section **3.2.2.3**. The measurements were done in duplicate for 1cy, 1cy40 and 1cy60 gels.

4.2.2.6. Structural stability

The structural stability was assessed by placing the hydrogels (13.8 mm diameter, 7–11 mm height) in water, solutions of NaCl 0.9% (w/w) and PBS (NaCl, 8.0 g/L; KCl, 0.20 g/L; K_2HPO_4, 1.77 g/L; KH_2PO_4, 0.24 g/L; pH 7.40). The NaCl 0.9 % represents physiological saline and PBS refers to 0.9 % of NaCl solution in phosphate buffer having KCl. The hydrogels were weighed

initially, and after 8 months immersed in the solutions. The final weight content (%) was determined by equation (9):

$$Weight\ content = \frac{m_{\,8\ months}}{m_{\,wet}} \text{ x } 100\ (\%) \quad (9)$$

where $m_{\,8\ months}$ is the hydrogel mass (g) after 8 months in the solutions, and $m_{\,wet}$ is the initial wet hydrogel mass (g). The measurements were done in triplicate for 1cy and 1cy60 gels.

4.2.2.7. Swelling properties

The swelling behaviour was assessed by the immersion of hydrogels (13.8 mm diameter, 7–11 mm height) in water, NaCl 0.9 % (w/w) and PBS (NaCl, 8.0 g/L; KCl, 0.20 g/L; K_2HPO_4, 1.77 g/L; KH_2PO_4, 0.24 g/L; pH 7.40). To study the effect of temperature and pH on swelling properties, the hydrogels were performed at 25°C, 37°C, and pH 2, at room temperature. The hydrogels were carefully removed from the solution and weighed every 30 min, throughout 8h. All the measurements were performed in triplicate for 1cy and 1cy60 gels and the swelling ratio (%) was calculated using equation (10):

$$Swelling\ ratio = \frac{m_{\,swollen}}{m_{\,wet}} \quad (10)$$

where the $m_{swollen}$ is the hydrogel swollen mass (g) and m_{wet} is the initial wet hydrogel mass (g).

4.2.2.8. Syneresis

4.2.2.8.1. Dehydration by centrifugation

The hydrogels were subjected to centrifugation (2000 x g, 20°C, for 25 min) with centrifuge filters (0.2 µm, Whatman) and the syneresis rate (%) was determined by gravimetry, using equation (11) as follows:

$$Syneresis\ rate = \frac{m_{\,wet} - m_{\,shrunk}}{m_{\,wet}} \text{ x } 100\ (\%) \quad (11)$$

where $m_{\,wet}$ (g) is the initial wet hydrogel mass and $m_{\,shrunk}$ (g) is the shrunk hydrogel mass. All measurements were made in octuplicate for 1cy and 1cy60 gels.

4.2.2.8.2. Dehydration by passive diffusion

The hydrogels (13.8 mm diameter, 7–11 mm height) placed in a Petri plate were submitted at different temperatures (25°C and 37°C), and the passive syneresis was determined by gravimetry using equation (11). The measurements were done for 1cy and 1cy60 hydrogels, in triplicate.

4.2.2.9. Loading and release ability

The evaluation of loading and release ability of the hydrogels (13.8 mm diameter, 7–11 mm height) was performed using a blue food dye (E133/E122) and for theophylline 99% (Sigma-Aldrich) as a model drug, which quantification was achieved by spectrophotometry. The maximum wavelength absorbance used was 629 nm and 298 nm, for the dye (Figure A8) and theophylline (Figure A9), respectively. Standard solutions were performed to obtain a calibration curve for the dye (Figure A10) and theophylline (Figure A11) in a concentration range between 0 to 0.8 g/L and 0 to 2.5 mM, respectively.

4.2.2.9.1. In aqueous media

To perform the dye load, hydrogels (13.8 mm diameter, 7–11 mm height) were immersed into 10 mL of blue dye solution (2.5 g/L) for 24 h. Then, they were placed into water, NaCl 0.9 % (w/w) and PBS solutions. To evaluate the release properties, the absorbance of the aqueous solutions was measured over 2.5, 24 and 51 h. The measurements were done in triplicate, for 1cy gels.

4.2.2.9.2. *In vitro* Franz diffusion cell

In vitro permeation experiments were conducted in a PermeGear V3B diffusion system, with Franz vertical diffusion cells with 10 mL capacity receptor compartment, filled with deionized water. The assays were carried out with a transdermal membrane (Strat-M transdermal diffusion test model 25 mm), with 3.14 cm^2 diffusion area, under a constant stirring (500 rpm), at 37°C.

The first experiments were performed by soaking hydrogels into 10 mL of blue dye solution (2.5 g/L), for 24 h. Then, the hydrogels were carefully placed on the diffusion system and the release was evaluated after 24 h (Figure 20). The released concentration was divided by each initial mass of the hydrogels. The measurements were performed in duplicate for 1cy gels.

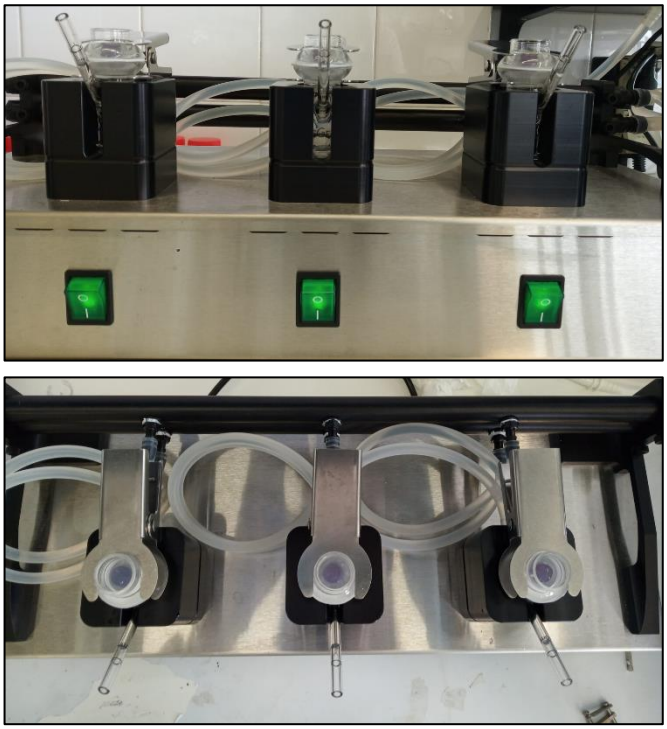

Figure 20: *In vitro* evaluation of the release ability of hydrogels immersed in dye solution, for 24 h, with Franz diffusion cells.

The assays with theophylline were done by soaking hydrogels into 30 mM of theophylline solution, for 24 h. The drug-loaded hydrogels were carefully placed on the diffusion system and the drug release was assessed through independent assays over 6, 12, 24, and 48 h. The released concentration was divided by each initial mass of the hydrogels. All the measurements were done in duplicate for 1cy and 1cy60 gels.

4.3. Results and discussion

4.3.1. Hydrogels formation and water content

Several conditions were applied to CGC solutions, in order to obtain desirable properties of final CGC hydrogels. First, the number of freeze/thaw cycles and time freezing, which can influence the CGC degree of acetylation. In fact, as reported by Araújo *et al*.[46], the hydrated alkali solvents disrupt the polymer chain at temperatures below the freezing point, by breaking the inter- and intra-molecular bonds of polymer matrix chain. Afterwards, the dialysis temperature, and finally, the CGC concentration and centrifugation, which may affect the chemical and physical properties of CGC hydrogels.

	1cycle	2cycle	3cycle	4cycle
CGC hydrogel	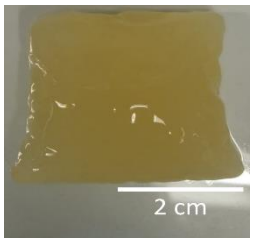	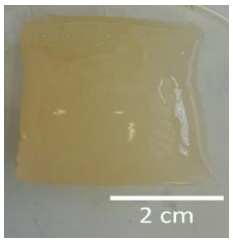	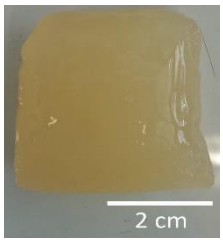	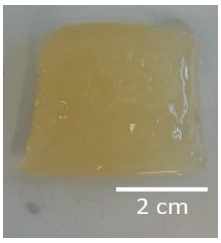
Water content (%)	98.22 (±0.20)	98.45 (±0.06)	98.57 (±0.02)	98.34 (±0.30)

	1cy	1cy30°C	1cy4%	1cy6%
CGC hydrogel	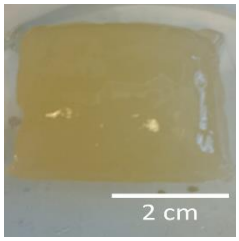	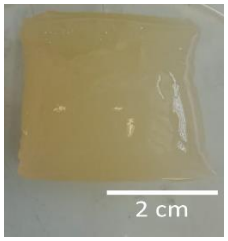	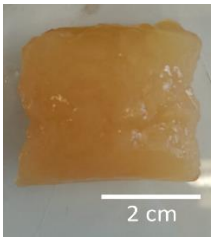	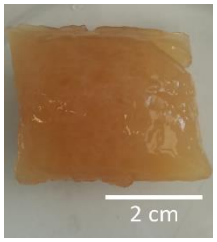
Water content (%)	97.63 (±0.12)	97.94 (±0.14)	97.27 (±0.13)	96.49 (±0.58)

	1cy40	1cy60
CGC hydrogel	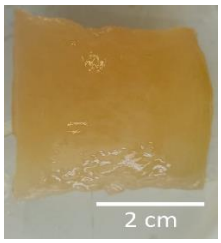	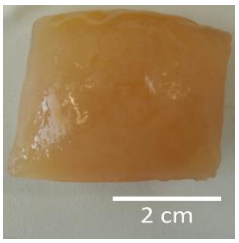
Water content (%)	97.64 (±0.16)	96.52 (±0.19)

Figure 21: Photographs and the respective water content of CGC hydrogels obtained with different freeze-thaw cycles (1cycle, 2cycle, 3cycle, and 4cycle), freezing time (1cy) temperature (1cy30°C), CGC concentration and centrifugation (1cy4%, 1cy40, 1cy6%, and 1cy60).

As can be seen in Figure 21, all hydrogels were translucid and presented a yellow colouration. The shape of the hydrogels was moulded by the dialysis tubing, and therefore, showing that CGC hydrogels performed by this methodology can be moulded into desirable shapes, by inducing gelation in adequate moulds[46]. Despite the hydrogels prepared with 2%

(w/w) of CGC (1cycle, 2cyle, 3cycle, 4cycle) presenting resembling visual features, as the initial CGC concentration increased to 4% and 6%, the final hydrogels (1cy4%, 1cy40 and 1cy6%, 1cy60, respectively) showed a noticeable changing to an orangish colour. Also, it can be seen that for the same initial polymer concentration, the 1cy4% and 1cy6% hydrogels seemed rougher than 1cy40 and 1cy60, respectively, probably caused to a higher fraction of insoluble CGC, which was attenuated by higher centrifugation conditions submitted to the latest hydrogels (40 000 and 60 000 x g, respectively).

To verify the significance of one freeze/thaw cycle, an attempt with no freeze/thaw cycle (0cycle) were performed, but only a viscous solution was formed, which may be due to the non-deacetylation that the freeze/thaw procedure induces, and consequently, low dissolution of CGC in NaOH. Also, the effect of dialysis at lower temperatures (4°C and 10°C, for 1cy4°C and 1cy10°C, respectively) was not possible to assess, probably caused by the harsh conditions which the dialysis membranes were submitted. In fact, it was reported that the solubility of cellulose, the membranes' material, become a little higher when subjected to NaOH water-based solvents at temperatures below 15°C[91].

As observed in Figure 21, all hydrogels exhibited a water content above 90%, typical of hydrogels structures. In fact, similar values were observed for hyaluronic acid (HA)- and Na CGC-based hydrogels (95.8%[92] and 97.72%[46], respectively). It seemed constant in the range of 1cycle to 4cycle (98.22–98.57%), with a slightly lower content for 1cy and 1cy30°C (97.63% and 97.94%, respectively). These values are similar to those reported in previous studies for CGC hydrogels prepared by the freeze-thaw method (97.72%)[46]. However, when the initial CGC concentration increased to 6% the water content of the final hydrogels (1cy6% and 1cy60) decreased significantly (96.49% and 96.52%, respectively), which indicates a higher final polymer content in the CGC hydrogel (3.51% and 3.48%, respectively), compared with previous studies (2.28%)[46].

4.3.2. Elemental analysis and degree of acetylation

Table 9 shows the chemical characterization of CGC polymer and hydrogels, compared with previous studies.

Table 9: Chemical characterization of original CGC and hydrogels, compared with previous studies.

	Sample	Elemental analysis (%)			Chitin content (%)	DA (%)
		C	H	N		
Literature[27]	CGC	43.6	7.2	1.7	23.8	61.3
	4cycle*	40.4–42.3	6.9–7.2	1.3–2.3	18.8–32.8	33.9–50.6
This study	CGC	43.9	7.2	2.5	35.6	63.4
	4cycle	41.1	6.8	1.8	25.7	40.6
	1cy	40.5	6.5	1.4	20.0	35.7
	1cy60	41.1	6.5	1.5	21.9	40.3

*NaOH/urea-based

As can be seen in Table 9, the chitin content of the original CGC was 35.6%. This value is quite higher comparing with those of the hydrogels (21.9–25.7 %), which is related to the fact that CGC solubility increases for lower chitin-glucan ratio present in the polymer content. Additionally, this chitin-glucan content (35.6%) also explains the higher value compared to that reported by Araújo *et al.*[27], in which the original CGC sample might be composed of polymer chains with lower chitin-glucan content. Nevertheless, the 1cy and 1cy60 chitin contents showed lower values (20.0% and 21.9%, respectively) than the 4cycle (25.7%), which can be explained by the number of freeze/thaw cycles. In fact, these values suggest that four freeze/thaw cycles can solubilize a higher chitin-glucan ratio than one freeze/thaw cycle.

It can be observed in Table 9 that the degree of acetylation decreased in the hydrogels (35.7–40.6%) when compared with the initial CGC (63.4%). This is related to the polymer dissolution process, where the NaOH solvent system associated with the freeze/thaw cycles convert chitin into chitosan, its N-deacetylated and soluble derivate[27]. Nonetheless, for the same freezing time, the degree of acetylation of 1cy (35.7%) presented lower values than the 1cy60 hydrogels (40.3%), which is possibly due to lower initial CGC concentration.

4.3.3. FT-IR

FTIR analysis was carried out to verify the impact of NaOH solvent system on the chemical structure of hydrogels (Figure 22).

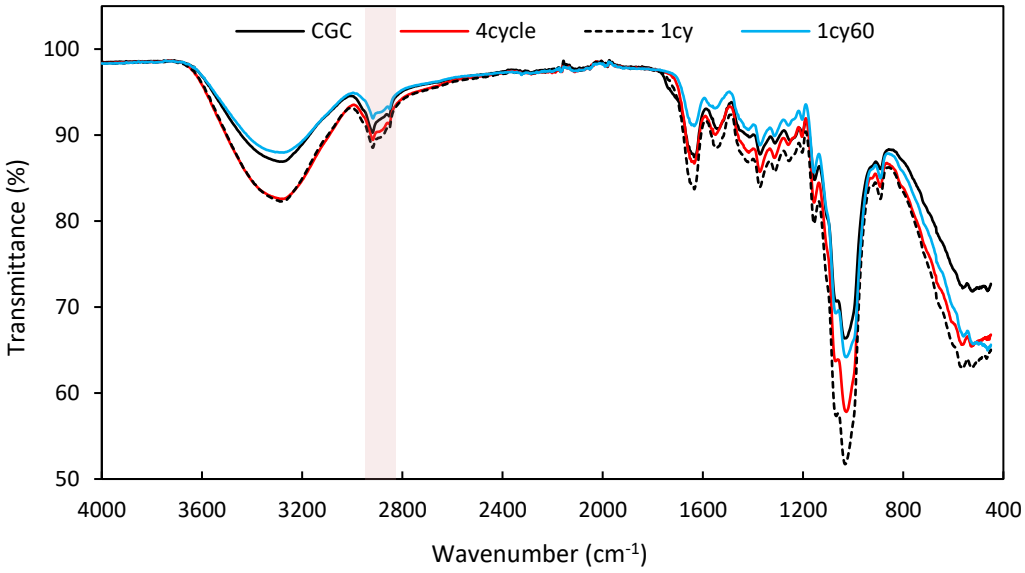

Figure 22: FTIR spectra of CGC polymer and dried CGC hydrogels (4cycle, 1cy and 1cy60).

As can be seen in Figure 22, no significant impact was observed among CGC and the final hydrogels. Still, all spectra exhibited a broad and intense band around 3400 cm^{-1}, typical of O–H stretching of hydroxyl groups, which is usual in chitin/chitosan complexes[27]. As reported by Araújo *et al.*[27] and Farinha *et al.*[61] this band overlaps the N–H symmetric and N–H asymmetric stretching peaks. The C–H stretching corresponding of CH_3 and CH_2 appeared at 2919 and 2852

cm^{-1} for CGC. In all hydrogel's spectra similar values were observed for the first peak at 2918 cm^{-1} (4cycle and 1cy) and 2917 cm^{-1} (1cy60), and for the second peak at 2852 cm^{-1} (4cycle and 1cy) and 2851 cm^{-1} (1cy60).

FTIR spectroscopy also enables to assess the nature of the β-glucan linkages. As described in previous studies[27,61], the characteristic small peaks of β-1,3-glucans are noticed around 891, 1154 and 1372 cm^{-1}, while β-1,6-glucans are represented by peaks at 922, 1045 and 1730 cm^{-1}. However, in all spectra, the β-1,3-glucans peaks are vague and doubtful whereas the β-1,6-glucans peaks are practically inexistent, due to the low β-1,6-glucans content present in *Komagataella pastoris* CGC[27].

For the texture profile, structural stability, passive syneresis, and releasing analysis, the hydrogels were shaped through a 13.8 mm diameter mould (Figure 19, section **4.2.2.4**) and cut with 7–11 mm height (Figure 23).

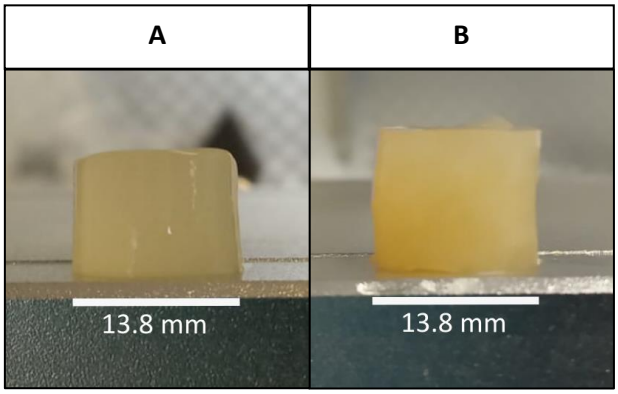

Figure 23: Photographs of typical hydrogels (**A**: 1cy, **B**: 1cy60) shaped with 13.8 mm diameter and height between 7–11 mm used for texture profile, structural stability, swelling, passive syneresis, and releasing analysis.

4.3.4. Texture profile analysis

The texture profile parameters were obtained as described by Araújo *et al*.[46]. It was applied a 50% strain of the hydrogel original height in a double compression cycle, and the hardness, springiness and cohesiveness results are represented in Figure 24.

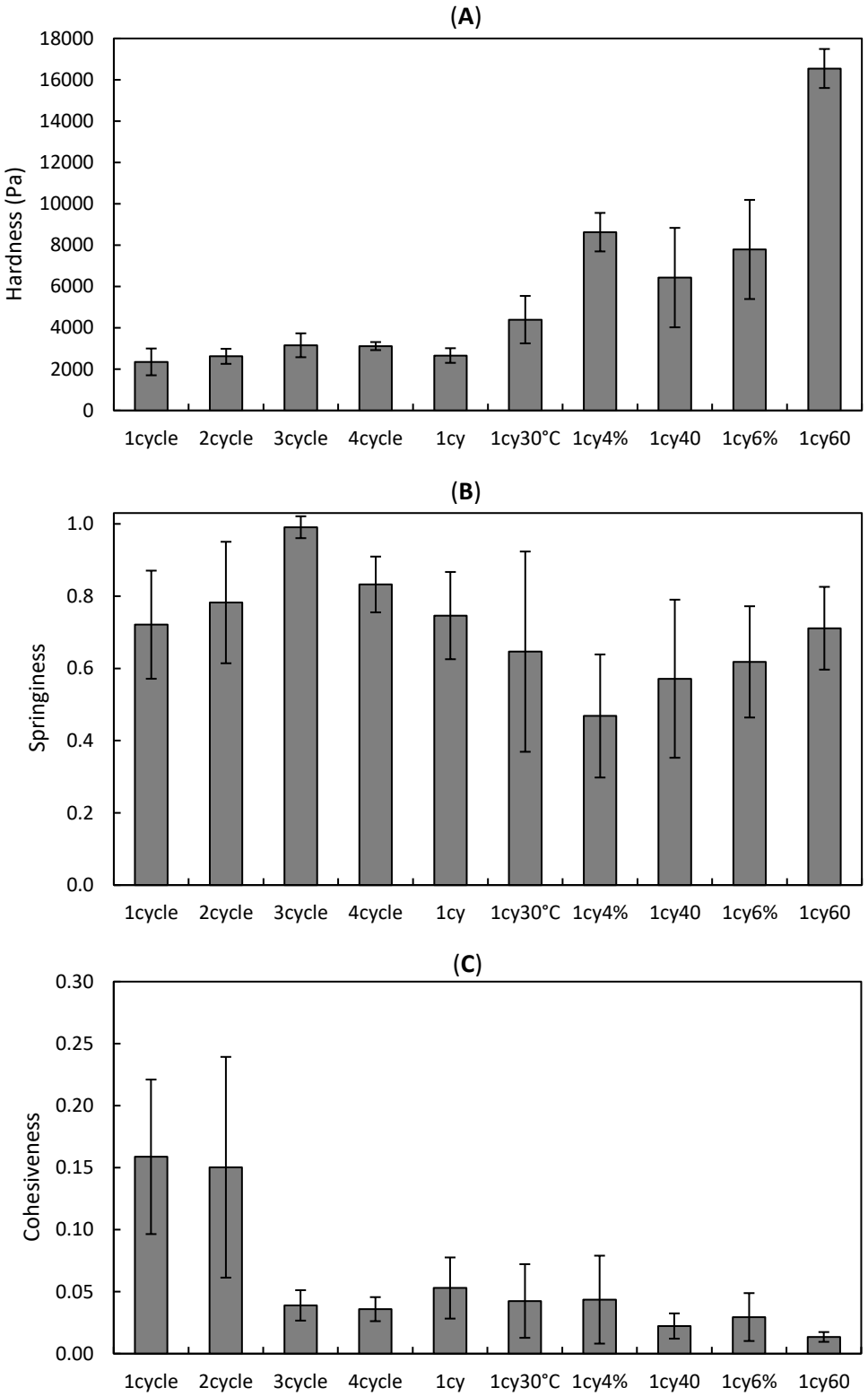

Figure 24: Texture profile parameters analysis hardness (**A**), springiness (**B**), and cohesiveness (**C**) for hydrogels prepared with different freeze-thaw cycles (1cycle, 2cycle, 3cycle, and 4cycle), freezing time (1cy) temperature (1cy30°C), CGC concentration and centrifugation (1cy4%, 1cy40, 1cy6%, and 1cy60).

The hardness is related to the maximum force required to cause the selected deformation in the gel. As can be observed in Figure 24**A** the number of freeze/thaw cycles seemed to have a slight positive effect in the hydrogel's hardness, since as the freeze/thaw cycles increased the hardness increased too (1cycle: 2352±648 Pa; 2cycle: 2621± 364 Pa; 3cycle: 3156±578 Pa; 4cycle: 3117±194 Pa), being similar for 3cycle and 4cycle, but relatively lower than the values reported in previous studies (4cycle: 7229±781 Pa)[46]. The decrease in freezing time for 18h (1cy: 2660±364 Pa) presented similar values to the values for 48h (1cycle: 2352±648), showing that the freezing time does not affect the hardness of hydrogels. However, a significantly higher hardness was observed at higher dialysis temperature (1cy30°C: 4397±1148 Pa), which may be related to the higher molecular aggregation and gelation rate increase with the increase of temperature, as reported by Nogueira *et al*.[93]. Nonetheless, CGC concentration was the parameter that most influenced the hydrogel's hardness. Although at 4% of CGC the 1cy4% presented slightly higher values than the 1cy40 (8628±932 Pa and 6430±2405 Pa, respectively), at 6% of CGC the 1cy60 presented a remarkable increase of hardness (16547±944 Pa) when compared with 1cy6%, which suggests that the increase in centrifugation from 20000 x g to 60000 x g (1cy6% and 1cy60, respectively) contributes to an increase in soluble CGC, allowing a final hydrogel with a stiffer structure. This value is slightly higher than those reported by Chen *et al*.[94] for HA-based hydrogels (2313–14309 Pa) with the same compression applied (50%).

Springiness expresses the capacity of the hydrogels to physically spring back after it has been deformed during the first compression, in which a period of time was allowed before the second compression. As can be seen in Figure 24**B**, the springiness for 1cy and among 1cycle to 4cycle were quite high (0.72–0.99), which is indicative of an elastic behaviour. These values are in the range of those reported by Araújo *et al*.[46] (0.85–0.93) and Chen *et al*.[94] (0.821–0.98). Besides, the hydrogels with higher initial CGC concentration (1cy4%, 1cy40, 1cy6% and 1cy60) presented lower elastic properties, except for the 1cy60, with a value of 0.71±0.11.

Cohesiveness reflects the ability of the hydrogel to withstand to compression, which means that a high cohesive product maintains its internal structure without failures when submitted to compression. Even though all the hydrogels presented (Figure 24**C**) a weak cohesiveness (0.013–0.053), having a slight increase for 1cycle and 2cycle (0.159±0.062 and 0.150±0.089, respectively), these values are quite lower when compared with the Na CGC-based (4cycle: 0.716)[46] and HA-based hydrogels (0.316–0.552)[94]. This fact suggests that the hydrogels had low strength of polymer chain molecular interactions, which induce this behaviour where the energy required for the second compression is notably lower than that for the first compression[46].

4.3.5. Rheology

The rheology of CGC hydrogels was studied in order to envisage their potential applications according to their viscoelastic properties.

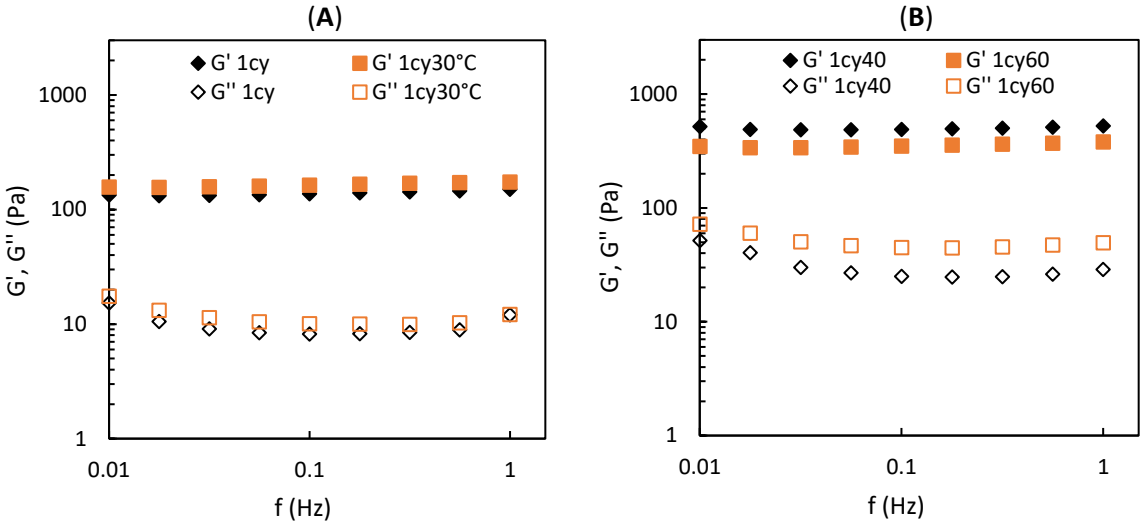

Figure 25: Rheological properties of CGC hydrogels, changing the temperature (**A**: 1cy and 1cy30°C) and CGC concentration (**B**: 1cy40 and 1cy60). Mechanical spectrum storage (G', solid symbols) and loss moduli (G'', open symbols).

As can be seen in Figure 25 for all CGC hydrogels the storage moduli (G') displayed values one order of magnitude higher than the loss moduli (G'') in the entire range of frequencies. This feature is concomitant with the gel-like nature of the samples. Comparing with similar hydrogels, the Na CGC-based[46] and hydrogels developed with HA cross-linked with divinyl sulfone[95] also exhibited similar behaviour. Although the identical profiles, CGC hydrogels (Figure 25**B**) exhibited improved mechanical properties. Indeed, for the same frequency (0.1 Hz), the 1cy40 and 1cy60 hydrogels presented storage moduli values of 489.7 and 347.9 Pa, respectively, which are higher than the HA-based hydrogels (304.3 Pa)[95] and in the same range than the values of Na CGC-based hydrogels (389 and 685 Pa) reported by Araújo *et al*. [46].

The dialysis temperature revealed to have low influence in the viscoelastic properties of hydrogels. In fact, similar dynamic moduli were observed with 1cy and 1cy30°C hydrogels, in the entire range of frequencies (Figure 25**A**). However, comparing with the mechanical spectra of Figure 25**B**, the dynamic moduli of 1cy40 and 1cy60 increased. This behaviour is consistent with the texture profile analysis, in which the hydrogels exhibited stronger mechanical properties as the CGC concentration increase. Interestingly, in the whole range of frequencies, the storage modulus of 1cy60 showed lower values (0.01 Hz, G'= 346.6 Pa) compared with 1cy40 (0.01 Hz, G'= 517.6 Pa) hydrogels, but higher loss moduli (0.01 Hz, G''= 71.8 Pa and 51.6 Pa, respectively). This indicates that the 1cy60 has low elastic capacity than 1cy40 hydrogels, but higher viscous properties when the shear stress is applied.

4.3.6. Structural stability

It is important to study the stability of hydrogels over time because it gives an idea not only regarding the shelf life of the product but also to find optimum storage conditions[96].

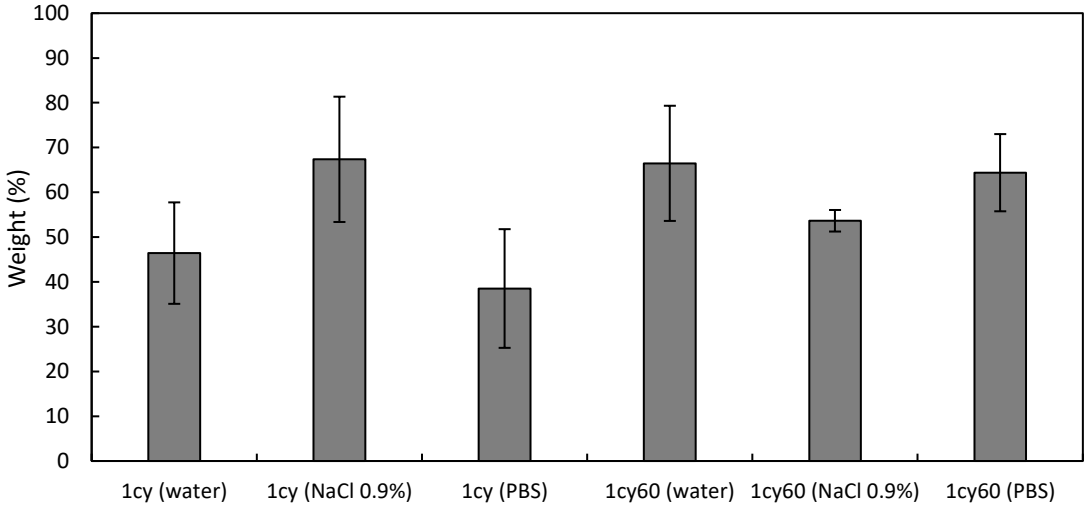

Figure 26: Stability of 1cy and 1cy60 hydrogels (wt.%) after 8 months in water, NaCl (0.9%) and PBS solutions.

The stability of CGC hydrogels was assessed by weighing the hydrogels initially and after 8 months in solutions. As observed in Figure 26, the 1cy hydrogels presented values in the range of 38.5–67.3% of initial weight, whereas 1cy60 hydrogels exhibited more constant values (53.6–66.5 %) in the conditions tested. This fact is probably due to the higher hardness of the 1cy60 hydrogels, which allowed a stiffer structure between polymer chains and a stabler final hydrogel. Considering 8 months as a long period of time, the obtained 1cy60 hydrogels were considerably stable in water (66.5±12.9%) and PBS (64.4±8.6%).

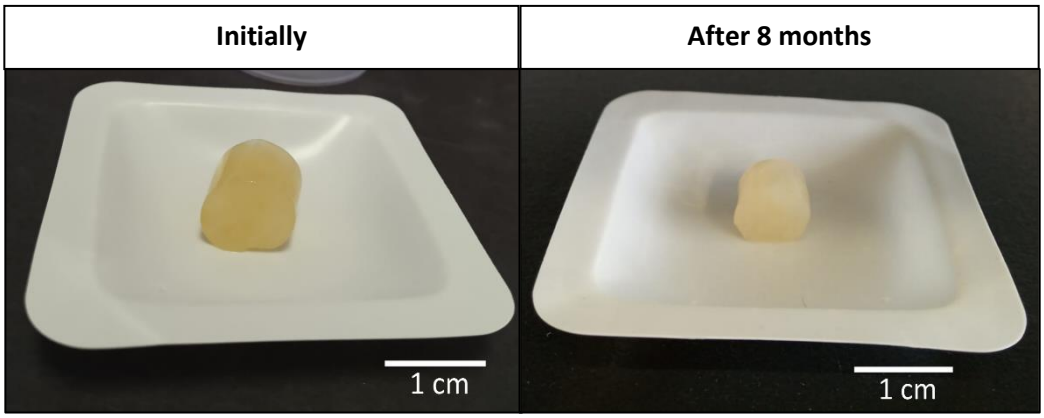

Figure 27: Photographs of 1cy60 hydrogels initially and after 8 months in water.

Nevertheless, as can be observed in Figure 27 the hydrogel differed mainly in size, being smaller after 8 months immersed in water, probably connected to the low cohesiveness of the hydrogels, in which parts with weaker molecular bonds of polymer matrix chain are loosed over time.

4.3.7. Swelling properties

Swelling behaviour is an important factor in applications as transdermal delivery systems since it can be directly related to the loading and delivery capability of drugs[97,98]. Indeed, the swelling behaviour of CGC hydrogels was assessed in different media.

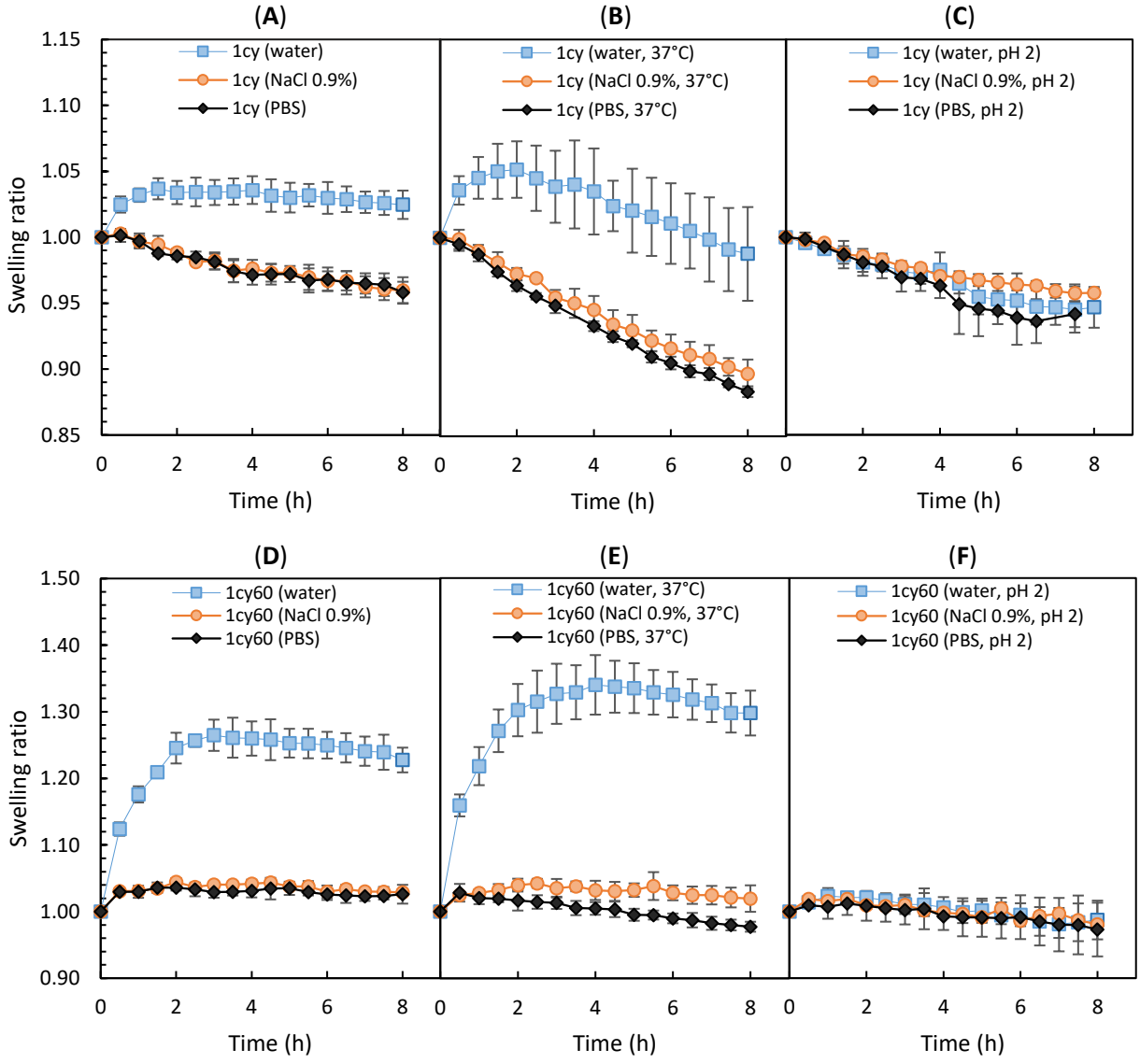

Figure 28: Effect of temperature (**A**: room temperature; **B**: 37°C) and pH (**C**: pH 2, room temperature) in 1cy and 1cy60 hydrogels in water, NaCl 0.9 %, and PBS.

The swelling of hydrogels may be influenced by several factors such as cross-linking density, temperature, salts, and pH of swelling media[98,99]. As noticed in Figure 28, the swelling capacity of CGC hydrogels was, except at pH 2, remarkably higher in water than in the other media. In fact, it was reported that for solutions with higher ionic strength, such as NaCl 0.9% and PBS, it is commonly observed a swelling decrease by polyelectrolyte hydrogels, due to the decrease of the osmotic pressure between the hydrogel structure and the solution[98]. Besides, as can be seen in Figure 28**C** and **F**, at pH 2, both 1cy and 1cy60 hydrogels did not swell, probably due to the high concentration of H^+ present in media, which led to a higher protonation of hydrophilic groups in the internal structure of the hydrogels, incapacitating the penetration of water molecules in the hydrogel structure[97].

As can be seen in Figure 28**B** and **E**, at 37°C, both 1cy and 1cy60 hydrogels displayed higher swelling values in water, when compared with the values at room temperature (Figure 28**A** and **D**, respectively). As reported by Ahmed *et al*.[99], the increase of temperature causes an increase in internal energy and entropy, which lead to a higher degree of movement and diffusion of water molecules into the hydrogel structure. Additionally, after 8 h soaked in PBS (Figure 28**B** and **E**, respectively), the 1cy exhibited lower swelling ratio values (0.88±0.01)) that 1cy60 hydrogel (0.98±0.01), which may be related to the stiffer structure of 1cy60 hydrogels.

Usually, the swelling behaviour is negatively influenced with the increase of polymer concentration, since the higher density of the polymer is associated with less stretching of the polymer chains, due to lower pores in the structure[98]. However, as observed in Figure 28, comparing **A** with **D**, and **B** with **E**, the increase of CGC concentration significantly increased the swelling capacity of hydrogels in water, reaching a maximum value of 1.26±0.03 (Figure 28**D**) and 1.34±0.04 (Figure 28**E**) of swelling ratio after 4 h immersed, for 1cy60 hydrogels. Comparing with the maximum swelling values of HA-based hydrogels (1.05–1.23) in PBS reported by Haridas *et al*.[96], the values obtained with 1cy60 hydrogels are slightly lower (1.03–1.04).

4.3.8. Syneresis

The syneresis is known as the spontaneous contraction of hydrogel and the exudation of liquid. This feature can be useful when used as drug delivery systems, and thus, the dehydration by centrifugation and by passive diffusion syneresis was evaluated.

4.3.8.1. Dehydration by centrifugation

The ability of hydrogels to withstand to external force was assessed by a centrifugation method (2000 x g, for 25 min, at 20°C). For the 1cy and 1cy60 hydrogels, 8.3% (±0.6) and 3.5% (±1.1) of syneresis rate were obtained, respectively, which is consistent with the fact that the stronger structure of 1cy60 hydrogels allowed to retain a higher amount of water, as well as mentioned by Danalache *et al*.[100].

4.3.8.2. Dehydration by passive diffusion

To evaluate the ability of the hydrogel structure to hold water inside, the syneresis by passive diffusion was evaluated at 25°C and 37°C.

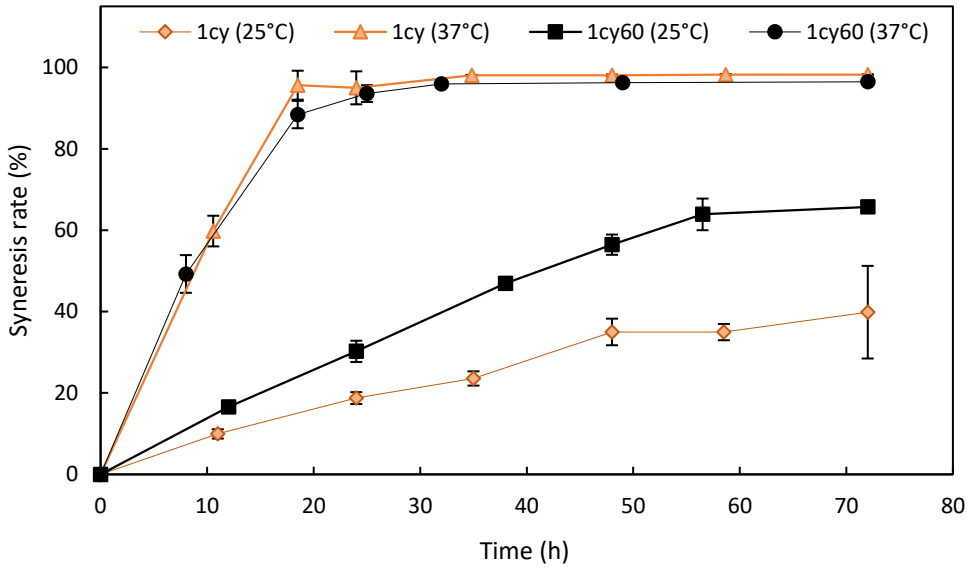

Figure 29: Effect of CGC concentration and temperature in syneresis rate of hydrogels.

As observed in Figure 29, at 37°C the syneresis rate was faster and similar for both 1cy and 1cy60 hydrogels, being totally dried about 35 h. After 10 h at 37°C, the 1cy and 1cy60 hydrogels showed a syneresis value about 59.8%, a value within the range of HA-based hydrogels (40–80%) reported by Atoufi *et al.*[101]. Interestingly at 25°C, a syneresis rate of 65.7% (±1.2) was obtained for 1cy60, a considerably higher value than for the 1cy hydrogels (39.9±11.4%). However, the 1cy60 showed lower syneresis value in the dehydration by centrifugation. As reported by Danalache *et al.*[100], brittle structures such as 1cy, with low polymer content, have lower syneresis rate with no external forces applied, but when submitted to external forces, a fracture may occur and the water molecules are expelled easier, leading to an increase in the syneresis rate.

4.3.9. Load and release properties

4.3.9.1. Release in aqueous media

In order to evaluate the release properties of hydrogels, preliminary assays with a blue food dye were assessed. The 1cy hydrogels were first soaked into a 2.5 g/L solution of dye, for 24 h (Figure 30**A**) and then released in aqueous media (Figure 30**B**).

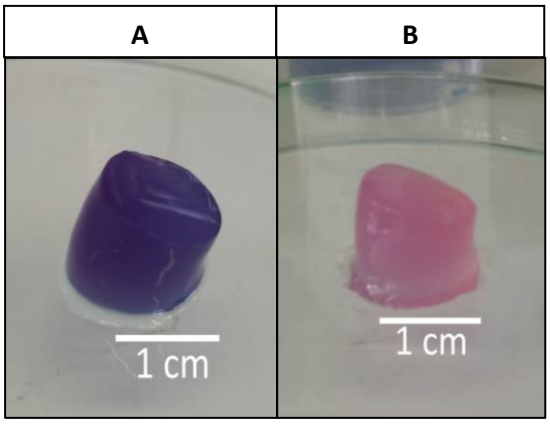

Figure 30:Photographs of: (**A**) 1cy hydrogel after immersed in blue dye solution (2.5 g/L), for 24 h. (**B**) The same hydrogel after 51 h releasing in water.

The release properties in aqueous media (10 mL) are represented in Figure 31, in which values in a range of 0.13–0.14 g/L of released dye were obtained in all media. These similar values suggest that the ionic strength of the NaCl 0.9% and PBS media did not affect the capacity of dye releasing from the hydrogel. Additionally, it can be seen about 24 h that the hydrogel released was constant until the end of the experience, which indicates that the hydrogel was in equilibrium with the media and possibly released all the loaded dye.

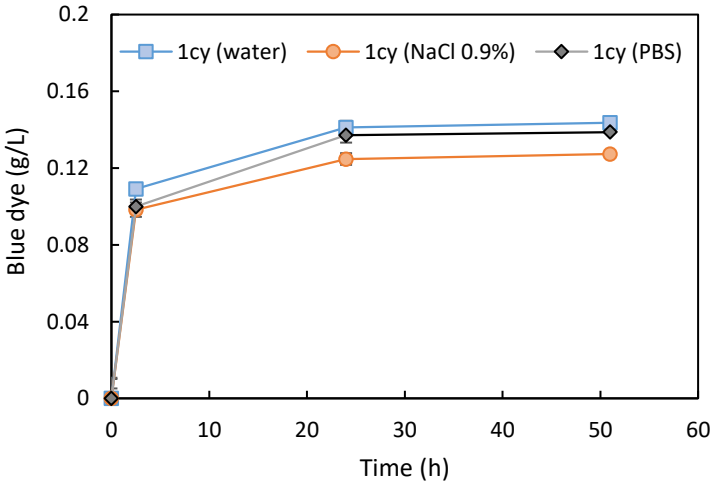

Figure 31: Dye cumulative release from 1cy hydrogels in 10 mL of aqueous media (water, NaCl 0.9 %, and PBS), at room temperature.

4.3.9.2. *In vitro* Franz diffusion cell

The *in vitro* experiments were first evaluated with the 1cy hydrogels soaked in 2.5 g/L solutions of dye, for 24 h. Then, the released properties were assessed after 24 h in the diffusion system. However, no dye concentration was detected in the receptor compartment, probably due to the high molecular mass of the dye (about 792 g/mol), which affect the permeation through the transdermal membrane. Indeed, small molecules are usually preferred because

they can cross through the membrane easier than large molecules[38]. Thus, the 1cy and 1cy60 hydrogels were immersed into a solution (0.03 M) of a smaller molecular weight molecule, theophylline (180 g/mol), for 24 h. Afterwards, taking into account the syneresis rate of the hydrogels at 37°C (Figure 29, section **4.3.8.2.**) the releasing ability was assessed through independent experiments in a time range between 6 and 48 hours, at 37°C.

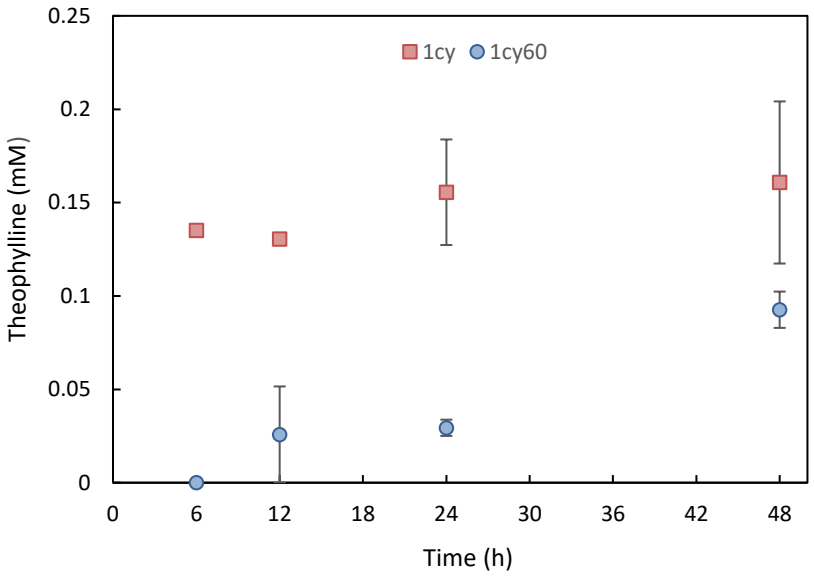

Figure 32: Theophylline *in vitro* release from 1cy and 1cy60 hydrogels in 10 mL of deionized water.

As can be observed in Figure 32, the 1cy hydrogels released a higher amount of theophylline among all the assays over time, which may be related to the fact that 1cy hydrogels have a less dense structure than 1cy60 hydrogels, allowing probably to a higher amount of loaded drug inside the hydrogel structure. It also can be seen for both hydrogels a slight increase of released theophylline as higher the hydrogels remained in the diffusion system. This fact might be explained with the higher shrink of hydrogels over time (Figure 33), leading to a higher release of the drug.

Time (h)	3	6	12
1cy60 hydrogels	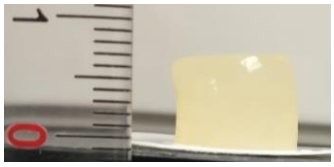	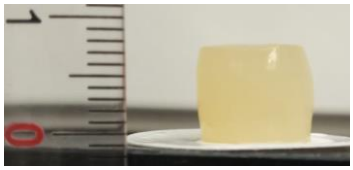	

Time (h)	24	48
1cy60 hydrogels	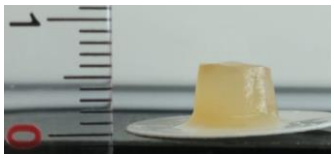	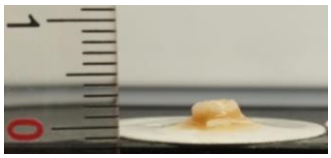

Figure 33: Photographs of 1cy60 hydrogels after 3, 6, 12, 24, and 48 h on the cell Franz, at 37°C.

Although the drug release results were not quite conclusive, for both 1cy and 1cy60 hydrogels this study encourage their use as promising biomaterials, especially, as transdermal delivery systems, due to their non-toxicity and biocompatibility[46]. Nevertheless, the *in vitro* experiments require a more detailed study and optimizations steps, such as the size of the gel, encapsulation efficiency and kinetics of drug release from the hydrogels.

4.4. Conclusion

Several conditions of CGC solutions were tested to evaluate the different properties of the final CGC hydrogels. Among them, the CGC concentration associated with high centrifugation conditions revealed to have a remarkable improving in texture properties hydrogel, reaching a hardness value of 16547±944 Pa. The viscoelastic measurements also demonstrated an improvement in mechanical properties for hydrogels with high polymer concentration (1cy40 and 1cy60). In terms of chemical properties, it was shown that the NaOH solvent combined with the freeze/thaw cycles decreased the degree of acetylation of CGC from 63.4% to 35.7–40.6%, converting chitin into chitosan, its N-deacetylated and soluble derivate. Although these changes, no significant impact was observed in FTIR analysis of hydrogels compared with the original polymer, meaning that the hydrogel polymer presented the same chemical characteristics than the original CGC.

The 1cy60 hydrogels exhibited good stability in water (66.5±12.9%) and PBS (64.4±8.6%), over a long period of time (8 months). On the other hand, 1cy hydrogels showed lower stability in water (46.4±11.3%) and PBS (38.5±13.3%), probably due to the lower stiffness of the polymer chains in the hydrogel structure. In terms of swelling properties, it was demonstrated that in solutions with higher ionic strength, such as NaCl 0.9% and PBS, the swelling behaviour decreased for 1cy and 1cy60 hydrogels, due to the decrease of the osmotic pressure between the hydrogel structure and media. In addition, at pH 2 both hydrogels did not swell, which is related to the higher protonation of hydrophilic groups in the internal structure of the hydrogels. In water, the 1cy60 hydrogels presented higher swelling values at room temperature (1.26±0.03) and 37°C (1.34±0.04).

The dehydration by centrifugation exhibited higher syneresis rates for 1cy (8.3±0.6%) than for 1cy60 (3.5±1.1%) hydrogels. Nevertheless, the dehydration by passive diffusion showed a higher syneresis rate for 1cy60 (65.7±1.2%) compared with 1cy hydrogels (39.9±11.4%). This might be explained by the fact that brittle structures (1cy) present lower syneresis rate when no external forces applied. However, when submitted to external forces, a fracture may occur and water is expelled easier, increasing the syneresis rate. The drug release of theophylline was demonstrated, in which the 1cy showed higher releasing capacity than the 1cy60, among the time range (48 h).

This extensive physical and chemical characterization of CGC hydrogels associated with their non-cytotoxicity strongly encourages its use in divers' areas, like biomedicine as drug-delivery systems and wound dressings.

Chapter 5- Conclusions and Future work

5.1. Conclusions and Future Work

The production and extraction of biopolymers reached values comparable to those of the literature. FucoPol bioreactor achieved a final polymer concentration of 6.2 g/L, with a polymer composition typical of FucoPol (35.7 mol.% of fucose, 26.0 mol.% of galactose, 33.1 mol.% of glucose, and 5.2 mol.% of glucuronic acid). CGC bioreactor produced 34.0 g/L of polymer with 35.6% of chitin content and a degree of acetylation of 63.4%.

For the first time, FucoPol hydrogels were produced by diffusion through dialysis tubing. The horizontal procedure allowed a more homogenous final hydrogel compared with the vertical procedure. Hydrogels prepared with the horizontal procedure showed that the crosslinked iron present in the hydrogel structure did not affect the characteristic chemical features of FucoPol. The rheology of hydrogels dialysed against 0.5 g/L of Fe^{3+} solution revealed improved mechanical properties compared with gellan- and xanthan-based hydrogels. The possibility of controlling the iron content associated to the non-toxicity and bioactivity allows their use as drug delivery carriers, for example, in iron deficiency anaemia. For future studies, the next step should focus on finding a procedure that enables the homogenous gelation of FucoPol hydrogels and thus, evaluate its physical and chemical characterization (texture profile analysis, rheology, microscopic observation of the structure, iron quantification). Further, the drug load and release ability should be assessed with *in vitro* studies.

CGC solutions were subjected to many different conditions in order to study their effect in the final hydrogels. Higher CGC concentration combined to higher centrifugation conditions originated the stiffer hydrogel (1cy60). Chemically, it was shown that the NaOH solvent and the freeze/thaw cycles caused a decrease in the degree of acetylation of CGC, from 63.4% to 35.7–40.6%. However, no significant changes were observed in FTIR analysis, meaning the final CGC present in the hydrogel exhibited the same chemical characteristics than the original CGC. The 1cy60 hydrogels showed good stability over 8 months in water (66.5±12.9%) and PBS (64.4±8.6%), and higher swelling values at room temperature (1.26±0.03) and 37°C (1.34±0.04). Higher syneresis rate by centrifugation was observed for 1cy (8.3±0.6%) than for 1cy60 (3.5±1.1%) even though the syneresis by passive diffusion showed higher values for 1cy60 (65.7±1.2%) compared with 1cy hydrogels (39.9±11.4%), due to the different brittleness of the structures. Finally, the drug release was demonstrated for 1cy and 1cy60, with higher values showed by 1cy hydrogels over time (48h). The physical and chemical characterization of CGC hydrogels combined with their non-cytotoxicity demonstrated that they can be used to prepare biomaterials in different applications, such as drug-delivery carriers in transdermal delivery systems and wound dressings. In terms of future work, it should focus on study and optimize the load and drug-release properties of 1cy and 1cy60 hydrogels. The size of the hydrogel must be higher in order to occupy all the membrane area, the encapsulation efficiency and kinetics of drug release should be studied, as well.

In addition, it would be interesting the microscopic observation of FucoPol and CGC hydrogel structures, which would allow the analysis of hydrogel pores (e.g. density, homogeneity, size) and certainly enable an easier comprehension and correlation with many results demonstrated in this thesis.

References

(1) Wang, X.; Majzoobi, M.; Farahnaky, A. Ultrasound-Assisted Modification of Functional Properties and Biological Activity of Biopolymers: A Review. *Ultrason. Sonochem.* **2020**, *65*, 105057. https://doi.org/10.1016/j.ultsonch.2020.105057.

(2) Nagarajan, S.; Radhakrishnan, S.; Kalkura, S. N.; Balme, S.; Miele, P.; Bechelany, M. Overview of Protein-Based Biopolymers for Biomedical Application. *Macromol. Chem. Phys.* **2019**, *220* (14), 1900126. https://doi.org/10.1002/macp.201900126.

(3) Endres, H.-J.; Siebert-Raths, A. State of Knowledge. In *Engineering Biopolymers*; Carl Hanser Verlag GmbH & Co. KG: München, **2011**; pp 19–43. https://doi.org/10.3139/9783446430020.002.

(4) George, A.; Sanjay, M. R.; Srisuk, R.; Parameswaranpillai, J.; Siengchin, S. A Comprehensive Review on Chemical Properties and Applications of Biopolymers and Their Composites. *Int. J. Biol. Macromol.* **2020**, *154*, 329–338. https://doi.org/10.1016/j.ijbiomac.2020.03.120.

(5) Ferreira, A. R. V.; Torres, C. A. V.; Freitas, F.; Sevrin, C.; Grandfils, C.; Reis, M. A. M.; Alves, V. D.; Coelhoso, I. M. Development and Characterization of Bilayer Films of FucoPol and Chitosan. *Carbohydr. Polym.* **2016**, *147*, 8–15. https://doi.org/10.1016/j.carbpol.2016.03.089.

(6) BeMiller, J. N. Polysaccharides: Occurrence, Structures, and Chemistry. In *Carbohydrate Chemistry for Food Scientists*; Elsevier, **2019**; pp 75–101. https://doi.org/10.1016/B978-0-12-812069-9.00004-2.

(7) Lourenço, S. C.; Torres, C. A. V.; Nunes, D.; Duarte, P.; Freitas, F.; Reis, M. A. M.; Fortunato, E.; Moldão-Martins, M.; da Costa, L. B.; Alves, V. D. Using a Bacterial Fucose-Rich Polysaccharide as Encapsulation Material of Bioactive Compounds. *Int. J. Biol. Macromol.* **2017**, *104*, 1099–1106. https://doi.org/10.1016/j.ijbiomac.2017.07.023.

(8) Torres, C. A. V; Marques, R.; Antunes, S.; Alves, V. D.; Sousa, I.; Ramos, A. M.; Oliveira, R.; Freitas, F.; Reis, M. A. M. Kinetics of Production and Characterization of the Fucose-Containing Exopolysaccharide from *Enterobacter* A47. *J. Biotechnol.* **2011**, *156* (4), 261–267. https://doi.org/10.1016/j.jbiotec.2011.06.024.

(9) Donot, F.; Fontana, A.; Baccou, J. C.; Schorr-Galindo, S. Microbial Exopolysaccharides: Main Examples of Synthesis, Excretion, Genetics and Extraction. *Carbohydr. Polym.* **2012**, *87* (2), 951–962. https://doi.org/10.1016/j.carbpol.2011.08.083.

(10) Ferguson, E. L.; Varache, M.; Stokniene, J.; Thomas, D. W. Polysaccharides for Protein and Peptide Conjugation. In *Polymer-Protein Conjugates*; Elsevier, **2020**; pp 421–453. https://doi.org/10.1016/B978-0-444-64081-9.00019-X.

(11) Schmid, J.; Sieber, V.; Rehm, B. Bacterial Exopolysaccharides: Biosynthesis Pathways and Engineering Strategies. *Front. Microbiol.* **2015**, *6* (496). https://doi.org/10.3389/fmicb.2015.00496.

(12) Antunes, S.; Freitas, F.; Sevrin, C.; Grandfils, C.; Reis, M. A. M. Production of FucoPol by *Enterobacter* A47 Using Waste Tomato Paste By-Product as Sole Carbon Source. *Bioresour. Technol.* **2017**, *227*, 66–73. https://doi.org/10.1016/j.biortech.2016.12.018.

(13) More, T. T.; Yadav, J. S. S.; Yan, S.; Tyagi, R. D.; Surampalli, R. Y. Extracellular Polymeric Substances of Bacteria and Their Potential Environmental Applications. *J. Environ. Manage.* **2014**, *144* (3), 1–25. https://doi.org/10.1016/j.jenvman.2014.05.010.

(14) Zupanc, M.; Pandur, Ž.; Stepišnik Perdih, T.; Stopar, D.; Petkovšek, M.; Dular, M. Effects of Cavitation on Different Microorganisms: The Current Understanding of the Mechanisms Taking Place behind the Phenomenon. A Review and Proposals for Further Research. *Ultrason. Sonochem.* **2019**, *57*, 147–165. https://doi.org/10.1016/j.ultsonch.2019.05.009.

(15) Arana, D. M.; Prieto, D.; Román, E.; Nombela, C.; Alonso-Monge, R.; Pla, J. The Role of the Cell Wall in Fungal Pathogenesis. *Microb. Biotechnol.* **2009**, *2* (3), 308–320. https://doi.org/10.1111/j.1751-7915.2008.00070.x.

(16) Aswathy, S. H.; Narendrakumar, U.; Manjubala, I. Commercial Hydrogels for Biomedical Applications. *Heliyon* **2020**, *6* (4), e03719. https://doi.org/10.1016/j.heliyon.2020.e03719.

(17) Xiang, J.; Shen, L.; Hong, Y. Status and Future Scope of Hydrogels in Wound Healing: Synthesis, Materials and Evaluation. *Eur. Polym. J.* **2020**, *130*, 109609. https://doi.org/10.1016/j.eurpolymj.2020.109609.

(18) Ahmed, E. M. Hydrogel: Preparation, Characterization, and Applications: A Review. *J. Adv. Res.* **2015**, *6* (2), 105–121. https://doi.org/10.1016/j.jare.2013.07.006.

(19) Zhu, T.; Mao, J.; Cheng, Y.; Liu, H.; Lv, L.; Ge, M.; Li, S.; Huang, J.; Chen, Z.; Li, H.; Yang, L.; Lai, Y. Recent Progress of Polysaccharide-Based Hydrogel Interfaces for Wound Healing and Tissue Engineering. *Adv. Mater. Interfaces* **2019**, *6* (17), 1900761. https://doi.org/10.1002/admi.201900761.

(20) Harrison, I.; Spada, F. Hydrogels for Atopic Dermatitis and Wound Management: A Superior Drug Delivery Vehicle. *Pharmaceutics* **2018**, *10* (2), 71. https://doi.org/10.3390/pharmaceutics10020071.

(21) Dave, P. N.; Gor, A. Natural Polysaccharide-Based Hydrogels and Nanomaterials: Recent Trends and Their Applications. In *Handbook of Nanomaterials for Industrial Applications*; Elsevier, **2018**; pp 36–66. https://doi.org/10.1016/B978-0-12-813351-4.00003-1.

(22) Camponeschi, F.; Atrei, A.; Rocchigiani, G.; Mencuccini, L.; Uva, M.; Barbucci, R. New Formulations of Polysaccharide-Based Hydrogels for Drug Release and Tissue Engineering. *Gels* **2015**, *1* (1), 3–23. https://doi.org/10.3390/gels1010003.

(23) Fernando, I. P. S.; Lee, W.; Han, E. J.; Ahn, G. Alginate-Based Nanomaterials: Fabrication Techniques, Properties, and Applications. *Chem. Eng. J.* **2020**, *391*, 123823. https://doi.org/10.1016/j.cej.2019.123823.

(24) Ullah, F.; Othman, M. B. H.; Javed, F.; Ahmad, Z.; Md Akil, H. Classification, Processing and Application of Hydrogels: A Review. *Mater. Sci. Eng. C* **2015**, *57*, 414–433. https://doi.org/10.1016/j.msec.2015.07.053.

(25) Atta, S.; Khaliq, S.; Islam, A.; Javeria, I.; Jamil, T.; Athar, M. M.; Shafiq, M. I.; Ghaffar, A. Injectable Biopolymer Based Hydrogels for Drug Delivery Applications. *Int. J. Biol. Macromol.* **2015**, *80*, 240–245. https://doi.org/10.1016/j.ijbiomac.2015.06.044.

(26) Fialho, L.; Araújo, D.; Alves, V. D.; Roma-Rodrigues, C.; Baptista, P. V.; Fernandes, A. R.; Freitas, F.; Reis, M. A. M. Cation-Mediated Gelation of the Fucose-Rich Polysaccharide FucoPol: Preparation and Characterization of Hydrogel Beads and Their Cytotoxicity Assessment. *Int. J. Polym. Mater. Polym. Biomater.* **2019**, *70* (2), 90–99. https://doi.org/10.1080/00914037.2019.1695205.

(27) Araújo, D.; Alves, V. D.; Marques, A. C.; Fortunato, E.; Reis, M. A. M.; Freitas, F. Low Temperature Dissolution of Yeast Chitin-Glucan Complex and Characterization of the Regenerated Polymer. *Bioengineering* **2020**, *7* (1), 28. https://doi.org/10.3390/bioengineering7010028.

(28) Kim, H. S.; Sun, X.; Lee, J.-H.; Kim, H.-W.; Fu, X.; Leong, K. W. Advanced Drug Delivery Systems and Artificial Skin Grafts for Skin Wound Healing. *Adv. Drug Deliv. Rev.* **2019**, *146*, 209–239. https://doi.org/10.1016/j.addr.2018.12.014.

(29) Das, M.; Giri, T. K. Hydrogels Based on Gellan Gum in Cell Delivery and Drug Delivery. *J. Drug Deliv. Sci. Technol.* **2020**, *56*, 101586. https://doi.org/10.1016/j.jddst.2020.101586.

(30) Sala, M.; Diab, R.; Elaissari, A.; Fessi, H. Lipid Nanocarriers as Skin Drug Delivery Systems: Properties, Mechanisms of Skin Interactions and Medical Applications. *Int. J. Pharm.* **2018**, *535* (1–2), 1–17. https://doi.org/10.1016/j.ijpharm.2017.10.046.

(31) Bolzinger, M.-A.; Briançon, S.; Pelletier, J.; Chevalier, Y. Penetration of Drugs through Skin, a Complex Rate-Controlling Membrane. *Curr. Opin. Colloid Interface Sci.* **2012**, *17* (3), 156–165. https://doi.org/10.1016/j.cocis.2012.02.001.

(32) Lai-Cheong, J. E.; McGrath, J. A. Structure and Function of Skin, Hair and Nails. *Medicine (Baltimore).* **2017**, *45* (6), 347–351. https://doi.org/10.1016/j.mpmed.2017.03.004.

(33) Campbell, K. L.; Lichtensteiger, C. A. Structure and Function of the Skin. In *Small Animal Dermatology Secrets*; Elsevier, **2003**; pp 1–9. https://doi.org/10.1016/B978-1-56053-626-0.50005-7.

(34) Mohammed, A.; Elshaer, A.; Sareh, P.; Elsayed, M.; Hassanin, H. Additive Manufacturing Technologies for Drug Delivery Applications. *Int. J. Pharm.* **2020**, *580*, 119245. https://doi.org/10.1016/j.ijpharm.2020.119245.

(35) Debnath, S.; Saha, A. *Transdermal Drug Delivery System : A*; Lambert Academic Publishing, **2012**.

(36) Prausnitz, M. R.; Langer, R. Transdermal Drug Delivery. *Nat. Biotechnol.* **2008**, *26* (11), 1261–1268. https://doi.org/10.1038/nbt.1504.

(37) Singh, P.; Carrier, A.; Chen, Y.; Lin, S.; Wang, J.; Cui, S.; Zhang, X. Polymeric Microneedles

for Controlled Transdermal Drug Delivery. *J. Control. Release* **2019**, *315*, 97–113. https://doi.org/10.1016/j.jconrel.2019.10.022.

(38) Dragicevic, N.; Maibach, H. I. Skin Deep: The Basics of Human Skin Structure and Drug Penetration; **2015**; pp 3–11. https://doi.org/10.1007/978-3-662-45013-0.

(39) Liu, H.; Wang, C.; Li, C.; Qin, Y.; Wang, Z.; Yang, F.; Li, Z.; Wang, J. A Functional Chitosan-Based Hydrogel as a Wound Dressing and Drug Delivery System in the Treatment of Wound Healing. *RSC Adv.* **2018**, *8* (14), 7533–7549. https://doi.org/10.1039/C7RA13510F.

(40) Pachuau, L. Recent Developments in Novel Drug Delivery Systems for Wound Healing. *Expert Opin. Drug Deliv.* **2015**, *12* (12), 1895–1909. https://doi.org/10.1517/17425247.2015.1070143.

(41) Saghazadeh, S.; Rinoldi, C.; Schot, M.; Kashaf, S. S.; Sharifi, F.; Jalilian, E.; Nuutila, K.; Giatsidis, G.; Mostafalu, P.; Derakhshandeh, H.; Yue, K.; Swieszkowski, W.; Memic, A.; Tamayol, A.; Khademhosseini, A. Drug Delivery Systems and Materials for Wound Healing Applications. *Adv. Drug Deliv. Rev.* **2018**, *127*, 138–166. https://doi.org/10.1016/j.addr.2018.04.008.

(42) Sinno, H.; Prakash, S. Complements and the Wound Healing Cascade: An Updated Review. *Plast. Surg. Int.* **2013**, *2013* (6), 1–7. https://doi.org/10.1155/2013/146764.

(43) Boateng, J. S.; Matthews, K. H.; Stevens, H. N. E.; Eccleston, G. M. Wound Healing Dressings and Drug Delivery Systems: A Review. *J. Pharm. Sci.* **2008**, *97* (8), 2892–2923. https://doi.org/10.1002/jps.21210.

(44) Cañedo-Dorantes, L.; Cañedo-Ayala, M. Skin Acute Wound Healing: A Comprehensive Review. *Int. J. Inflam.* **2019**, *2019*, 1–15. https://doi.org/10.1155/2019/3706315.

(45) Singh, B.; Kumar, A. Graft and Crosslinked Polymerization of Polysaccharide Gum to Form Hydrogel Wound Dressings for Drug Delivery Applications. *Carbohydr. Res.* **2020**, *489*, 107949. https://doi.org/10.1016/j.carres.2020.107949.

(46) Araújo, D.; Alves, V. D.; Lima, S. A. C.; Reis, S.; Freitas, F.; Reis, M. A. M. Novel Hydrogels Based on Yeast Chitin-Glucan Complex: Characterization and Safety Assessment. *Int. J. Biol. Macromol.* **2020**, *156*, 1104–1111. https://doi.org/10.1016/j.ijbiomac.2019.11.141.

(47) Roca, C.; Alves, V. D.; Freitas, F.; Reis, M. A. M. Exopolysaccharides Enriched in Rare Sugars: Bacterial Sources, Production, and Applications. *Front. Microbiol.* **2015**, *6:288*, 1–7. https://doi.org/10.3389/fmicb.2015.00288.

(48) Freitas, F.; Alves, V. D.; Torres, C. A. V.; Cruz, M.; Sousa, I.; Melo, M. J.; Ramos, A. M.; Reis, M. A. M. Fucose-Containing Exopolysaccharide Produced by the Newly Isolated *Enterobacter* Strain A47 DSM 23139. *Carbohydr. Polym.* **2011**, *83* (1), 159–165. https://doi.org/10.1016/j.carbpol.2010.07.034.

(49) Antunes, S.; Freitas, F.; Alves, V. D.; Grandfils, C.; Reis, M. A. M. Conversion of Cheese Whey into a Fucose- and Glucuronic Acid-Rich Extracellular Polysaccharide by *Enterobacter* A47. *J. Biotechnol.* **2015**, *210*, 1–7. https://doi.org/10.1016/j.jbiotec.2015.05.013.

(50) Cimini, D.; De Rosa, M.; Schiraldi, C. Production of Glucuronic Acid-Based Polysaccharides by Microbial Fermentation for Biomedical Applications. *Biotechnol. J.* **2012**, *7* (2), 237–250. https://doi.org/10.1002/biot.201100242.

(51) Araújo, D.; Alves, V. D.; Campos, J.; Coelhoso, I.; Sevrin, C.; Grandfils, C.; Freitas, F.; Reis, M. A. M. Assessment of the Adhesive Properties of the Bacterial Polysaccharide FucoPol. *Int. J. Biol. Macromol.* **2016**, *92*, 383–389. https://doi.org/10.1016/j.ijbiomac.2016.07.035.

(52) Torres, C. A. V.; Ferreira, A. R. V.; Freitas, F.; Reis, M. A. M.; Coelhoso, I.; Sousa, I.; Alves, V. D. Rheological Studies of the Fucose-Rich Exopolysaccharide FucoPol. *Int. J. Biol. Macromol.* **2015**, *79*, 611–617. https://doi.org/10.1016/j.ijbiomac.2015.05.029.

(53) Ferreira, A. R. V.; Torres, C. A. V.; Freitas, F.; Reis, M. A. M.; Alves, V. D.; Coelhoso, I. M. Biodegradable Films Produced from the Bacterial Polysaccharide FucoPol. *Int. J. Biol. Macromol.* **2014**, *71*, 111–116. https://doi.org/10.1016/j.ijbiomac.2014.04.022.

(54) Freitas, F.; Alves, V. D.; Gouveia, A. R.; Pinheiro, C.; Torres, C. A. V.; Grandfils, C.; Reis, M. A. M. Controlled Production of Exopolysaccharides from *Enterobacter* A47 as a Function of Carbon Source with Demonstration of Their Film and Emulsifying Abilities. *Appl. Biochem. Biotechnol.* **2014**, *172* (2), 641–657. https://doi.org/10.1007/s12010-013-0560-0.

(55) Crini, G. Historical Review on Chitin and Chitosan Biopolymers. *Environ. Chem. Lett.* **2019**, *17* (1), 1623–1643. https://doi.org/10.1007/s10311-019-00901-0.

(56) Roca, C.; Chagas, B.; Farinha, I.; Freitas, F.; Mafra, L.; Aguiar, F.; Oliveira, R.; Reis, M. A. M. Production of Yeast Chitin-Glucan Complex from Biodiesel Industry Byproduct. *Process Biochem.* **2012**, *47* (11), 1670–1675. https://doi.org/10.1016/j.procbio.2012.04.004.

(57) Araújo, D.; Ferreira, I. C.; Torres, C. A. V.; Neves, L.; Freitas, F. Chitinous Polymers: Extraction from Fungal Sources, Characterization and Processing towards Value-added Applications. *J. Chem. Technol. Biotechnol.* **2020**, *95* (5), 1277–1289. https://doi.org/10.1002/jctb.6325.

(58) Cui, J.; Yu, Z.; Lau, D. Effect of Acetyl Group on Mechanical Properties of Chitin/Chitosan Nanocrystal: A Molecular Dynamics Study. *Int. J. Mol. Sci.* **2016**, *17:61* (1), 1–13. https://doi.org/10.3390/ijms17010061.

(59) Ferreira, I. C.; Araújo, D.; Voisin, P.; Alves, V. D.; Rosatella, A. A.; Afonso, C. A. M.; Freitas, F.; Neves, L. A. Chitin-Glucan Complex – Based Biopolymeric Structures Using Biocompatible Ionic Liquids. *Carbohydr. Polym.* **2020**, *247*, 116679. https://doi.org/10.1016/j.carbpol.2020.116679.

(60) Ahmad, S. I.; Ahmad, R.; Khan, M. S.; Kant, R.; Shahid, S.; Gautam, L.; Hasan, G. M.; Hassan, M. I. Chitin and Its Derivatives: Structural Properties and Biomedical Applications. *Int. J. Biol. Macromol.* **2020**, *164*, 526–539. https://doi.org/10.1016/j.ijbiomac.2020.07.098.

(61) Farinha, I.; Duarte, P.; Pimentel, A.; Plotnikova, E.; Chagas, B.; Mafra, L.; Grandfils, C.; Freitas, F.; Fortunato, E.; Reis, M. A. M. Chitin-Glucan Complex Production by K*omagataella pastoris*: Downstream Optimization and Product Characterization. *Carbohydr. Polym.* **2015**, *130*, 455–464. https://doi.org/10.1016/j.carbpol.2015.05.034.

(62) Chagas, B. F. Production and Characterization of Chitin-Glucan Complex by *Komagataella pastoris*, PhD Thesis in Chemical and Biochemical Engineering, FCT UNL, **2015**.

(63) Farinha, I.; Araújo, D.; Freitas, F. Optimization of Medium Composition for Production of Chitin-Glucan Complex and Mannose-Containing Polysaccharides by the Yeast

Komagataella pastoris. *J. Biotechnol.* **2019**, *303*, 30–36. https://doi.org/10.1016/j.jbiotec.2019.07.007.

(64) Alves, V. D.; Freitas, F.; Torres, C. A. V.; Cruz, M.; Marques, R.; Grandfils, C.; Gonçalves, M. P.; Oliveira, R.; Reis, M. A. M. Rheological and Morphological Characterization of the Culture Broth during Exopolysaccharide Production by *Enterobacter Sp*. *Carbohydr. Polym.* **2010**, *81* (4), 758–764. https://doi.org/10.1016/j.carbpol.2010.03.048.

(65) Patil, J. S.; Kamalapur, M. V.; Marapur, S. C.; Kadam, D. V. Ionotropic Gelation and Polyelectrolyte Complexation: The Novel Techniques to Design Hydrogel Particulate Sustained, Modulated Drug Delivery System: A Review. *Dig. J. Nanomater. Biostructures* **2010**, *5* (1), 241–248.

(66) Nayak, A. K.; Hasnain, M. S. Ionotropically Gelled Alginate Particles in Sustained Drug Release. In *Alginates in Drug Delivery*; Elsevier, **2020**; pp 203–230. https://doi.org/10.1016/B978-0-12-817640-5.00009-1.

(67) Costa, L.; Silva-Correia, J.; Oliveira, J. M.; Reis, R. L. Gellan Gum-Based Hydrogels for Osteochondral Repair. In *Advances in Experimental Medicine and Biology*; Springer International Publishing AG, **2018**; Vol. 1058, pp 281–304. https://doi.org/10.1007/978-3-319-76711-6_13.

(68) Bacelar, A. H.; Silva-Correia, J.; Oliveira, J. M.; Reis, R. L. Recent Progress in Gellan Gum Hydrogels Provided by Functionalization Strategies. *J. Mater. Chem. B* **2016**, *4* (37), 6164–6174. https://doi.org/10.1039/C6TB01488G.

(69) Abasalizadeh, F.; Moghaddam, S. V.; Alizadeh, E.; Akbari, E.; Kashani, E.; Fazljou, S. M. B.; Torbati, M.; Akbarzadeh, A. Alginate-Based Hydrogels as Drug Delivery Vehicles in Cancer Treatment and Their Applications in Wound Dressing and 3D Bioprinting. *J. Biol. Eng.* **2020**, *14* (1), 1–22. https://doi.org/10.1186/s13036-020-00239-0.

(70) Lascol, M.; Bourgeois, S.; Barratier, C.; Marote, P.; Lantéri, P.; Bordes, C. Development of Pectin Microparticles by Using Ionotropic Gelation with Chlorhexidine as Cross-Linking Agent. *Int. J. Pharm.* **2018**, *542* (1–2), 205–212. https://doi.org/10.1016/j.ijpharm.2018.03.011.

(71) Harper, B. A.; Barbut, S.; Lim, L.-T.; Marcone, M. F. Effect of Various Gelling Cations on

the Physical Properties of “Wet” Alginate Films. *J. Food Sci.* **2014**, *79* (4), E562–E567. https://doi.org/10.1111/1750-3841.12376.

(72) Lee, K. Y.; Mooney, D. J. Alginate: Properties and Biomedical Applications. *Prog. Polym. Sci.* **2012**, *37* (1), 106–126. https://doi.org/10.1016/j.progpolymsci.2011.06.003.

(73) Klontzas, M. E.; Reakasame, S.; Silva, R.; Morais, J. C. F.; Vernardis, S.; MacFarlane, R. J.; Heliotis, M.; Tsiridis, E.; Panoskaltsis, N.; Boccaccini, A. R.; Mantalaris, A. Oxidized Alginate Hydrogels with the GHK Peptide Enhance Cord Blood Mesenchymal Stem Cell Osteogenesis: A Paradigm for Metabolomics-Based Evaluation of Biomaterial Design. *Acta Biomater.* **2019**, *88*, 224–240. https://doi.org/10.1016/j.actbio.2019.02.017.

(74) Balitaan, J. N. I.; Hsiao, C.-D.; Yeh, J.-M.; Santiago, K. S. Innovation Inspired by Nature: Biocompatible Self-Healing Injectable Hydrogels Based on Modified-β-Chitin for Wound Healing. *Int. J. Biol. Macromol.* **2020**, *162*, 723–736. https://doi.org/10.1016/j.ijbiomac.2020.06.129.

(75) Debnath, S.; Suresh Kumar, R.; Niranjan Babu, M. Ionotropic Gelation - A Novel Method to Prepare Chitosan Nanoparticles. *Res. J. Pharm. Technol.* **2011**, *4* (4), 492–495.

(76) Pedroso-Santana, S.; Fleitas-Salazar, N. Ionotropic Gelation Method in the Synthesis of Nanoparticles/Microparticles for Biomedical Purposes. *Polym. Int.* **2020**, *69* (5), 443–447. https://doi.org/10.1002/pi.5970.

(77) Bajpai, M.; Shukla, P.; Bajpai, S. K. Enhancement in the Stability of Alginate Gels Prepared with Mixed Solution of Divalent Ions Using a Diffusion through Dialysis Tube (DTDT) Approach. *J. Macromol. Sci. Part A* **2017**, *54* (5), 301–310. https://doi.org/10.1080/10601325.2017.1294452.

(78) Liu, L.; Wang, B.; Gao, Y.; Bai, T. Chitosan Fibers Enhanced Gellan Gum Hydrogels with Superior Mechanical Properties and Water-Holding Capacity. *Carbohydr. Polym.* **2013**, *97* (1), 152–158. https://doi.org/10.1016/j.carbpol.2013.04.043.

(79) Shahria Disha, J.; Hosney, M.; Begum, A.; Mahfuz, M.; Shawan, A. K.; Khatun, N.; Ahmed, S.; Islam, M. S.; Karim, R.; Islam, R.; Hossain, M.; Hasan, M. A. Preparation and Characterization of Xanthan Gum-Based Biodegradable Polysaccharide Hydrogels. *Res. J. Mater. Sci.* **2016**, *4* (4), 13–18.

(80) Dobashi, T.; Yamamoto, T. Anisotropic Gel Formation Induced by Dialysis. In *Encyclopedia of Biocolloid and Biointerface Science, 2 Volume Set*; John Wiley & Sons, Inc.: Hoboken, NJ, USA, **2016**; Vol. 2, pp 487–497. https://doi.org/10.1002/9781119075691.ch39.

(81) Modepalli, N.; Shivakumar, H.; Kanni, K. P.; Murthy, S. N. Transdermal Iron Replenishment Therapy. *Ther. Deliv.* **2015**, *6* (6), 661–668. https://doi.org/10.4155/tde.15.24.

(82) Zhang, R.; Tao, Y.; Xu, W.; Xiao, S.; Du, S.; Zhou, Y.; Hasan, A. Rheological and Controlled Release Properties of Hydrogels Based on Mushroom Hyperbranched Polysaccharide and Xanthan Gum. *Int. J. Biol. Macromol.* **2018**, *120* (Part B), 2399–2409. https://doi.org/10.1016/j.ijbiomac.2018.09.008.

(83) Ambebila, E. N.; Santamaría, E.; Maestro, A.; Gutiérrez, J. M.; González, C. Gellan Hydrogels: Preparation, Rheological Characterization and Application in Encapsulation of Curcumin. *Food Biophys.* **2019**, *14* (2), 154–163. https://doi.org/10.1007/s11483-019-09568-0.

(84) Feng, Y.; Taraban, M.; Yu, Y. B. The Effect of Ionic Strength on the Mechanical, Structural and Transport Properties of Peptide Hydrogels. *Soft Matter* **2012**, *8* (46), 11723–11731. https://doi.org/10.1039/c2sm26572a.

(85) Shen, X.; Shamshina, J. L.; Berton, P.; Gurau, G.; Rogers, R. D. Hydrogels Based on Cellulose and Chitin: Fabrication, Properties, and Applications. *Green Chem.* **2016**, *18* (1), 53–75. https://doi.org/10.1039/C5GC02396C.

(86) Tamura, H.; Furuike, T.; Nair, S. V.; Jayakumar, R. Biomedical Applications of Chitin Hydrogel Membranes and Scaffolds. *Carbohydr. Polym.* **2011**, *84* (2), 820–824. https://doi.org/10.1016/j.carbpol.2010.06.001.

(87) Gong, P.; Wang, J.; Liu, B.; Ru, G.; Feng, J. Dissolution of Chitin in Aqueous KOH. *Cellulose* **2016**, *23* (3), 1705–1711. https://doi.org/10.1007/s10570-016-0932-z.

(88) Duan, J.; Liang, X.; Cao, Y.; Wang, S.; Zhang, L. High Strength Chitosan Hydrogels with Biocompatibility via New Avenue Based on Constructing Nanofibrous Architecture. *Macromolecules* **2015**, *48* (8), 2706–2714. https://doi.org/10.1021/acs.macromol.5b00117.

(89) Chang, C.; Chen, S.; Zhang, L. Novel Hydrogels Prepared via Direct Dissolution of Chitin at Low Temperature: Structure and Biocompatibility. *J. Mater. Chem.* **2011**, *21* (11), 3865. https://doi.org/10.1039/c0jm03075a.

(90) Muñoz, G.; Valencia, C.; Valderruten, N.; Ruiz-Durántez, E.; Zuluaga, F. Extraction of Chitosan from *Aspergillus niger* Mycelium and Synthesis of Hydrogels for Controlled Release of Betahistine. *React. Funct. Polym.* **2015**, *91–92*, 1–10. https://doi.org/10.1016/j.reactfunctpolym.2015.03.008.

(91) Budtova, T.; Navard, P. Cellulose in NaOH–Water Based Solvents: A Review. *Cellulose* **2016**, *23* (1), 5–55. https://doi.org/10.1007/s10570-015-0779-8.

(92) Dhanasingh, A.; Salber, J.; Moeller, M.; Groll, J. Tailored Hyaluronic Acid Hydrogels through Hydrophilic Prepolymer Cross-Linkers. *Soft Matter* **2010**, *6* (3), 618–629. https://doi.org/10.1039/B917113D.

(93) Nogueira, G. M.; de Moraes, M. A.; Rodas, A. C. D.; Higa, O. Z.; Beppu, M. M. Hydrogels from Silk Fibroin Metastable Solution: Formation and Characterization from a Biomaterial Perspective. *Mater. Sci. Eng. C* **2011**, *31* (5), 997–1001. https://doi.org/10.1016/j.msec.2011.02.019.

(94) Chen, Y.-H.; Li, J.; Hao, Y.-B.; Qi, J.-X.; Dong, N.-G.; Wu, C.-L.; Wang, Q. Preparation and Characterization of Composite Hydrogels Based on Crosslinked Hyaluronic Acid and Sodium Alginate. *J. Appl. Polym. Sci.* **2015**, *132* (19), 41898. https://doi.org/10.1002/app.41898.

(95) Borzacchiello, A.; Russo, L.; Malle, B. M.; Schwach-Abdellaoui, K.; Ambrosio, L. Hyaluronic Acid Based Hydrogels for Regenerative Medicine Applications. *Biomed Res. Int.* **2015**, *2015* (4), 1–12. https://doi.org/10.1155/2015/871218.

(96) Haridas, N.; Rosemary, M. J. Effect of Steam Sterilization and Biocompatibility Studies of Hyaluronic Acid Hydrogel for Viscosupplementation. *Polym. Degrad. Stab.* **2019**, *163*, 220–227. https://doi.org/10.1016/j.polymdegradstab.2019.03.019.

(97) Saeed, A. M. Effect of PH on Swelling Properties of Commercial Polyacrylic Acid Hydrogel Bead. *J. Atoms Mol.* **2014**, *4* (1), 656–665.

(98) Kong, B. J.; Kim, A.; Park, S. N. Properties and *in Vitro* Drug Release of Hyaluronic Acid-

Hydroxyethyl Cellulose Hydrogels for Transdermal Delivery of Isoliquiritigenin. *Carbohydr. Polym.* **2016**, *147*, 473–481. https://doi.org/10.1016/j.carbpol.2016.04.021.

(99) Saeed, A. M. Temperature Effect on Swelling Properties of Commercial Polyacrylic Acid Hydrogel Beads. *Int. J. Adv. Biol. Biomed. Res.* **2013**, *1* (12), 1614–1627.

(100) Danalache, F. A. Novel Ready-to-Eat Mango Product Using Gellan Gum as Gelling Agent: Physico-Chemical, Microbial and Sensory Characteristics, PhD Thesis in Sustainable Chemistry, FCT-UNL, **2014**.

(101) Atoufi, Z.; Kamrava, S. K.; Davachi, S. M.; Hassanabadi, M.; Saeedi Garakani, S.; Alizadeh, R.; Farhadi, M.; Tavakol, S.; Bagher, Z.; Hashemi Motlagh, G. Injectable PNIPAM/Hyaluronic Acid Hydrogels Containing Multipurpose Modified Particles for Cartilage Tissue Engineering: Synthesis, Characterization, Drug Release and Cell Culture Study. *Int. J. Biol. Macromol.* **2019**, *139*, 1168–1181. https://doi.org/10.1016/j.ijbiomac.2019.08.101.

Appendices

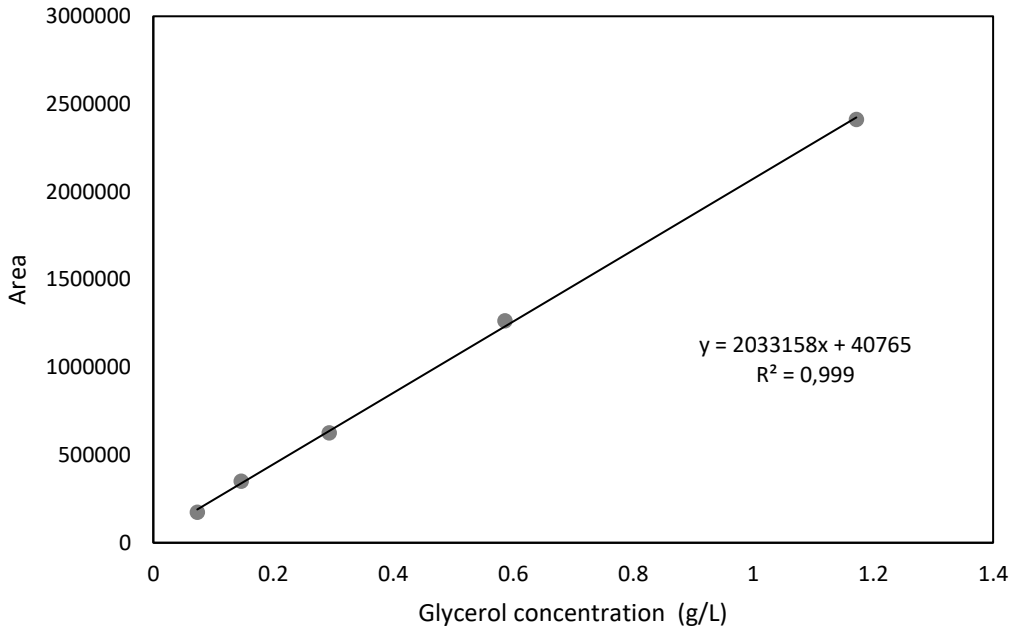

Figure A1: Glycerol calibration curve used in glycerol quantification of the FucoPol bioreactor assay.

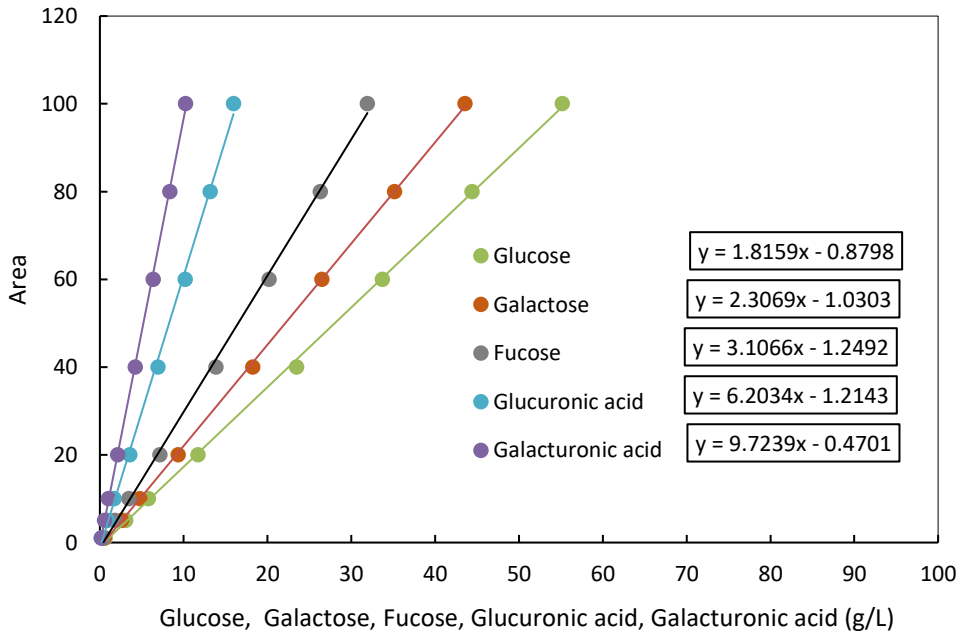

Figure A2: Calibration curve used in EPS sugar monomers characterization (glucose, galactose, fucose, and glucuronic acid).

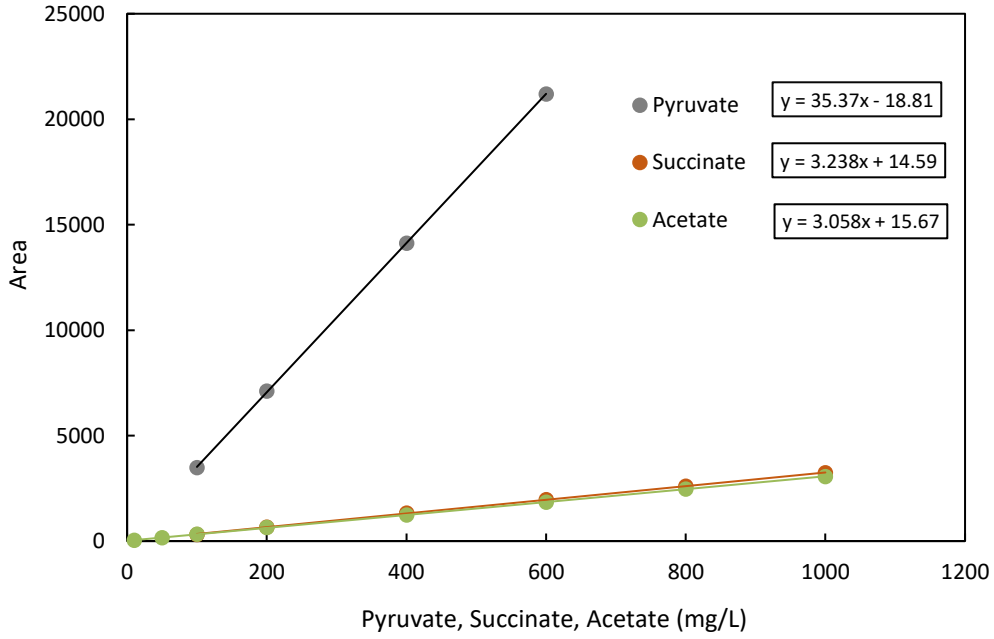

Figure A3: Calibration curve used in the EPS quantification of acyl groups (pyruvate, succinate, and acetate).

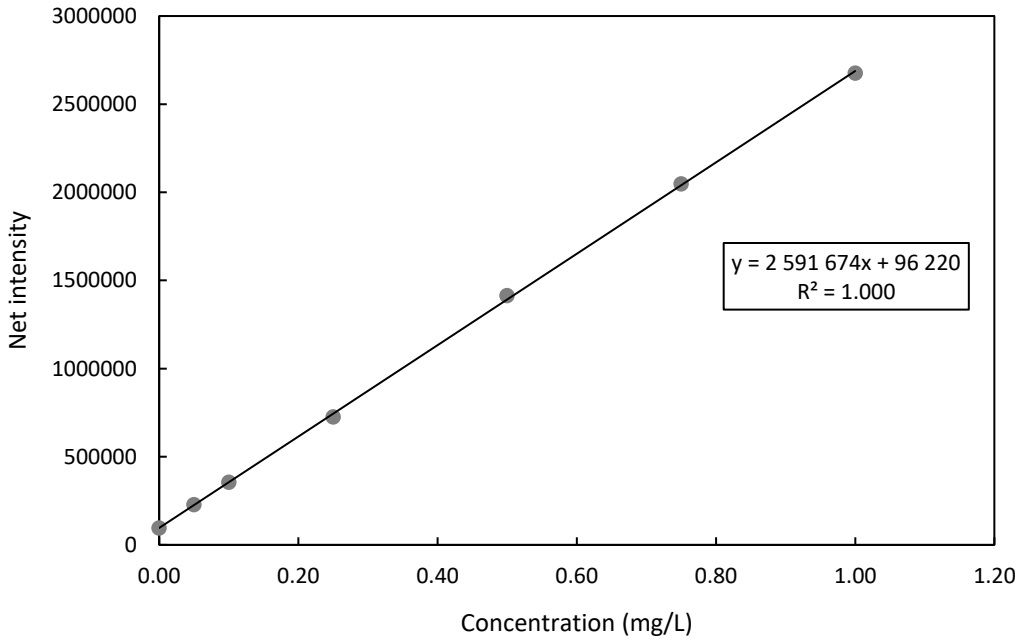

Figure A4: Calibration curve used in iron quantification of FucoPol hydrogels.

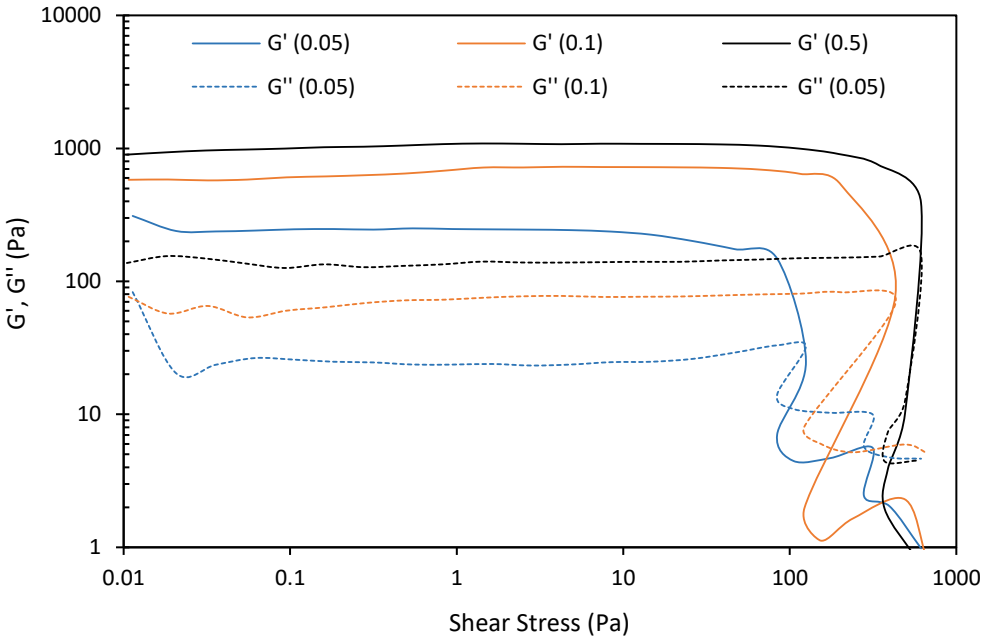

Figure A5: Stress sweeps of FucoPol hydrogels dialysed against iron solutions (0.05, 0.1 and 0.5 g/L of Fe^{3+}). Mechanical spectrum storage (G', solid line) and loss moduli (G''dotted line).

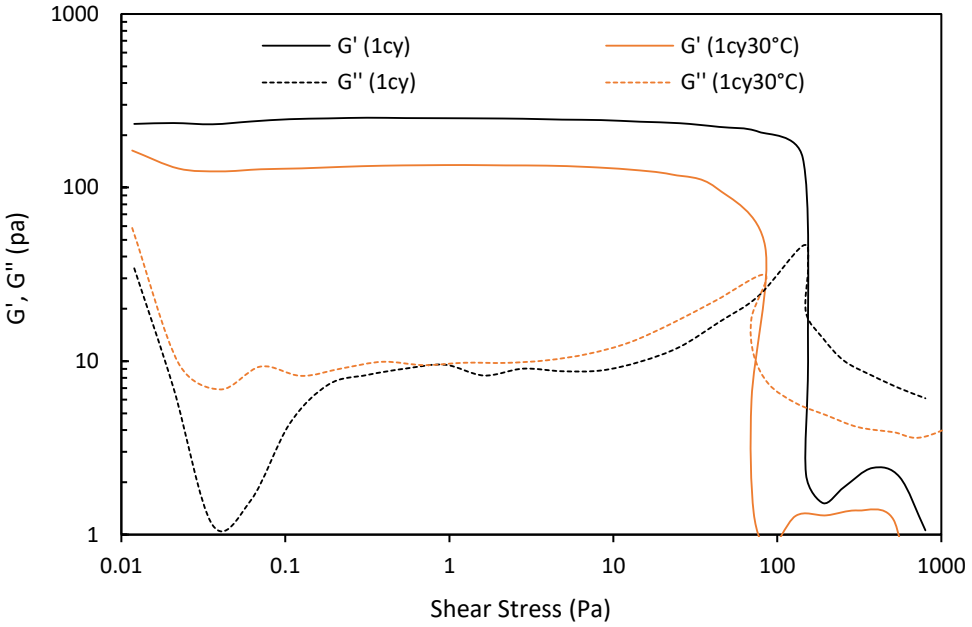

Figure A6: Stress sweeps of 1cy and 1cy30°C CGC hydrogels. Mechanical spectrum storage (G', solid line) and loss moduli (G''dotted line).

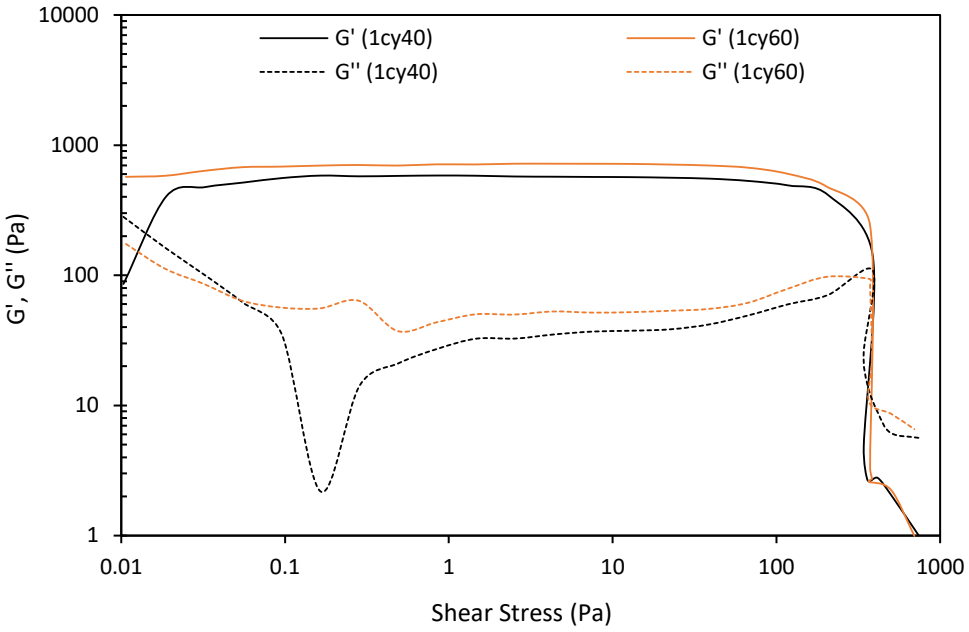

Figure A7: Stress sweeps of 1cy40 and 1cy60 CGC hydrogels. Mechanical spectrum storage (G', solid line) and loss moduli (G''dotted line).

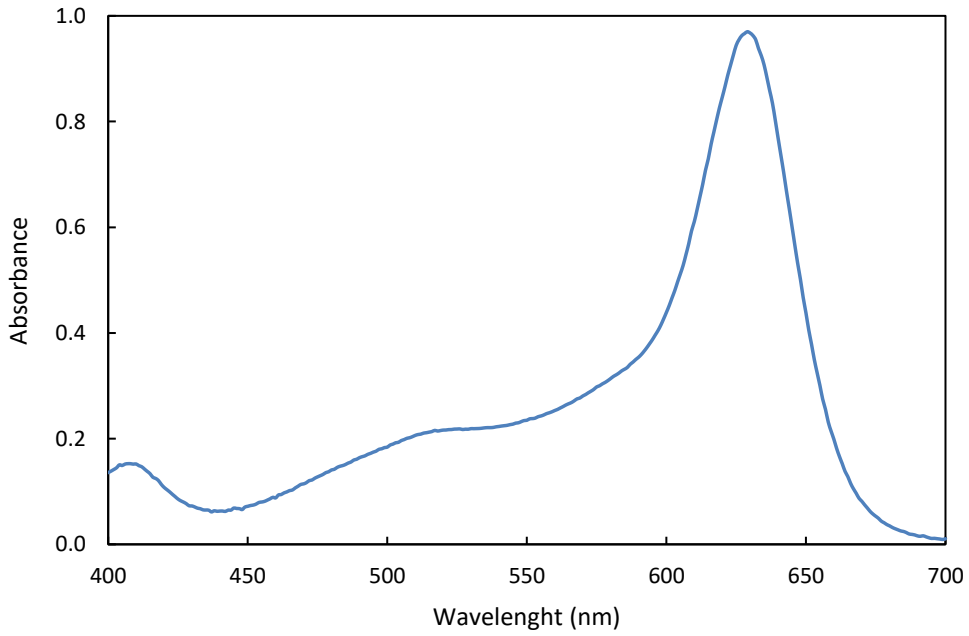

Figure A8: UV-vis spectra of the blue food dye in water.

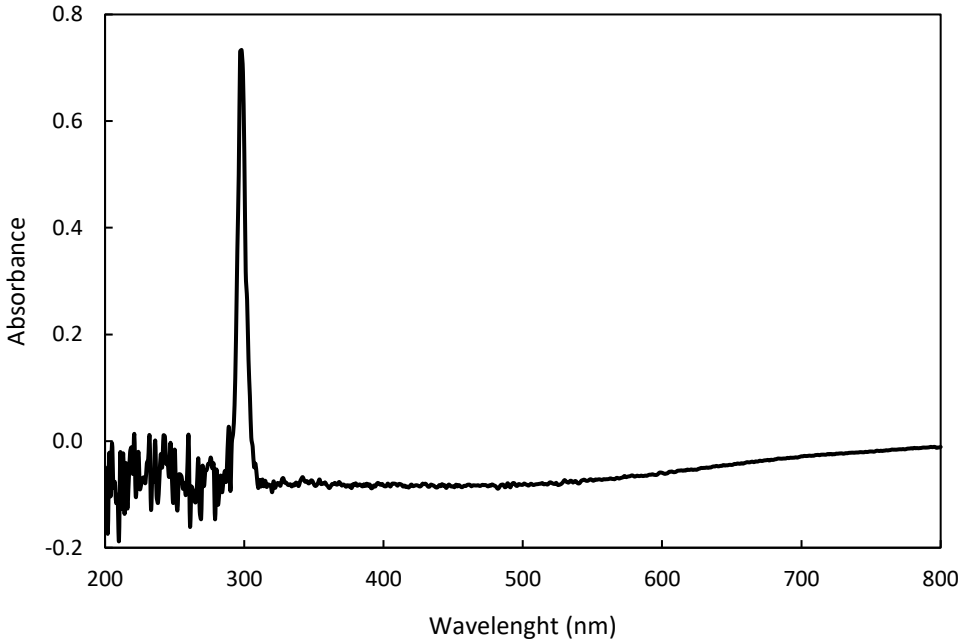

Figure A9: UV-vis spectra of theophylline in water.

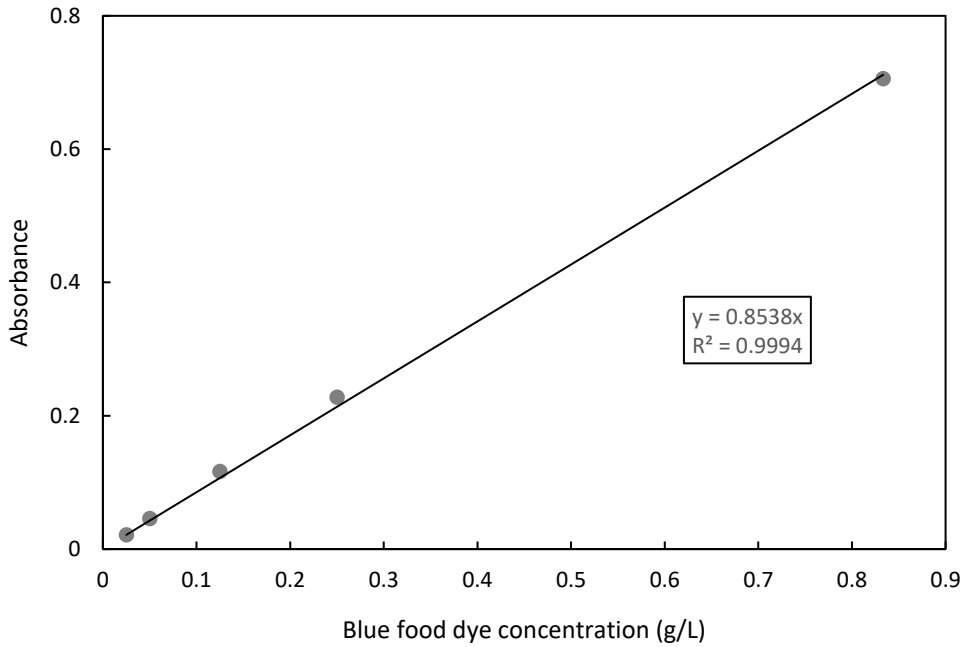

Figure A10: Calibration curve of the blue food dye used in the quantification of release properties of 1cy hydrogels.

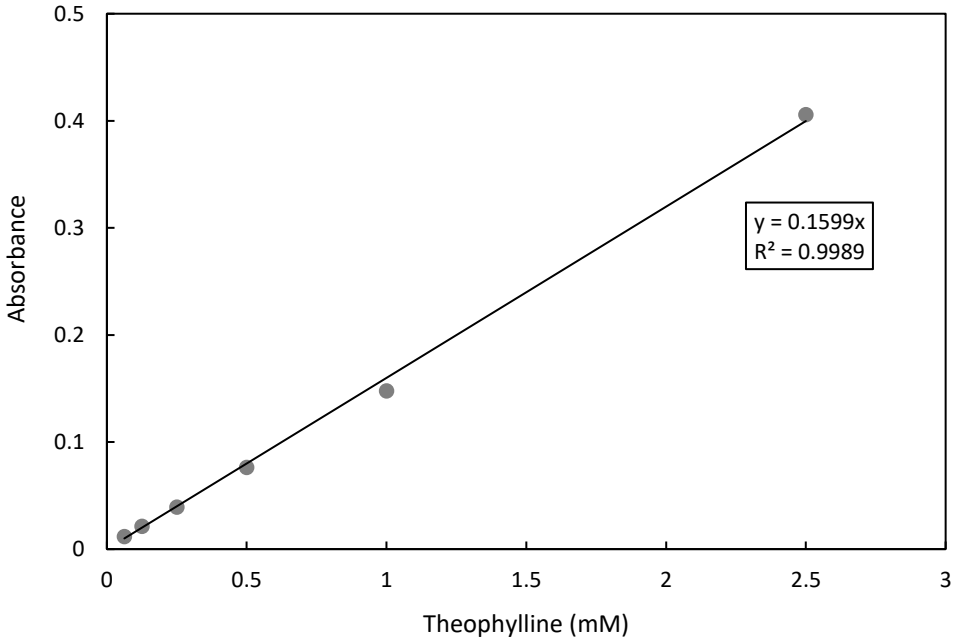

Figure A11: Calibration curve of theophylline used in the quantification of release properties of 1cy and 1cy60 hydrogels.